

1N-44

0224747

Thermal Evaluation of Advanced Solar Dynamic Heat Receiver Performance

Roger A. Crane
The University of South Florida
Tampa, Florida

March 1989

Prepared for
Lewis Research Center
Under Grant NAG3-851

NASA

National Aeronautics and
Space Administration

(NASA-CR-185117) THERMAL EVALUATION OF
ADVANCED SOLAR DYNAMIC HEAT RECEIVER
PERFORMANCE Final Report, Jan - Dec. 1988
(University of South Florida) 131 pCSCL 10A

N89-27256

Unclas
0224747

G3/44

Table of Contents

1	Introduction.	1
1.1	Advanced Solar Dynamic Systems	2
1.1.1	Advanced Solar Dynamic Brayton Cycle	2
1.1.2	Advanced Solar Dynamic Stirling Cycle	3
1.2	Advanced Solar Dynamic Receiver Design	4
1.3	Project Scope.	6
2	Analysis Approach	11
2.1	Basic Cycles	11
2.2	Concentrators	12
2.3	PCM Enhancement	14
2.4	Receiver Concepts	15
2.4.1	Base Receiver Concept	15
2.4.2	Heat Pipe Concept	16
2.4.3	Pebble Bed Concept	17
2.4.4	Cavity Heat Pipe	17
2.4.5	Brayton Cycle Cavity Receiver	19
2.5	Hybrid Elements	20
2.6	Model	22
2.6.1	Physical model.	24
2.6.2	Void model.	24
2.6.3	Energy equation.	26
2.6.4	Computer Program.	27
3	Parametric Study	28
3.1	Base Line Receiver.	28
3.2	Heat Pipe Receiver.	34
3.3	Pebble Bed Receiver.	39
3.4	Cavity Heat Pipe Receiver.	41
3.5	Cavity Receiver.	45
4	Discussion	50
4.1	Attainable Performance	50
4.2	PCM Thermal Enhancement	53
4.3	Parametric Studies	54
5	Conclusions.	56
6	References	57

Table of Figures

Advanced Solar Dynamic Brayton Cycle	3
Advanced Solar Dynamic Stirling Cycle	4
Weight Distribution for Solar Dynamic System.	6
Incident Solar Flux Distribution.	12
Receiver Energy Distribution.	13
Finite Difference Element Arrangement.	24
Base Line Orbital Turbine Inlet Temperature.	29
Effects of PCM Enhancement on Base Line Turbine Inlet Temp.	30
Effects of Element Number on Base Line Turbine Inlet Temp.	30
Effects of Base Line Receiver L/D on Turbine Inlet Temp. .	31
Effects of Base Line Element P/D on Turbine Inlet Temp. ..	32
Effects of Base Line Element Number on Canister Temp.	32
Effects of Base Line Receiver L/D on Canister Temp.	33
Effects of Base Line P/D on Canister Temp.	33
Effects of PCM Selection on Heat Pipe Orbital Vapor Temp.	34
Effects of PCM Enhancement on Heat Pipe Vapor Temp.	35
Effects of Element Number on Heat Pipe Vapor Temp.	36
Effects of Receiver L/D on Heat Pipe Vapor Temp.	36
Effects of Element Number on Heat Pipe Canister Temp.	37
Effect of Receiver L/D on Heat Pipe Canister Temp.	38
Effect of PCM Enrichment on Heat Pipe Canister Temp.	38
Effect of Element P/D on Pebble Bed Turbine Inlet Temp. ..	39
Effect of Pebble Bed Receiver L/D on Turbine Inlet Temp. .	40
Effect of Pebble Bed Element P/D on Canister Temp.	40
Effect of Pebble Bed Receiver L/D on Canister Temp.	41
Effects of Cavity Heat Pipe Element Number on Canister Temp.	42
Effect of Cavity Heat Pipe Apex Angle on Cavity Temp.	43
Effects of Cavity Heat Pipe Receiver L/D on Cavity Temp. .	44
Effects of PCM Enhancement on Cavity Heat Pipe Cavity Temp.	45
Cavity Receiver Orbital Turbine Inlet Temperature.	46
Effects of Cavity Receiver Element P/D on Canister Temp. .	47
Effects of Cavity Receiver PCM Absorptivity on Cansiter Temp	47
Effects of Cavity Receiver L/D on Canister Temp.	48
Effects of Cavity Receiver Element P/D on Canister Temp. .	49

1 Introduction.

A study has been conducted by the University of South Florida to evaluate elements of Advanced Solar Dynamic power generation. This effort has been designed to determine the thermal performance of basic receiver concepts and the effects of various phase change materials. The study was funded by the NASA-Lewis Research Center under contract NAG3-851 and conducted during the period of January 1988 through December 1988 at the University of South Florida, Tampa, Florida.

Associated with a significant increase in space exploration, scientific research, commercial development and potential military weapons systems, comes the need for increased capacity, space operable, electrical power sources. Photovoltaic power generation is now a well developed technology successfully utilized in numerous commercial and military satellites. The technology is especially attractive for space applications in terms of mechanical simplicity, utilizing no moving parts and easing problems of deployment and maintenance. Their major limitation is relatively low energy efficiency, typically in the range of 8 percent. This is well below the levels encountered in many relatively simple terrestrial systems which regularly achieve efficiencies of 20 to 25 percent.

As power requirements in space increase, the size penalties placed on design by the photovoltaic technology become less acceptable. Whereas current satellites have generally required less than 10 kWe, missions planned within the next 10 years [1] require one to two orders of magnitude increase. Advanced phases of the space station incorporate design plans for a number of solar dynamic cycle electrical generators providing a total power level of between 300 and 1000 kWe. Other unclassified large scale missions include a GEO communications platform, an air/ocean traffic control system, a GEO payload delivery system and a micro g materials processing system. With a clear need established for an advanced, light weight, increased capacity power generation system, NASA has undertaken the development of a space solar dynamic technology. It is clear that with the development of such advanced technologies, substantial improvements can be made in system size and weight.

Concepts currently under consideration are for applications in low earth orbit (LEO). These include solar powered Brayton and Stirling cycles operation at peak cycle temperatures of between 1000 and 1400 K. To ensure continuous power during the eclipse portion of the LEO, thermal energy storage is accomplished through the use of a suitable phase change material (PCM). With proper selection of materials the use of latent energy storage will provide relatively compact, low weight storage at a uniform high temperature. Both fluoride salts and metallic alloys are being evaluated for these applications. Typically the fluoride salts provide large

heats of fusion with suitable containment chemical compatibility; they are limited by poor thermal transport properties and large volume changes. Metallic alloys provide outstanding thermal transport properties and restricted volume changes but do not have demonstrated containment materials.

The work described herein addresses a portion of that development effort. The goal is first to examine a number of alternative receiver designs to determine their basic thermal performance. Designs providing large thermal gradients or large temperature swings during orbit are susceptible to early mechanical failure. In addition significant temperature variations in the working fluid have an adverse impact on the thermal efficiency of the cycle. By reviewing the thermal performance of each basic design, the relative merits of the basic concepts are to be compared. In addition, the effect of thermal enhancement and metal utilization provides a partial characterization of the performance improvements to be achieved by developing these technologies. The results are then thought to be applicable in determining the justification for development of new technologies. Finally the analysis includes a basic geometrical parametric study of each of the designs. Near the optimal design point it appears that there is generally a trade off between thermal performance and receiver weight. The results of this study will show how design parameters thermally affect overall system weight.

1.1 Advanced Solar Dynamic Systems

Initially the ASD program gave consideration to three basic power cycles: the Rankine, Brayton and Stirling engines. An organic Rankine cycle, using toluene as a working fluid, was considered but determined to be of limited potential for advanced applications. Organics tend to break down chemically at elevated temperatures, limiting the cycle to about 700 K. Since improvements in thermodynamic efficiency can most easily be achieved by increases in peak cycle temperature, consideration of the Rankine cycle then turned to either using liquid metals as working fluids or to finding an alternative stable, high temperature fluid. Preliminary design studies have shown that such systems are of significantly greater specific mass than their alternatives so that attention is currently concentrating on future development of the Brayton and Stirling cycles.

1.1.1 Advanced Solar Dynamic Brayton Cycle

A schematic of the Brayton cycle is shown in Figure 1. The cycle utilizes a mixture of xenon and helium as the working fluid. Earlier studies have indicated that a suitable combination of high and low molecular weight gases provides an optimum mixture with relatively high density and high thermal

conductivity [2]. The gas is compressed in a single stage mixed flow compressor, heated as it is passed successively through a recuperator and a receiver, expanded through a turbine and finally cooled by returning through the recuperator and passing through the heat exchanger. Energy is supplied by focusing solar energy from a parabolic collector into the receiver; waste heat is radiated into space.

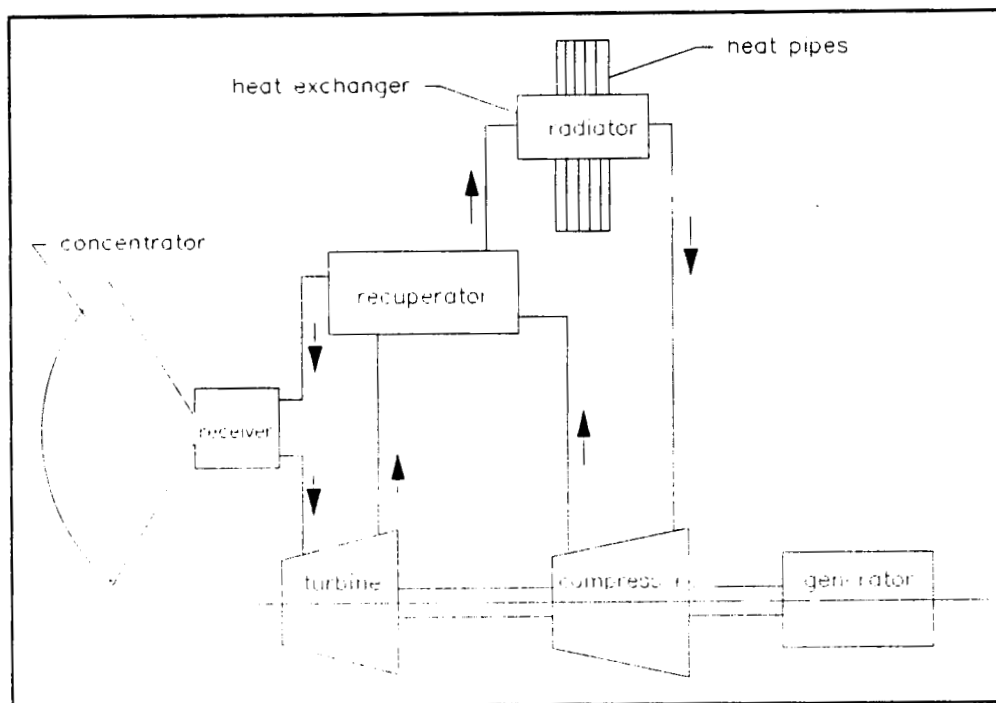


Figure 1. Advanced Solar Dynamic Brayton Cycle.

1.1.2 Advanced Solar Dynamic Stirling Cycle

The Stirling cycle is represented schematically in Figure 2. The engine includes a piston and cylinder arrangement in which the working fluid moves alternately to chambers above and below the piston via a set of bypass ports in the cylinder walls. The upper chamber is thermally connected to the radiator. The piston is attached directly to a linear alternator to provide for a very simple system of electrical power generation.

The Stirling engine represents a technological step beyond the Brayton engine. Whereas the Brayton cycle is widely used in terrestrial applications the Stirling engine is still in its infancy. The advantage lies primarily in its high specific power in larger generator sizes. Results of an earlier study [4] show that a 7 kWe Stirling system will weigh about 20% less than a comparable Brayton system, 40% less than a planer photovoltaic array, and 45% less than a photovoltaic array with a focused concentrator; at 35 kWe the advantage increases

to about 25% below the Brayton cycle, 50% less than a photovoltaic planer array, and 85% less than a photovoltaic array with a focused concentrator. NASA is currently testing a prototype Stirling engine to obtain additional data for evaluating its suitability for long term space applications.

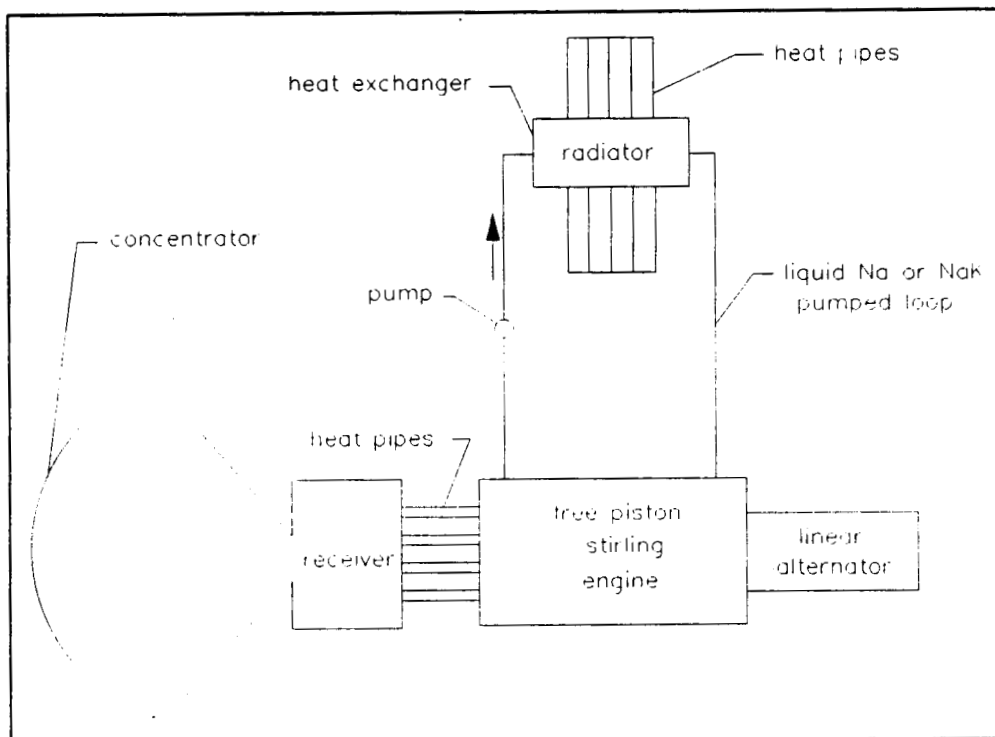


Figure 2. Advanced Solar Dynamic Stirling Cycle.

1.2 Advanced Solar Dynamic Receiver Design

Both the Brayton and Stirling cycles are adaptable to a wide range of high power applications. In low earth orbit provisions are made for uninterrupted power generation during the eclipse portion of the orbit by storing excess energy in periods of solar incidence as a sensible and/or latent heat. A receiver containing the storage media and designed for use with the Space Station is shown in Figure 3. On the right side of the receiver is an aperture placed at the focal point of the concentrator. Energy passing through the aperture is absorbed in the elements containing the PCM located on the inside perimeter of the receiver; a portion is stored for later use while the remainder is transferred to the working fluid flowing through a concentric passage inside the PCM.

ORIGINAL PAGE IS
OF POOR QUALITY

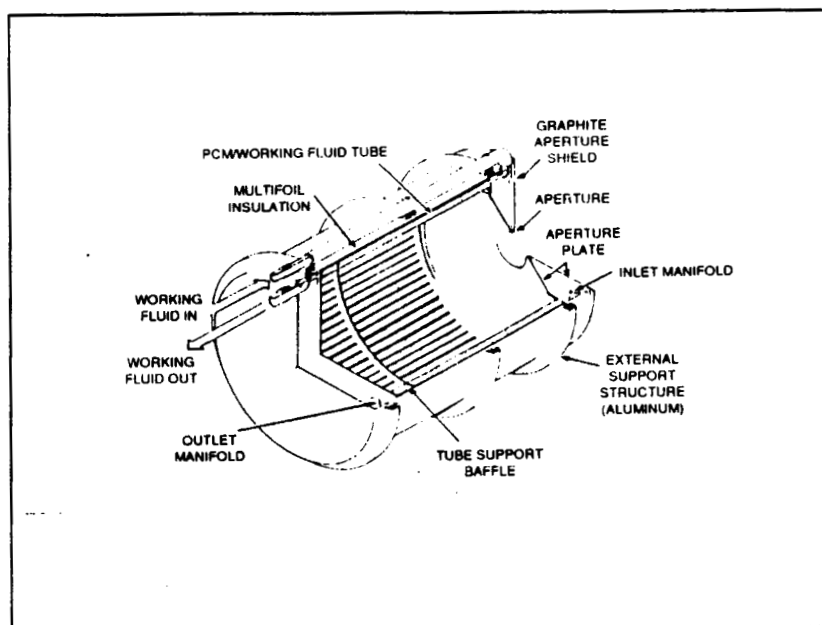


Figure 3. Space Station Receiver Design. [3]

Design studies [4] initiated to determine the overall weight distribution within a typical solar dynamic system have clearly established design targets for substantial performance improvements. Results, shown in Figure 4, indicate that the receiver would likely be the single heaviest component with about 45% of the overall system weight. This is followed by the concentrator, with about 20% of the system weight, and the structure and radiator, each constituting about 10%. In an attempt to reduce overall system weight, it is natural that attention focus first on the receiver. In so doing it is also important to note that in most receiver designs, the PCM constitutes only a small fraction of the actual receiver weight. Receiver weight distributions for the base case design are shown in Table I. Here the PCM constitutes only 70 kg out of an overall receiver weight of 461 kg. This is a meager 15% and clearly suggests substantial opportunity for system weight savings through improved receiver design.

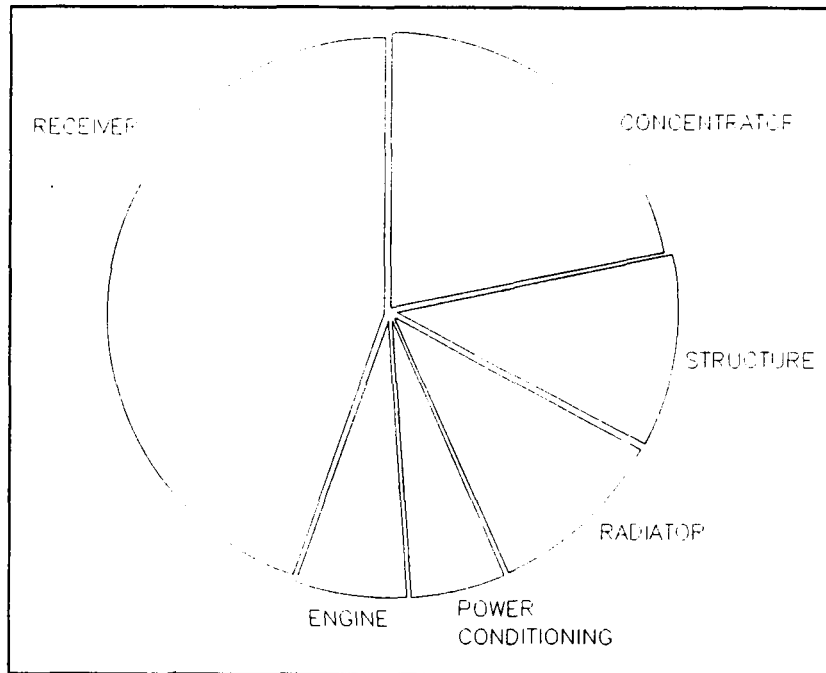


Figure 4. Weight Distribution for Space Station Solar Dynamic System.

1.3 Project Scope.

This study is designed to compare the basic thermal performance of five receiver concepts. The goal is to determine the efficiency of each in utilization of the PCM, the magnitude of the thermal gradients resulting, the extent of the resultant peak cycle temperature swings and their impact on overall cycle efficiency. Concepts were selected for analysis based partially on their respective merit, but also with the goal of including the widest possible range of distinct design approaches. Those selected include (a) a base case taken from the Space Station design effort, (b) a heat pipe configuration, (c) a pebble bed concept, (d) a Sanders Brayton cycle design and (e) a cavity heat pipe arrangement. The base case design is shown in Figure 3. The remaining concepts are shown in Figures 5 through 8 respectively.

TABLE I. BASIC CASE RECEIVER WEIGHT DISTRIBUTION

Component	Weight, kg
Phase Change Material	70
Working Fluid Tube	17
Containment Canister	132
Manifold	21
Formed Insulation Mandrel	32
Backwall support Plate	15
Multifoil Insulation	47
Aluminum Outer Shell	59
Baffels and Supports	23
Aperture Plate	30
Aperture Shield	15
TOTAL	461

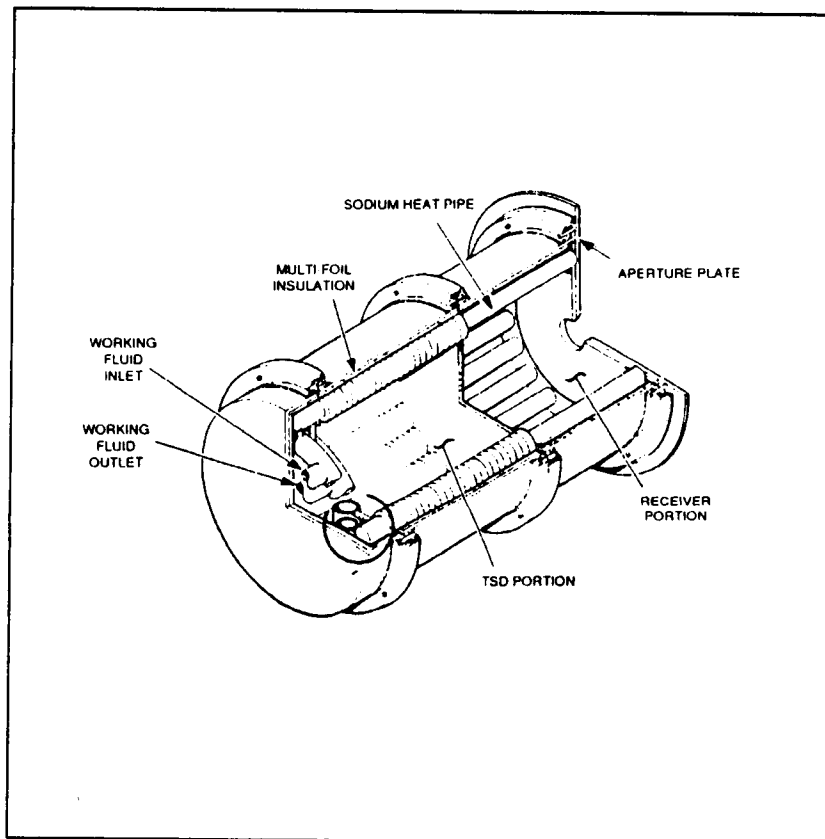


Figure 5. Heat Pipe Receiver. [3]

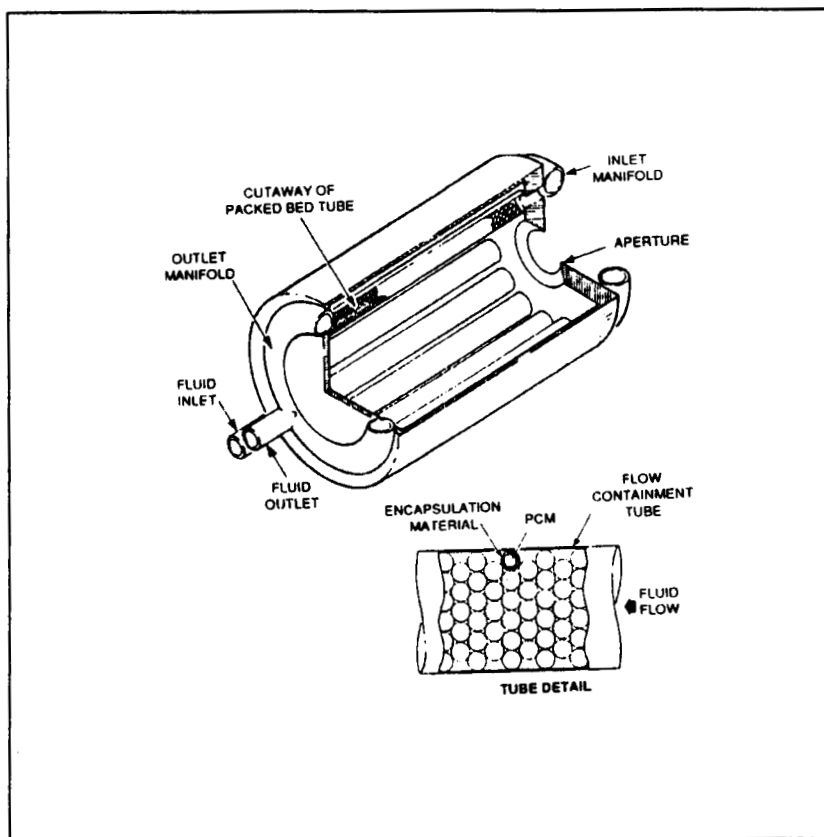


Figure 6. Pebble Bed Receiver. [3]

Each concept has been proposed by one or more outside contractors to NASA. However, the approach undertaken here is not to attempt to compare specific designs. These designs have been used to identify basic configurations. Each configuration has then been normalized to utilize the same group of PCMs and evaluated under a similar set of operation conditions irrespective of those originally proposed. The results are not seen as a basis for comparison of the respective proposals but instead are intended as a thermal comparison of the overall configurations.

In addition to considerations of basic receiver configuration, optimal selection of those dimensional parameters which affect thermal performance will be of concern. Specifically this study will include a parametric study of each of the basic receiver designs to establish the range of performance achievable with each. While no direct trade-off will be performed between improvements in thermal performance and possible adverse effects on receiver weight, it is envisioned that the results might be useful in such a comparison.

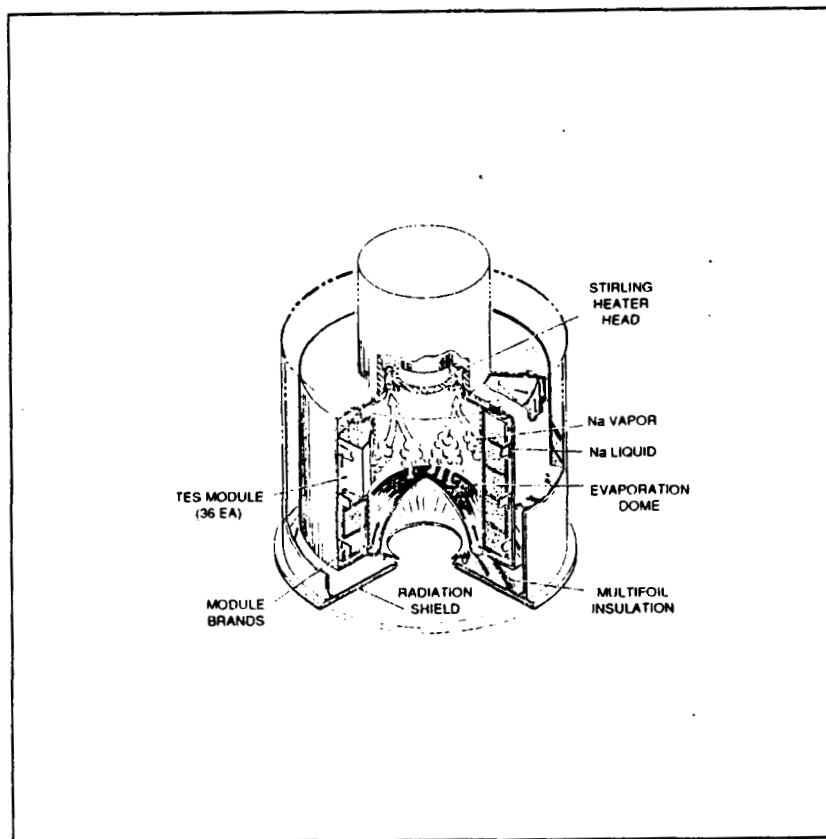


Figure 7. Cavity Heat Pipe Receiver. [5]

The third consideration in this study is that of PCM selection. Thermodynamic considerations would normally lead to a design in which all heating would occur at a temperature as high as practical below that imposed by the physical characteristics of the high temperature structure. This has led to the search for a material having a melting point near that imposed by the strength limitations of existing high temperature alloys and simultaneously possessing a high heat of fusion.

A preliminary list of candidate phase change materials indicates numerous possibilities. The choice is complicated by the fact that many of these materials do not have well defined thermo-physical properties [6]. The characteristics sought here are not generally duplicated in other applications so that there has not heretofore been an intensive effort to establish properties. Moreover the high temperature range of interest makes measurement particularly difficult. At such high temperatures materials are frequently quite corrosive making containment itself a problem. This analysis has been undertaken to determine the relative merits in utilization of either thermal conductivity

enhanced salts or of metallic PCMs. By including direct evaluations of the thermal performance of the respective receiver concepts incorporating such alternative materials is possible to ascertain the potential for improved performance from each. Ultimately such results may offer insight or lend weight to the decision to pursue development of the more promising technologies.

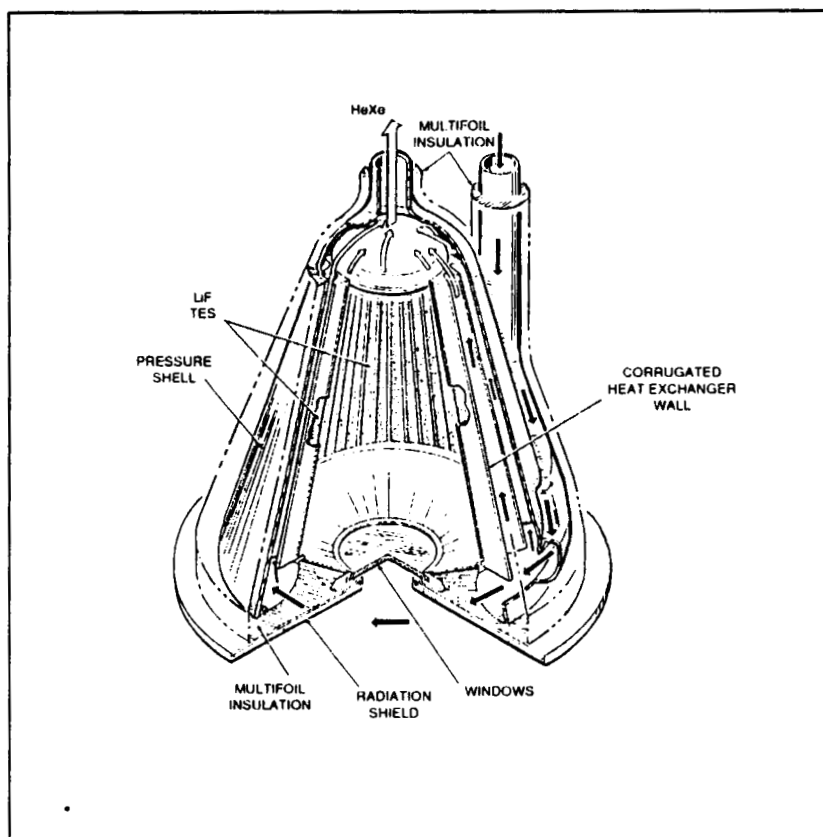


Figure 8. Brayton Cycle Cavity Receiver. [5]

2 Analysis Approach

2.1 Basic Cycles

Performance parameters for the cycle have been established from typical Brayton Cycle conditions. The selection of the Brayton cycle appears natural in that the receivers selected for comparison were, with the exception of the Cavity Heat Pipe and the Stirling Heat Pipe designs, originally designed for that cycle. It is not thought that this assumption will significantly detract from the generality of the results. There appears little reason to believe that operating conditions would change dramatically with either cycle so that results are thought to be generally applicable.

The basic cycle performance characteristics are shown in Table II. The base design for comparison is a Brayton cycle engine producing 7 kW_e from a continuous 25.9 kW_t input. This corresponds to an overall cycle efficiency of 27%. Variations in the turbine inlet temperature will affect both cycle efficiency and power output; these effects may probably be best handled by controlling the working fluid flow rate or bypassing a portion of the flow around the receiver. In any case these control mechanisms are not used for purposes of this analysis and both receiver inlet temperature and flow rate are maintained at a constant level. The coolant composition, inlet temperature and flow rate are taken as the nominal values used in the base design. This selection might be considered to favor the base case but in preliminary studies, designs have not shown a significant sensitivity to the selection. In any case it was desired to compare the respective designs under similar operating conditions so that utilization of base case parameters appeared more reasonable than selecting conditions proposed with one of the advanced designs.

TABLE II. BASIC CYCLE PERFORMANCE CHARACTERISTICS

Parameter	Specification
Engine Power	7 kW_e
Engine Thermal Input	25.9 kW_t
Receiver Losses	3.1 kW_t
Solar Incidence Period	54 min.
Eclipse Period	36 min.
Working Fluid	71% He 29% Xe
Coolant Flow Rate	0.25 kg/s
Coolant Inlet Temperature	800 K

2.2 Concentrators

The performance of any receiver in which the PCM is directly irradiated by the incident solar flux will be strongly a function of the incident flux distribution. In the study reported here all flux distribution have been determined from the CAV2 [7] computer program. The input parameters used in each of the cases are as given in Table III. The receiver diameter and depth were selected to accommodate the PCM elements in each case without additional clearance. The elements were located at a distance from the aperture so that the incident flux would begin to become significant at the first PCM cannister and was extended to exactly the element length. The inside diameter of the receiver was set at the outer diameter formed by the PCM elements.

TABLE III. BASIC CONCENTRATOR CHARACTERISTICS

Parameter	Specification
Dish diameter	3.59 m
Rim angle	45°
Slope error	1%
Aperture radius	0.091 m
Aperture offset	0 m
Dish misalignment	0 mr

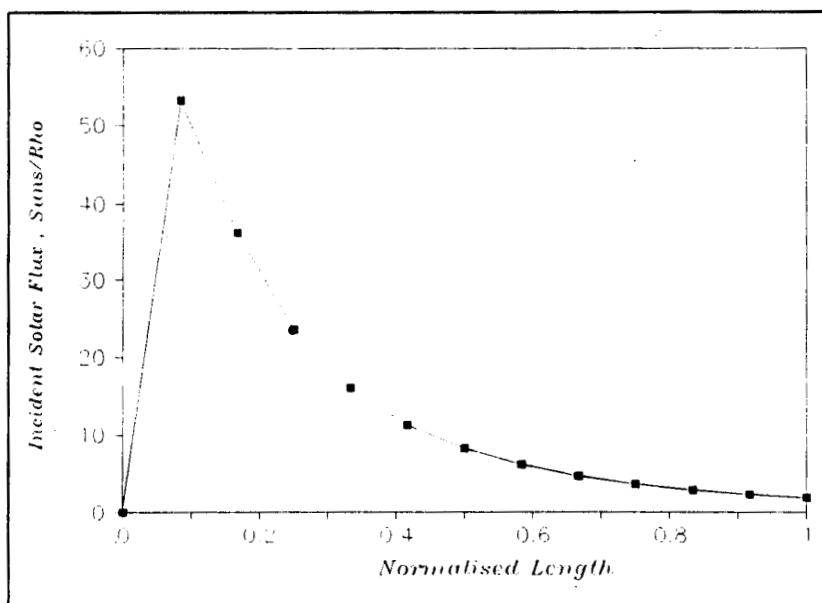


Figure 9. Base Case Incident Solar Flux Distribution.

ORIGINAL PAGE IS
OF POOR QUALITY

The resultant flux distribution calculated for the base case configuration is shown in Figure 9. The distribution is shown for receiver arrangements with L/D ratios varying from 1 to 2 as used in the parametric evaluation. Clearly the flux is quite high near the aperture end of the receiver leading to difficulties in obtaining uniform PCM utilization. The problem is somewhat more severe with the higher L/D ratios indicating a higher incident flux to compensate for the lower reflectance from the bottom of the receiver. Receivers utilizing a truncated cone configuration can provide a more uniform incident flux distribution and a more appropriate PCM allocation.

The shape of the incident flux curves, while relatively simple in form, are somewhat difficult to represent numerically without introducing certain round off error. In order to smooth the function it has been decided to integrate the area under the curve allowing representation of the cumulative heat input as a function of axial position. The integration has been performed using standard numerical techniques and resultant curve is shown in Figure 10. Also shown is a third order curve fit of the integral used in the receiver program. The technique allows for relatively accurate representation of the CAV2 results but also provides a somewhat clearer picture of the tendency for poor flux distribution. It may be noted that 48% of the incident energy enters the first 20% of the receiver length.

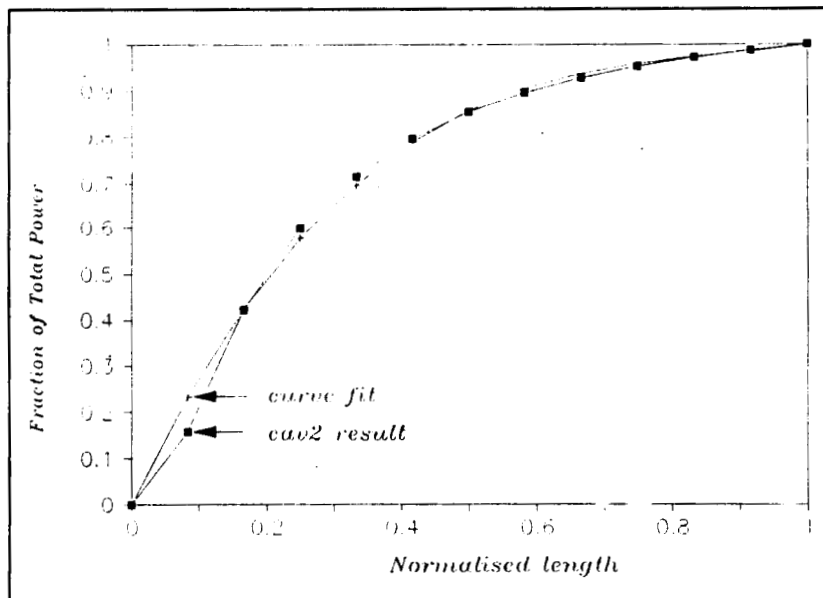


Figure 10. Receiver Energy Distribution.

2.3 PCM Enhancement

While fluoride salts have been considered as prime candidates for selection as the phase change material, they are characterized by a low thermal conductivity. In order to achieve a high level of thermal utilization and low temperature gradients designers have relied on a variety of thermal enhancement schemes. Proposed schemes have included high conductivity metal fins extending through the PCM, wire meshes within the PCM, metallic foams in which the PCM can be placed and a graphite matrix in which individual PCM pellets are to be arrayed. Manufacturing of certain of these concepts represents an unproven technology. Also unproven is the long term integrity of the concepts during normal orbital cycles. Nevertheless there remains the need to develop techniques of improving the thermal performance of such materials and it would seem prudent at this time to evaluate the impact of specific material enhancement schemes so as to perhaps limit development to only the most promising concepts.

The approach used here has been to develop a model based largely around a "random" metal mesh. It is probably easiest to envision such a mesh as being constructed from layers of wires lying in a plane. Stacked on the first layer will be a second layer of wires arranged so that the wires in adjacent lamina appear to form a square grid. The model is designed around a large number of such planes. If one of these laminas is viewed from the edge so as to be seen from the end of the wires, the wires and PCM may be considered to act to transfer heat in parallel. The thermal resistance associated with this plane is:

$$R_p = \frac{2}{(1 - \epsilon) \cdot k_{PCM} + \epsilon \cdot k_{ENH}}$$

Adjacent planes, when viewed from the same perspective, will appear as layers of PCM acting in series with the wire segments. The effective thermal resistance of these laminas are given as:

$$R_s = \frac{\ln\left(\frac{k_{PCM}}{k_{ENH}}\right) \cdot \frac{1}{k_{PCM} - k_{ENH}} + \frac{P - 2 \cdot r}{0.5 \cdot k_{PCM}}}{P}$$

The composite system will appear as a large number of such planes all acting in parallel with one another:

$$\frac{1}{R_1} = \frac{1}{R_p} + \frac{1}{R_s}$$

When this system is viewed from a direction normal to both layers of wires, each lamina will appear as a cylinder in parallel with PCM. The equivalent resistance of this arrangement is given as:

$$R_2 = \frac{2 \cdot P \cdot \ln\left(\frac{k_{PCM}}{k_{ENH}}\right) \cdot \frac{1}{k_{PCM} - k_{ENH}} \cdot \frac{0.5}{(P-2 \cdot r) \cdot k_{PCM}}}{\ln\left(\frac{k_{PCM}}{k_{ENH}}\right) \cdot \frac{1}{k_{PCM} - k_{ENH}} + \frac{0.5}{(P-2 \cdot r) \cdot k_{PCM}}}$$

It is assumed that these two orientations are randomly dispersed within the elements so that the overall effect is to produce an isotropic effective conductivity. It is further assumed that these resistances will combine in the same manner as structural properties in a composite material. From random orientations of fibers in a composite materials:

$$\frac{1}{R_{EFFECTIVE}} = \frac{3}{8} * \frac{1}{R_1} + \frac{5}{8} * \frac{1}{R_2}$$

This approach has been utilized to evaluate the effect of adding the various enhancement materials. The results are shown in Table IV. In the listing, the density is given as the density of PCM per unit volume. Since voids are assumed to remain distributed within the solid phase the same value is reported for liquid and solid. Likewise, the specific heat reported is based solely on the PCM so that the enhancement material does not add to sensible energy storage capacity. The thermal conductivity values include the effects of distributed voids within the solid and may be taken as the effective enhanced conductivity.

Table IV. Thermal Transport Properties of Enhanced PCM

Material	Density kJ/m ³	Specific Heat kJ/kg K (Sol/liq)	Thermal Conductivity kW/m K (Sol/liq)	Heat of Fusion kJ/kg	Energy Density gJ/m ³
LiF 22 CaF ₂	2097.0	1.84/1.97	.00413/.00173	753	1.597
10% BN	1887.3	1.84/1.97	.00492/.00254	753	1.421
18% BN	1719.4	1.84/1.97	.00554/.00320	753	1.295
10% Grap.	1887.3	1.84/1.97	.00643/.00387	753	1.421
18% Grap.	1719.4	1.84/1.97	.00825/.00559	753	1.295
Ge	5010.2	0.38/0.39	.0405/.0424	481	2.410

2.4 Receiver Concepts

2.4.1 Base Receiver Concept

The base case receiver design is essentially similar to that shown in Figure 3 for the space station. In this design

the PCM is contained in individual canisters. These canisters are constructed as a concentric annulus with each end closed. Several of these individual canisters are then stacked by placing them over a central coolant tube. The coolant tube with the canisters forms a single PCM element. Several elements are then placed inside the inner circumference of the receiver shell with equal azimuthal spacing. The coolant tubes are connected by separate manifolds at each end of the receiver to form the inlet and outlet gas passages. Dimensions on the base case receiver are shown in Table IV.

TABLE V. BASE CASE RECEIVER CHARACTERISTICS

Parameter	Specification
Tube Length, m	1.8
Number of Tubes	75
Sidewall/PCM Thickness	12.5%
Coolant Tube ID	0.00841 m
Canister ID	0.01095 m
Canister OD	0.015 m
Canister Wall Thickness	0.00071 m
Element P/D	1.66
PCM	LiF 22 CaF ₂
PCM Mass	96 kg

2.4.2 Heat Pipe Concept

The heat pipe receiver design is shown in Figure 5. The receiver is constructed in three axial sections. The first of these sections is located nearest the receiver aperture and includes no PCM canisters. Solar energy entering through the aperture strikes the central tubes directly. Inside the tube is a heat pipe working fluid. The evaporated fluid then transports the energy into the remaining two sections. In the central section the tube is surrounded by PCM canisters, with a configuration much like those in the base case design. A portion of the energy from the heat pipe fluid is conducted into the PCM and stored as latent energy during periods of solar incidence. The remaining energy from the heat pipe is transported to the last section of the receiver where a heat exchanger couples the heat pipe to the engine. During the solar eclipse the heat pipe drops in pressure and temperature and begins to remove energy from the PCM and transports it to the heat exchanger in the last section of the receiver. Dimensions on the base case receiver are shown in Table V.

TABLE VI. HEAT PIPE RECEIVER CHARACTERISTICS

Parameter	Specification
Tube Length, m	0.7116 m
Number of Tubes	20
Sidewall/PCM Thickness	12.5%
Coolant Tube ID	0.0482 m
Canister ID	0.0522 m
Canister OD	0.0820 m
Canister Wall Thickness	0.00127 m
PCM	LiF 22 CaF ₂
PCM Mass	91.5 kg

2.4.3 Pebble Bed Concept

The pebble bed receiver is shown in Figure 6. In this case the PCM is stored in individual capsules, each coated with a suitable high temperature material. The capsules are contained within the coolant passage. The outside surface of the coolant tubes is directly exposed to the solar flux. Energy is then conducted across the tube wall where a portion is convected directly to the cycle working fluid and the remainder is conducted to those solid particles adjacent to the wall. Energy is transported to the interior elements by a combination of conduction and convection through the working fluid. Dimensions for the pebble bed concept are shown in Table VI.

TABLE VI. PEBBLE BED RECEIVER CHARACTERISTICS

Parameter	Specification
Tube Length, m	0.91 m
Number of Tubes	15
Packing Fraction	70.0%
Coolant Tube ID	0.82 m
Canister Wall Thickness	0.00127 m
PCM	LiF 22 CaF ₂
PCM Mass	96 kg
PCM Sphere OD	0.014 m

2.4.4 Cavity Heat Pipe

The system under consideration will consist of a cavity heat pipe, shown in the Figure 7. This design is intended for use in conjunction with the Stirling engine, but it is believed that a similar design could be developed for the

Brayton engine with the inclusion of a suitable heat exchanger within the receiver. In this design the receiver is configured as a right cylinder. The solar incidence from a parabolic collector arrives at the receiver and passes through an aperture at the bottom. Inside the aperture the flux strikes the evaporator section of the cavity. The vapor then transfers heat to condensing surfaces on both the thermal storage material (TSM) and the engine high temperature heat exchanger.

The thermal storage material is contained in a number of canisters arranged around the periphery of the receiver. The side walls of these structures are tapered inward toward the apex, so that as the canisters are placed side by side they bend into a closed cylinder configuration. This cylinder is then banded together and placed inside the receiver. The apex of the canisters are covered with a condenser/evaporator material, generally a wire mesh. During the period of solar incidence, this area receives a continuous heat input, gradually melting the TSM. During the eclipse portion of the orbit, energy is removed from the TSM by evaporating the heat pipe fluid from this area.

The shape of individual canisters has been established as a method of thermal enhancement. In effect, if one were to consider the region between roofs, this region acts as a triangular shaped fin with the heat pipe fluid replacing the fin material. The arrangement provides for fins of extremely high effective conductivity and of relatively low equivalent mass. Increasing the number of fins will necessarily imply an increased number of canisters, so that careful trade-offs are necessary between thermal enhancement and system weight.

The high apex shape may also serve to alleviate the problem of void management, but this has not yet been confirmed. Certainly the narrowing walls are reminiscent of geometries proposed for fuel management within zero g environments. However Marangoni forces may well counter these effects during the heating phase and a careful analysis will be required to ascertain the final deposition.

From a thermal aspect, the problem is not so severe as in those designs which allow direct solar incidence onto the canisters. In those cases the heat flux at any point in the receiver was fixed by the collector and receiver geometries. If there were inadequate material to absorb the incident radiation, surface temperatures would rise and a thermally induced failure might occur. In the cavity heat pipe design it is not the flux on the canister surface which is fixed, but rather the temperature. The temperature throughout the cavity will be nearly uniform and adequate to drive the energy into

the TSM, neither more nor less. At any point where low thermal storage capacity might occur, the energy input would simply decrease locally and the corresponding energy would be stored elsewhere. Only in the case where the void covered a significant fraction of the overall heat transfer surface would a problem arise. In this analysis it is assumed that massive void coverage of the heated surface will be avoided.

TABLE VII. CAVITY HEAT PIPE CHARACTERISTICS

Parameter	Specification
Tube Length, m	0.91 m
Number of Tubes	15
Packing Fraction	70.0%
Coolant Tube ID	0.82 m
Canister Wall Thickness	0.00127 m
PCM	LiF 22 CaF ₂
PCM Mass	96 kg

2.4.5 Brayton Cycle Cavity Receiver

The Brayton cycle cavity receiver concept is shown in Figure 8. A major feature of this particular design are a number of innovative concepts to decrease receiver weight. Most notable is the method used for PCM containment. The overall configuration of the receiver is that of a truncated cone with corrugations running from the base toward the apex. The PCM is held into the troughs of the corrugations by capillary action while being contained within the receiver by a suitable window across the receiver aperture. A second smooth conical section is situated outside the first, with the interstitial space then serving as a passage for coolant. This particular arrangement is interesting in that it provides for a relatively light structure and includes a relatively limited number of fabrication steps.

Solar radiation which enters the receiver impinges directly on the PCM. Since the PCM is normally highly transparent to the incident radiation, suitable additives are to be included to ensure adequate absorption. While this approach is as yet unproven, it is interesting from a heat transfer viewpoint in that it allows the designer a degree of control over the absorbed energy distribution. An indirect consequence of this is that high element P/D ratios are not required to achieve effective distribution of the stored energy. The net result is an extremely compact receiver with associated weight savings in structure and insulation.

This concept is the only one of the designs considered which utilizes the truncated cone geometry to distribute PCM with higher fractions near the aperture and a decreasing fraction at the more distant locations. By situating the PCM where it can be most effectively utilized a somewhat decreased mass is required.

TABLE IX. BRAYTON CYCLE RECEIVER CHARACTERISTICS

Parameter	Specification
Corrugation Length	0.654 m
Number of Corrugations	100
Height of Corrugation	.064127 m
Corrugation Wall Thickness	.001 m
Base Radius of Truncated Cone	.386 m
Top Radius of Truncated Cone	.154 m
PCM	Lif 22 Caf
PCM Mass	96 Kg

2.5 Hybrid Elements

Within the parametric studies performed on each of the receiver concepts, four PCM concepts have been evaluated. These have included (a) a fluoride salt, (b) a fluoride salt enhanced with Boron Nitride, (c) a fluoride salt enhanced with ATJ graphite and (d) a metallic PCM. This grouping, while considering only a limited number of alternatives, is thought to bracket the range of thermal transport properties of most materials under consideration for Advanced Solar Dynamic applications at this time.

As a part of this study several additional materials were considered and, while not included in the parametric evaluation, were evaluated for thermal properties. In this case NaF was selected as the fluoride salt with Germanium being selected as the metallic alternative. Enhanced combinations each included NaF with the following enhancement schemes: (a) 12% of volume consisting of Niobium fins, (b) 12% Nickel fins, (c) 18% niobium wire mesh, (d) 18% nickel wire mesh and (e) 18% pyrolytic graphite mesh.

An alternative arrangement considered was to encapsulate Germanium into spheres and to fill the interstices in the packing with either a conductivity enhancement material, i.e. graphite, or with a nonencapsulated PCM, i.e. NaF. Using uniform sized spheres it is possible to achieve packings of spheres of about 60%. By using 2 significantly different sphere sizes packing densities of up to about 80% are achievable.

A final arrangement considered included packings of uniform sized spheres of encapsulated Germanium with pyrolytic graphite fibers traveling along the major axis of the packing to enhance thermal conductivity. The interstitial spaces were then filled with NaF to completely utilized the available volume.

The results of an analysis of each of these schemes to determine the effective thermal transport properties is shown in Table X. In each of these comparisons the most important thermal properties are the effective thermal conductivity and the energy density. The effective conductivity is of course that hypothetical thermal conductivity which would produce the same temperature difference in a large sample as would the nonhomogeneous material under consideration. It may be viewed as indicative of the temperature gradients which each sample would produce in an operating system. The energy density is the latent energy stored per unit volume by the nonhomogeneous element. It may be viewed as an indication of the required size of receiver which might incorporate that particular PCM.

What is not indicated within this comparison is the ease of development of each of the respective concepts. Whereas Germanium appears to be the choice candidate on the basis of energy density and thermal conductivity, problems of containment may suggest an alternative selection. However almost any other selection of Germanium in combination with other materials considered here tends to result in an improved energy density. The potential combination with NaF, if it could be fabricated, certainly indicates a potential for compact design. However this particular combination results in an unusually low thermal conductivity and it not thought to merit further consideration.

The enhancement of NaF with either of the two graphites, ATJ or pyrolytic graphite, will serve to significantly improve the effective thermal conductivity. The use of pyrolytic graphite offers a significant advantage over nickel additions. However any addition of a nonmelting material will necessarily decrease the energy density. The choice of a fluoride salt with any of the thermal enhancement additions is a low risk choice in terms of technological development while offering satisfactory thermal conductivity improvement. It will, of course, require a relatively large and heavy receiver.

Table X. Thermal Transport Properties of Advanced Enhancement PCM

Material	Density kJ/m ³	Specific Heat kJ/kg K (Sol/liq)	Thermal Conductivity kW/m K (Sol/liq)	Heat of Fusion kJ/kg	Energy Density gJ/m ³
NaF	1948.6	1.12/1.24	.003/.00013	798	1.537
Ge	5010.2	.381/.396	.0405/.0424	481	2.401
Fins:					
NaF/Nio.	2744.4	1.01/	.0087/.0069	493	1.360
NaF/Ni.	2744.4	1.01	.0105/.0081	493	1.360
Mesh:					
NaF/Nio.	3142.3	.964/1.06	.0044/.0035	401	1.261
NaF/Ni.	3142.3	.967/1.07	.0052/.0042	401	1.261
NaF/Pyro.				401	1.261
Matrix:					
.4NaF/.6Ge	3785.6	.680/.730	.0045/.0021	545	2.061
.2NaF/.8Ge	4397.9	.530/.560	.0053/.0026	508	2.235
.6Ge/Pyro.	3685.3	.90/.91	.0559/.0577	392	1.446
.8Ge/Pyro.	4347.7	.640/.652	.0340/.0365	443	1.926
.8Ge/ATJ	4347.7	.640/.652	.0188/.0203	443	1.926
Hybrid:					
NaF/Ge/Pyro	3864.9	.499/.516	.0204/.0179	455	1.757

By a process of elimination it would appear that the aggressive, high payback choice would be a combination of Germanium encapsulated or contained in graphite. If high density, i.e. 80%, packing can be achieved this approach combines both unusually high thermal conductivity and high energy density.

2.6 Model

In this study effort, a number of semi-two dimensional, transient, finite difference code were developed to evaluate each of the receiver systems. The codes were then used to perform several pertinent parametric studies. These studies were directed not only as establishing the performance of the proposed systems, but also toward optimizing such performance and establishing directions of future development.

While describing the model, reference will be made to the base line configuration. In certain of the other concepts this approach has been modified to represent the specific arrangements, but in general the overall methods remain uniform throughout. The approach has been to utilize a two dimensional, transient analysis with an implicit formulation. All conduction is assumed to occur in the axial (R-Theta or X-Y, depending on the coordinate system selected) plane. A series of such axial elements are stacked between the coolant inlet and outlet. For each axial element the solar input is determined based on the results of the CAV2 output. Heat input into the coolant is determined based on the calculated convective coefficient, coolant inlet temperature and the average wall temperature. Successive axial elements are connected thermally through the change in coolant temperature as it flows downstream. This approach utilizing the implicit calculational scheme provides for stable solutions for relatively long time steps and therefore is thought to be most applicable to computations involving medium to small computers.

The two dimensional finite difference program is designed to describe the system shown in Figure 11. Symmetry is assumed so that only one half of the element is modeled. Within the semi-annulus an arbitrary number of elements is used in the R and Theta directions. Generally this will require annular segmental elements where the dR segments are uniformly spaced and, in general, unequal to $d\theta$. Within the metal containment representing the first and last radial elements, a somewhat different radial length is used corresponding to the actual thickness of the containment wall.

All radiant heat transfer is assumed to occur through the outside circumference. In general this flux will be nonuniformly distributed azimuthally. In the model the total incident flux is constituted from a uniformly distributed portion representing the indirect radiation and a frontal portion representing a direct radiation component. Because of symmetry both the 0 and 180 degree walls are insulated. All convective losses are assumed to occur through the inside circumference. Convective coefficients are determined from conventional pipe flow correlations and assume a developing thermal boundary layer based on the distance from the inlet to the first element.

There are, within the literature, a number of methods of presenting the energy equation for solution of problems involving phase change. The method employed here is not taken directly from any of these but is a logical extension of the methods proposed by Pantankar [8] for the general solution of conduction problems. Emphasis is placed on writing relatively short, simple programs using methods that are broadly understood within the heat transfer community. While it might be argued that certain

of the advanced procedures provide for improved accuracy or stability, the advantages of presenting a scheme generally understood within the potential range of users or reviewers and ease of technical support are considered to be compelling.

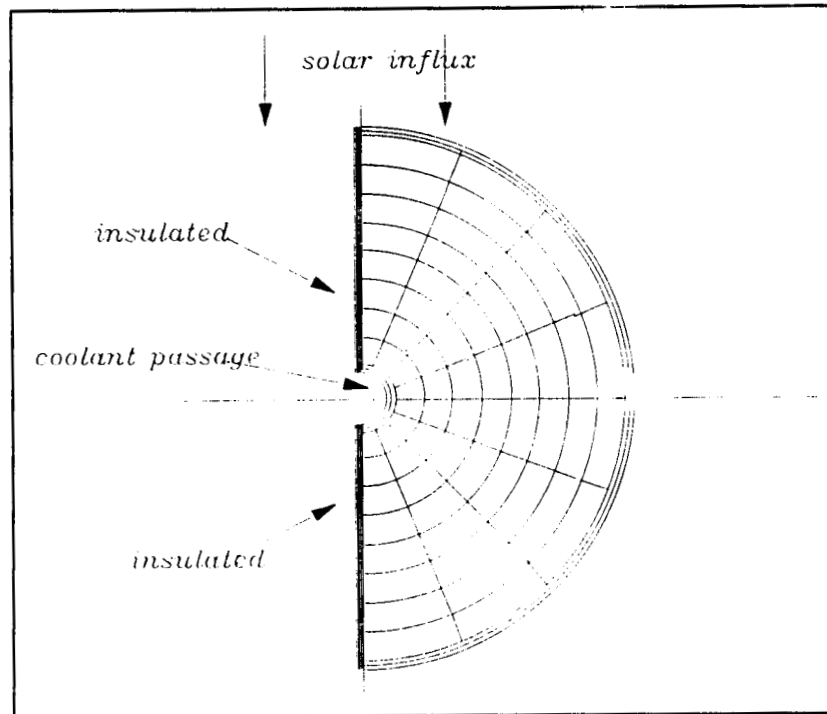


Figure 11. Finite Difference Element Arrangement.

2.6.1 Physical model.

The physical model is somewhat complicated by a number of factors including zero g effects, inadequate physical property data and the need for generality where various thermal enhancement devices might be considered. Particular caution must be employed in such choices in that the selection of differing models for alternative conditions may, in fact, overshadow all other parameters under consideration. This is particularly true in terms of the void model and while alternate enhancement schemes may actually justify differing models a uniform model has been incorporated here in an attempt at generality.

2.6.2 Void model.

Considerable uncertainty exists as to void location during the heating/cooling cycle. A characteristic of the fluoride salts currently being considered is that they tend to undergo significant density changes with phase change. Normally this will involve a density increase of between 10 and 25% as the material solidifies. Thus upon solidification voids will tend

to form so that the question remains as to how such voids react. If they fail to coalesce then such voids will likely remain dispersed within the solid phase. If they do coalesce then the question remains as to how such voids migrate and to what position.

At this time an experiment is planned for a space flight test in an attempt to gain actual data on void migration. Prior to acquiring such data any model will be, at best, only speculative. In those cases where a high conductivity foam is to be used for enhancement of the thermal conductivity, it might reasonably be anticipated that migration will be restricted and that voids will remain within the cells where they are formed. It is thought possible that viscous effects might produce similar distributions in the more general case.

In the absence of experimental data it is assumed that all voids form microspheres which are uniformly distributed within the solid. The remaining material will then exhibit no convective component to heat transfer and will retain a uniform effective density throughout. Note that the thermal conductivity will be affected. In this case the granular material model proposed by Meredith and Tobias [9] is utilized to predict the effective thermal conductivity of the overall system. For the case in which radiation is neglected, the voids may be assumed to have zero thermal conductivity and the equation reduces to the form:

$$\frac{k_{eff}}{k_{TSM}} = \frac{2 \cdot (1 - \epsilon) + 0.6135 \cdot \epsilon^{2.333} - 1.6 \cdot \epsilon^{3.333}}{2 + \epsilon + 0.6135 \cdot \epsilon^{2.333} - 0.6975 \cdot \epsilon^{3.333}}$$

where ϵ = the void fraction.

An alternate approach is used in the case of the cavity receiver. In this case if voids are assumed to coalesce they may be assumed to migrate to the liquid-cavity interface and to leave a 100% dense solid phase. This is in contrast to those enclosed PCM systems where the final location of void migration remains unanswered. To remain consistent with the analysis of the original contractor proposing this concept it was decided to assume such migration in this one case. This approach will tend to result in higher calculated thermal conductivities between the melt front and the gas coolant. The effect will clearly be most significant when the PCM is largely solidified. This occurs early in the heating cycle and late in the cooling cycle. It should be noted that the time early in the heating cycle does not correspond to a time of temperature extremes so that the consequences on engine

performance and thermal stresses are not thought to be significant. However, the period late in the cooling cycle is a time of temperature extremes. The minimum predicted turbine inlet temperatures may be somewhat nonconservative. Thermal stresses at this same point in time are not thought to be as severe as those occurring late in the heating cycle so that these results remain unaffected.

Computationally the void migration is accomplished by allowing a mass interchange between any element undergoing a phase change and the outermost element within the same radial segment. At each time step the movement of the melt front is calculated within the element undergoing phase change. The change in mass is then calculated. It is further assumed that the transferred mass leaves and enters the respective elements at the melting temperature as a method of ensuring that appropriate energy balances are maintained.

2.6.3 Energy equation.

The general transient energy equation for a stationary system may be written in terms of sensible and latent energy accumulation and conductive transport as:

$$\rho c_v \frac{dT}{d\tau} + \rho h_{fv} v = \bar{k} \cdot \nabla T$$

where v = melt front velocity.

In finite difference form this equation may be written as:

$$\left(\frac{\rho c}{\Delta \tau} + 2k \frac{\Delta x}{\Delta y} + 2k \frac{\Delta y}{\Delta x} \right) T^{r+1} = 2k \frac{\Delta x}{\Delta y} (T_e + T_w)^{r+1} + 2k \frac{\Delta y}{\Delta x} (T_n + T_s)^{r+1} + \frac{\rho c}{\Delta \tau} T^r + \rho h_{fv} v$$

The major feature in discretizing this formula is in the treatment of the latent accumulation term. The resultant equation is nonlinear so that a trial and error procedure is required. Since it is anticipated that the temperature of any element with a partial phase change should be near the melting temperature, the velocity may be adjusted in each iteration so as to cause the associated node temperature to vanish.

$$v = \frac{\mu c_v (T - T_{melt})}{h_{fg}}$$

where μ = a convergence factor.

In the cases reviewed here the convergence factor could be taken as between 0.25 and 2.0. The velocity term obtained in this manner is cumulative. That is, it is underevaluated in each iteration so that summing the value for subsequent iterations will eventually lead to a convergent value where the local temperature approaches the melting value. A second convergence criteria is also included based on an energy balance for the overall axial segment. In general the goal is to seek energy convergence to within .1%.

2.6.4 Computer Program.

Selection of an implicit scheme to solve the nodal equations is designed to enhance numerical stability and to permit the use of reasonably long time increments. This is viewed as a necessity for such programs when utilizing relatively small computational facilities. A major advantage to such an approach is that the resultant program is highly portable, being designed primarily for PC usage.

In order to simplify the programming and to reduce the number of parameters being stored a hybrid computational scheme is employed which included features of both Gaussian elimination and Gauss Seidel. Considering the figure of the finite difference scheme, the approach is to successively solve for the temperatures along each of the vertical columns, using a one dimensional (tridiagonal) method. While evaluating the temperatures along any one column, temperatures along any other column are assumed to be known based on the last iteration. Utilizing successive sweeps, this method provides for a rapid convergence while limiting memory requirements.

3 Parametric Study

In the parametric studies which follow, the effects of the basic geometric parameters influencing overall thermal performance of the canisters are examined. These include the number of canisters, element geometry or spacing and the use of alternative thermal enhancement materials. During the transient, temperatures are evaluated at two times, 54 and 90 minutes. These times correspond to the end of the solar incidence, where maximum temperatures are achieved, and to the end of the solar eclipse, where minimum temperatures are encountered. The implications of such temperatures, while largely qualitative, directly influence both receiver life and cycle efficiency.

One important aspect of the study is to underline the differences in thermal performance between metals and salts as PCM's. Because of the inherently low thermal conductivity of the salts, their parametric range has been extended with a view of establishing potential for improved performance with improved geometry. In the case of metals this same extension has appeared unnecessary.

3.1 Base Line Receiver.

The base line receiver utilizes convective transport directly to the working fluid rather than utilizing a heat pipe as the other designs considered here. The nature of the design constrains the parametric study to some extent so that certain combinations of enhancement and configuration perturbation are not possible. This is not a limitation of the design, but rather of the parameters selected. In order to take advantage of the full range of enhancement the system would require a different inlet temperature and/or flow rate. The values chosen for the study basically correspond to those initially proposed in the design. This decision has meant that considerations of enhancement are thus addressed on a more limited scale.

It should also be noted that any enhancement effect due to the canister side walls is neglected. If foam enhancement is added it is assumed that the foam will provide for the void management so that a large number of individual canisters is not required. Since exclusion of the canister walls is thought necessary for evaluation of enhancement effects it has also been omitted from the base case to fully indicate relative improvements.

The turbine inlet temperature for the base line case during normal orbit is shown in Figure 12. Thermodynamically the outlet temperature must average 1000 K (LiF 22 CaF₂ melts at 1039 K) and variations around this value are due to alternate melting and sensible heating or solidifying and sensible cooling of the PCM. The temperature is seen to increase during the solar

incidence reaching a value about 30 degrees above the average and cooling rapidly during eclipse to about 30 degrees below the average.

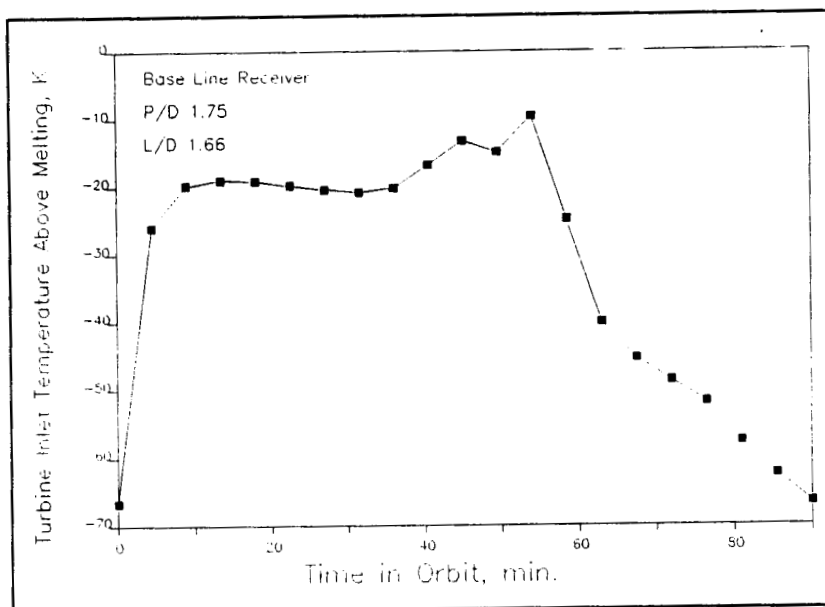


Figure 12. Base Line Orbital Turbine Inlet Temperature.

The effects of thermal enhancement are seen in Figure 13. Note that the plotted values do not extend to include the 18% enhancement value. A projection of the partial low temperature lines would indicate that this case would fall above the average gas temperature violating the first law. However it is seen that over the effective range the lower temperature is increased an average of 3.4° and 4.2° for each percent addition of BN and pyrolytic graphite, respectively and that the enhanced materials can be utilized effectively to control temperature swings. Full utilization of the enhancement would require either an increase in coolant flow rate or reoptimization of the inlet temperature.

Increasing the number of elements serves to reduce the radius of the individual canisters and subsequently reduces the thermal resistance within each. As indicated in Figure 14 the effect is fairly significant up to between 60 and 75 elements producing about a 3° improvement per element. In view of the weight advantage of reducing the number of elements it would appear that the optimal condition would occur at a number near 60 or 65 elements.

ORIGINAL PAGE IS
OF POOR QUALITY

ORIGINAL PAGE IS
OF POOR QUALITY

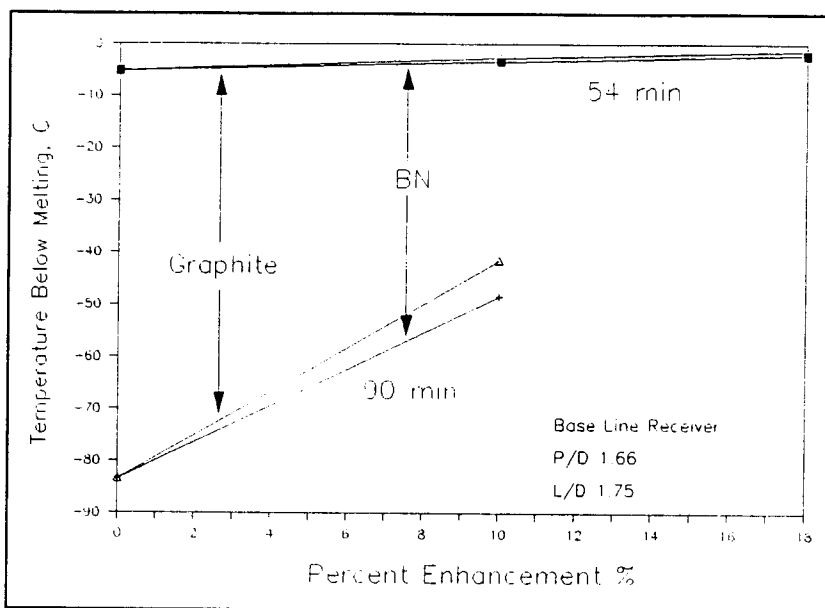


Figure 13. Effects of PCM Enhancement on Turbine Inlet Temperature.

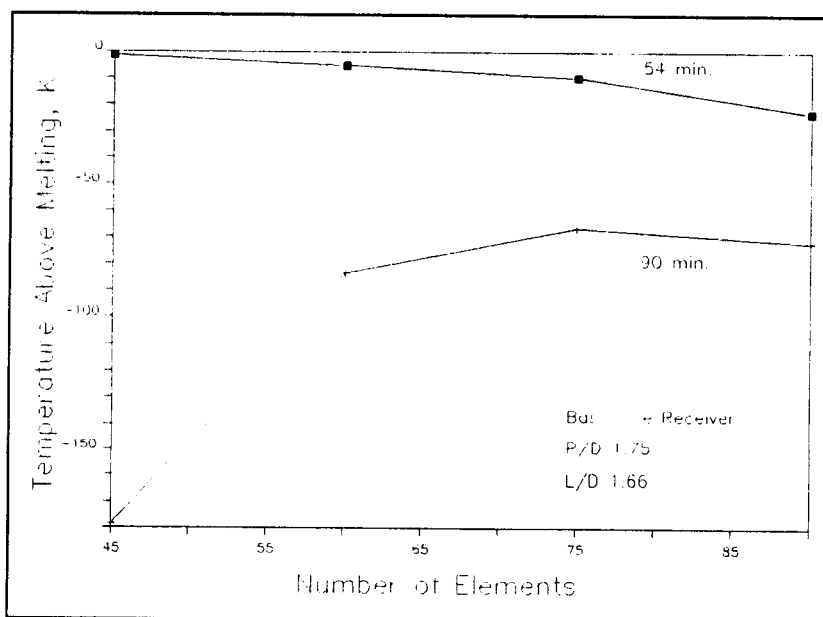


Figure 14. Effects of Element Number on Turbine Inlet Temperature.

The effects of increasing the receiver L/D ratio are shown in Figure 15. Again increasing the length of each element tends to reduce the radius of individual canisters again reducing the effective thermal resistance. The magnitude of improvement is only about 1.3° per percent change in L/D. While the effect shown is relatively small it may, in fact, be something of an overstatement. In the cases demonstrated here the receiver flux

distribution was assumed to remain constant with each of the configurations. In fact as the L/D increases the heat flux will tend to become somewhat more maldistributed. In this case the improvements seen at high L/D ratios will be somewhat reduced.

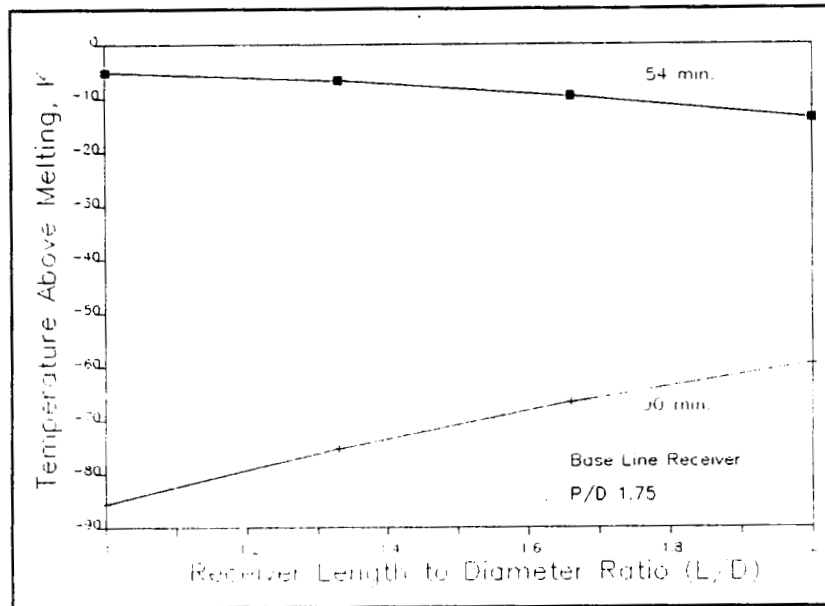


Figure 15. Effects of Receiver L/D on Turbine Inlet Temperature.

The effect of increasing the element circumferential pitch to diameter ratio would be to decrease the azimuthal variation in the incident heat flux. The improvement in the utilization of the PCM will then lead to an improvement in the uniformity of the inlet turbine gas temperature. This effect is seen in Figure 16. It is noted that the reduction in variation appears nearly linear over the P/D range of 1.25 to 2.0 with a corresponding improvement of 30°.

In Figures 17 through 19 the maximum and minimum canister temperatures are shown at 54 minutes in the first section of the element. These values are obtained from the same runs in which the turbine inlet temperatures were calculated. What will be generally noted is that the PCM temperatures show much the same trends but are much more sensitive to the geometrical parameters. Where poor PCM utilization is encountered there is a shift from storing energy in its latent form to storage as sensible heat. The inevitable results include large variations in turbine inlet temperature accompanied by high peak PCM temperatures.

The PCM temperature differential as a result of increasing the element number is shown in Figure 17. The design is subjected to considerable peaking of the incident heat flux and shows considerable sensible heating until the number of elements nears

90. The temperature difference across the canister is also decreased with increasing number of elements. The improvement is somewhat compressed by the scale of the figure. In this case the temperature differential decreases from about 60° to 25° as the number of elements is increased from 45 to 90. Note that improvement in canister temperature differences is over 50%.

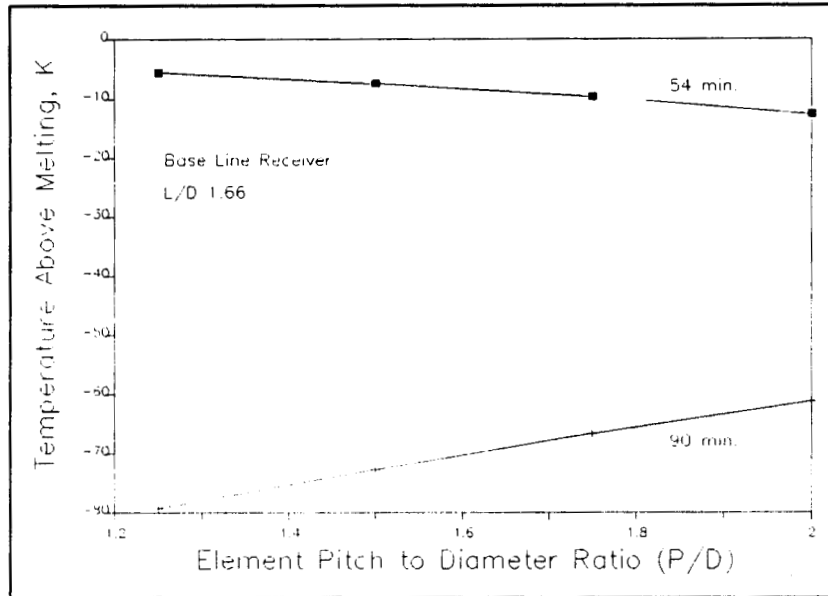


Figure 16. Effects of Element P/D on Turbine Inlet Temperature.

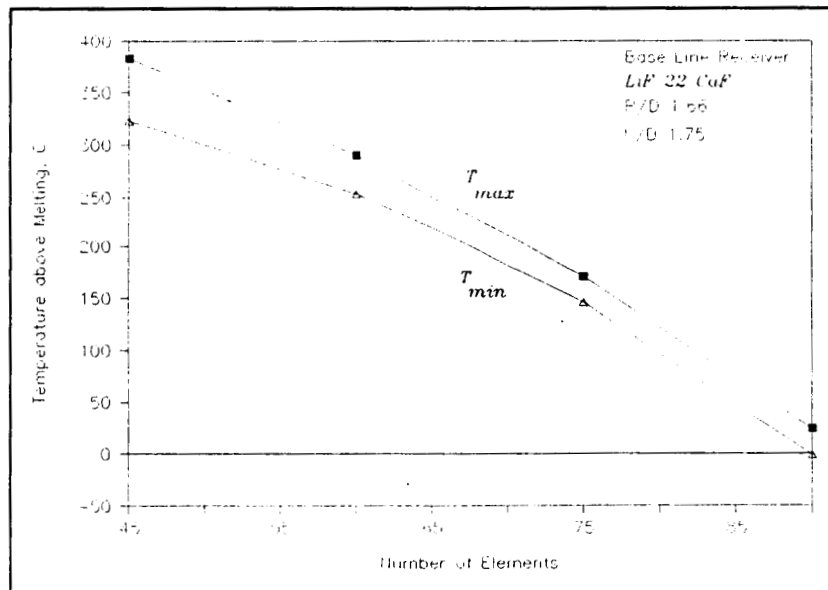


Figure 17. Effects of Element Number on Canister Temperature Difference.

The variation in PCM temperature with receiver length to diameter ratio is seen in Figure 18. The improved utilization of PCM serves to decrease the peak temperature from about 305° to about 110° above melting as the L/D increases from 1 to 2. The canister temperature difference is seen to decrease from about 40° to nearly 20° over the same range.

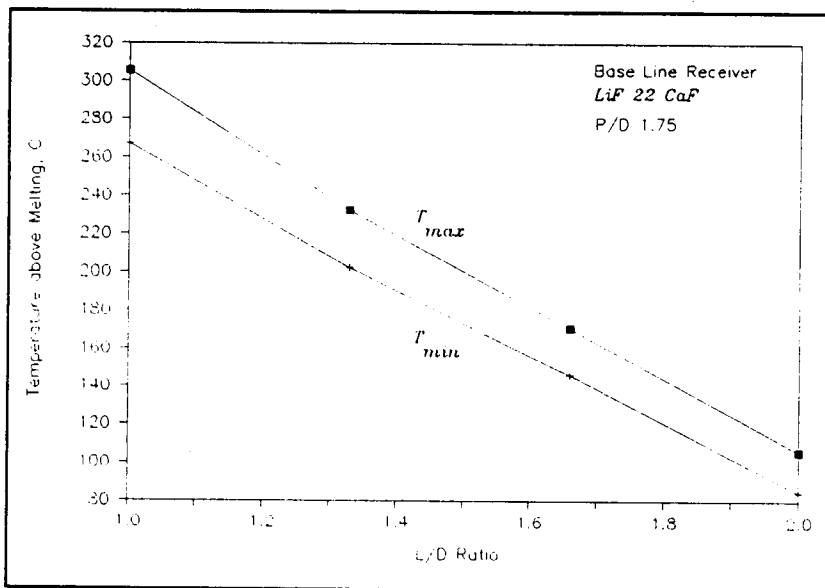


Figure 18. Effects of Receiver L/D on Canister Temperature Difference.

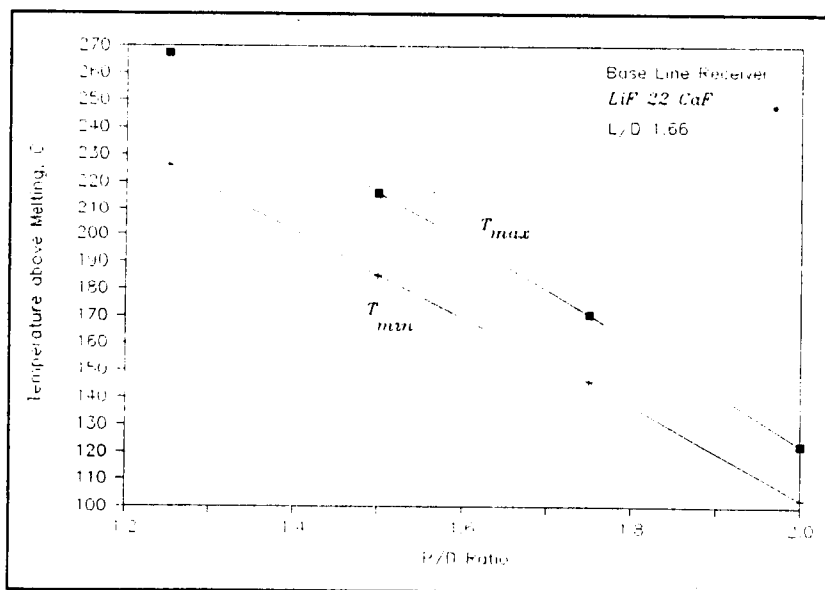


Figure 19. Effects of Element P/D on Canister Temperature Difference.

The effect of element pitch to diameter ratio on PCM temperatures is shown for the base line receiver in Figure 19. Peak temperatures decrease from about 270° to about 125° above melting as the P/D increases from 1.25 to 2. Canister temperature differences decrease from about 40° to about 20° over the same range.

3.2 Heat Pipe Receiver.

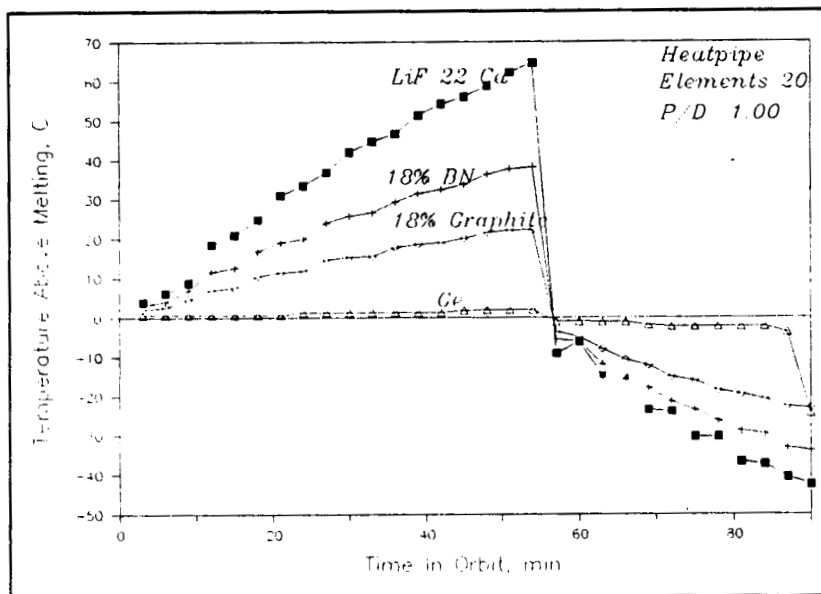


Figure 20. Effects of PCM Selection on Heat Pipe Vapor Temperature.

In Figure 20 the heat pipe vapor temperature is indicated through the steady orbit. It can be seen that temperatures change markedly between eclipse and solar incidence. The heat pipe fluid must operate at above melting to store energy during the incidence period and below melting to remove energy during eclipse. As either period progresses the melt front advances through the PCM so that a continually increasing temperature difference is required to sustain the heat transfer rate. One can also see the effects of thermal enhancement of the PCM. Additions of 18% by volume of BN or ATJ graphite substantially reduce the indicated temperature variations with overall variations decreasing from about 110° to about 75° and 60° respectively. The use of a metal PCM is seen to virtually eliminate all such variations providing only about a 25° change. Note that virtually all of the variation in the last case occurs in the very last time step. This is an indication of excessive solidification and use of only sensible energy. With some adjustment of the operating conditions this drop can be eliminated reducing the overall variation to only about 5°.

The maximum and minimum heat pipe vapor temperatures corresponding to the end of solar incidence (54 min.) and the end of solar eclipse (90 min.) as a function of the percent of thermal enhancement are shown in Figure 21. Also shown are the corresponding swings encountered with the metal PCM (Germanium). Enhancement materials serve to improve the radial conduction but the effect is partially countered by displacing PCM. This produces an improved conductivity but requires that heat be conducted over a larger distance. While the effect is significant in either of the enhancement materials, both are substantially less effective than the use of metals. From the heat pipe vapor temperatures produced it would appear the between 8 and 15% of either enhancement material is required to produce a significant improvement.

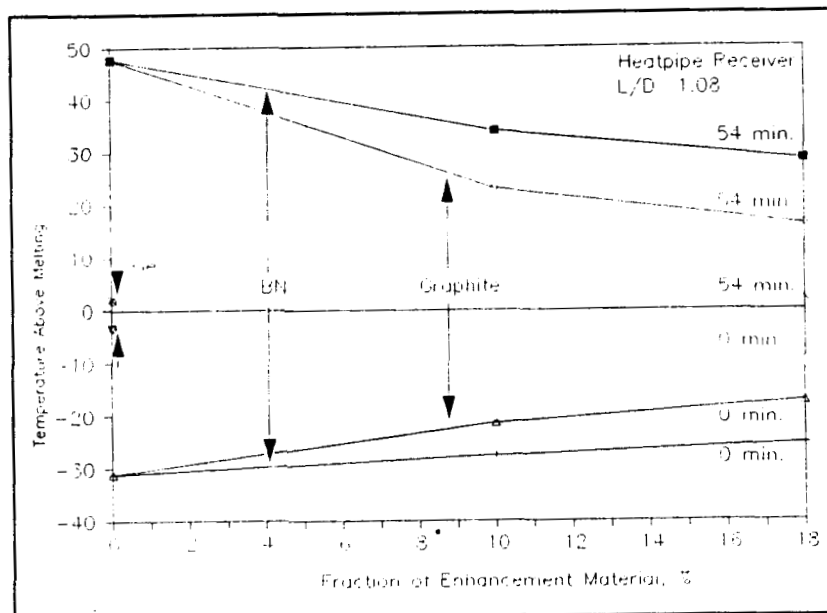


Figure 21. Effect of Enhancement Fraction on Heat Pipe Vapor Temperature.

An increased number of elements has the effect, as seen in Figure 22, of decreasing the radial thickness of PCM in each canister. The result should be a decrease in heat pipe vapor temperature variation as the thermal resistance between the heat pipe fluid and the melt front is decreased. With $\text{LiF } 22 \text{ CaF}_2$ the variation in heat pipe vapor temperatures is seen to be substantially reduced as the number of elements is increased to between about 20 and 25. Beyond this point the impact of further additions appears limited. The effect can be achieved with far fewer elements with some degree of thermal enhancement. The metal PCM is shown only for the case of 15 elements. It would be expected that the effect of increasing the canister number for the Ge PCM would result in a similar curve for the salts.

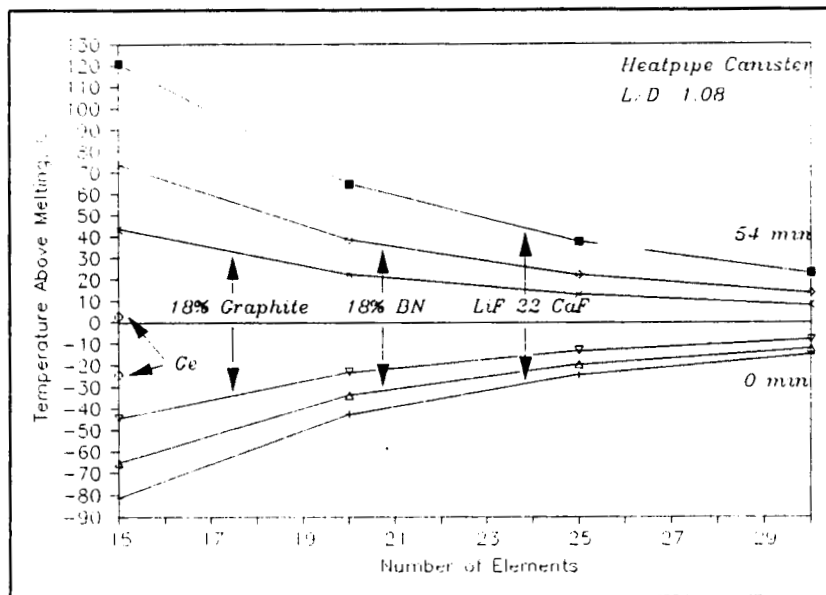


Figure 22. Effect of Element Number on Heat Pipe Vapor Temperatures.

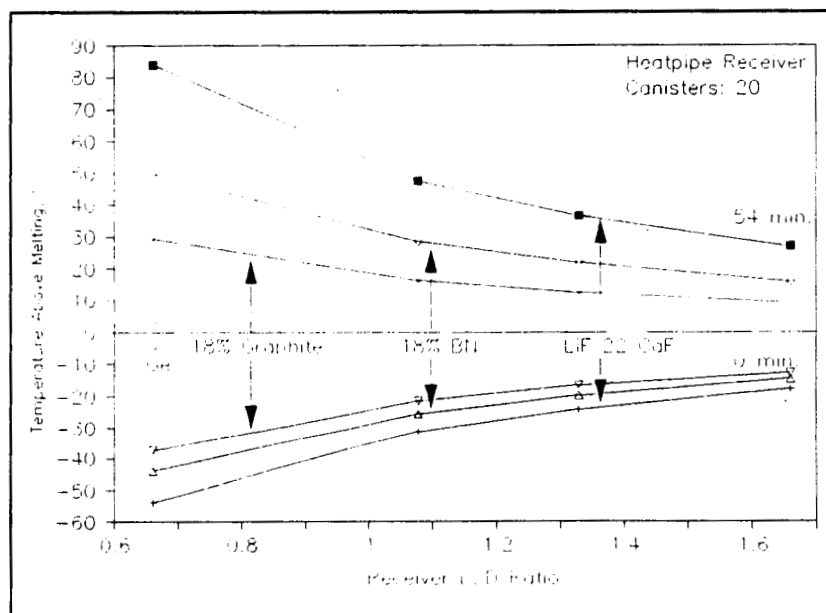


Figure 23. Effect of Receiver L/D Ratio on Heat Pipe Vapor Temperatures.

As the receiver is made longer the radial dimension of the individual canisters is decreased. Thermally this results in a decrease in both the heat flux and the radial resistance through which energy must flow. As seen in Figure 23 the effect appears to be relatively large for ratios up to 1. For longer receivers

there appears to be only a small improvement in the variation. Again the effect of the solar flux profile would be to moderate the improvement at the longer L/D ratios.

Both the absolute PCM temperature and the temperature difference across the canister are seen to decrease as the number of elements is increased. Results shown in Figure 24 indicate that the LiF 22 CaF₂, having a relatively low thermal conductivity, will require considerable sensible energy storage to ensure adequate potential to transfer heat to the heat pipe vapor during the eclipse phase. The increase in the number of canisters from 15 to 30 serves to drop the peak temperature from about 120 above melting to about 30°. This is seen to occur in an exponentially decaying fashion. The minimum temperature is not shown here but will, by design, be quite close to melting. Thus the peak temperature above melting is essentially the same as the temperature difference.

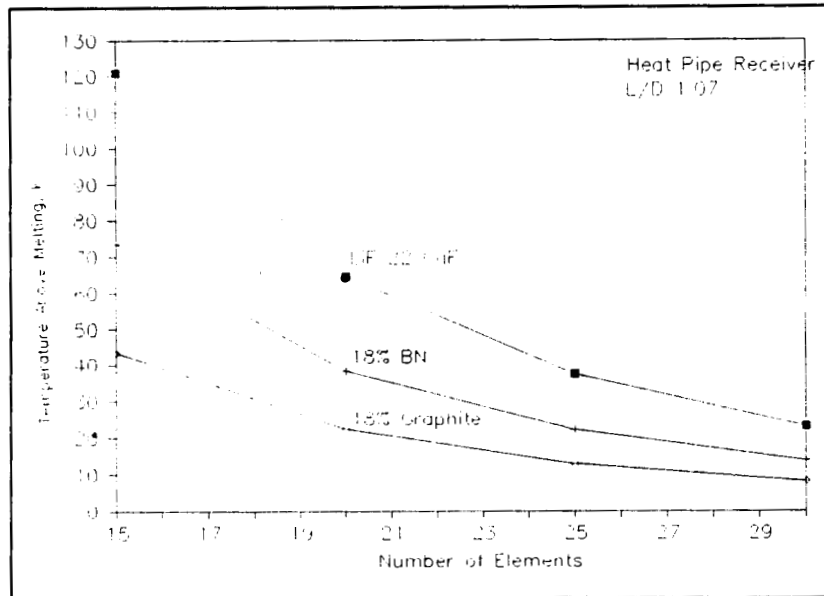


Figure 24. Effects of Element Number on Canister Temperature Difference.

As seen in Figure 25 the effect of increasing the receiver length to diameter ratio is also to decrease both PCM temperature and temperature difference. In this case the temperature difference for LiF 22 CaF₂ is decreased from about 100 to about 40 degrees as the L/D ranges from 0.66 to 1.66.

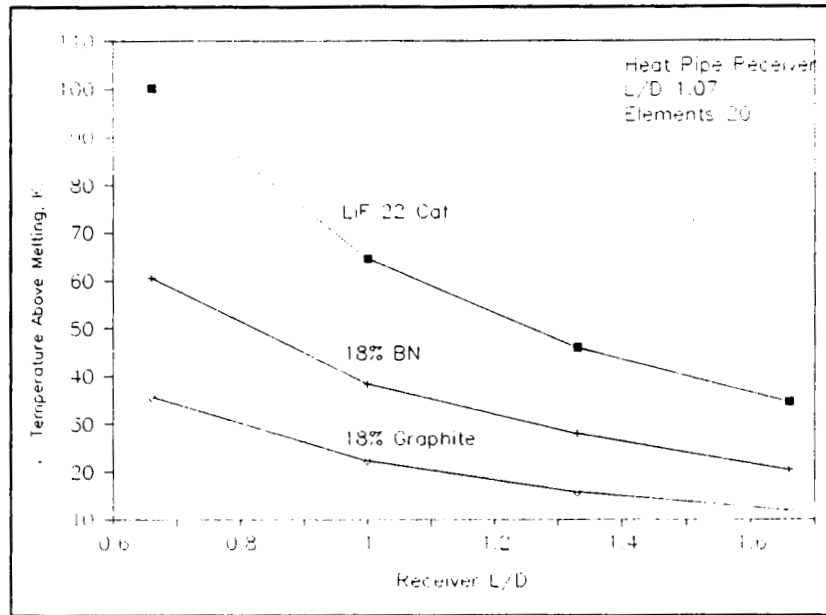


Figure 25. Effects of Receiver L/D on Canister Temperature Difference.

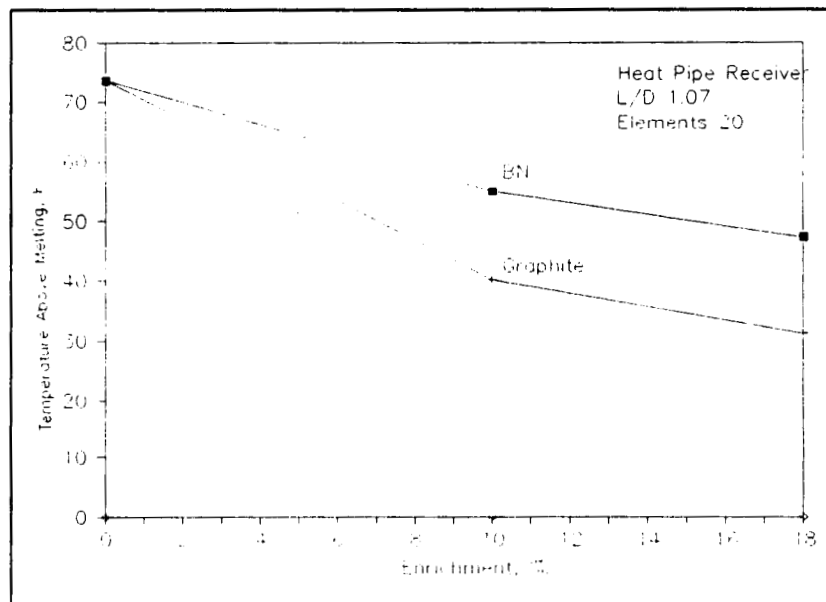


Figure 26. Effects of PCM Enrichment on Canister Temperature Difference.

The PCM maximum and minimum temperatures are plotted against the element enrichment in Figure 26. As noted earlier, the effect of enrichment is to improve thermal conductivity but this occurs at the cost of increasing the length of the path through which heat conduction must occur. The utilization of 18% Boron Nitride or Graphite is to decrease the peak Element temperature from about 75 degrees above melting to around 50 and 30 respectively.

In this case the minimum temperature remains, by design, essentially at the melt temperature. The element temperature differences will, therefore, have the same value.

3.3 Pebble Bed Receiver.

The modeling of the pebble bed assumed that the pebble stacking would provide for efficient gas mixing so that the working fluid provides for a degree of PCM enhancement. This effect reduces the radial thermal resistance in the elements so that the impact of the maldistribution of input heat flux associated with low element circumferential pitch to diameter ratios is significantly reduced. As seen in Figure 27 the effect of varying the P/D between 1.4 and 2 is negligible on the minimum turbine inlet temperature, typically about 990 K throughout the range. The maximum turbine inlet temperature, corresponding to the end of solar incidence is seen to vary only between about 1050 down to 1070 K over this same range. The effect of graphite enhancement is seen to be small but typically reduces the maximum temperature by 20 to 30 degrees over this same range.

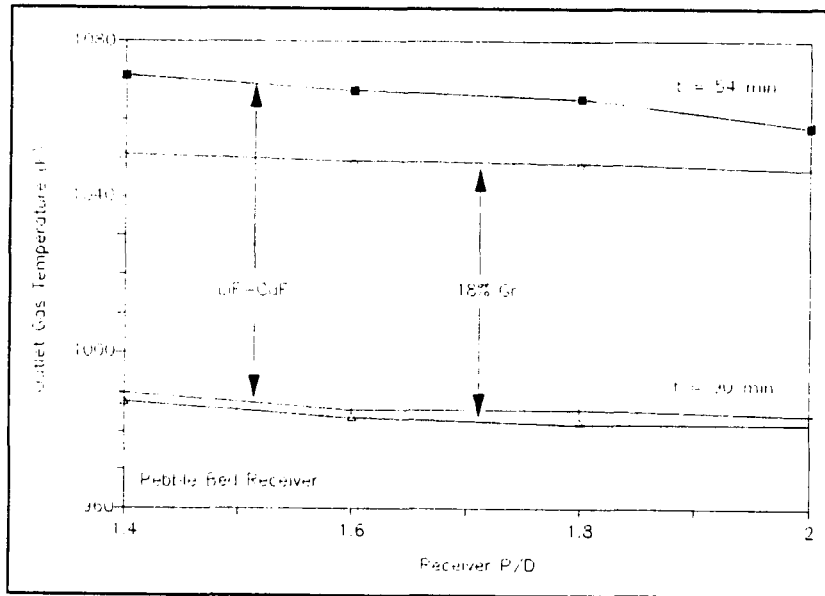


Figure 27. Effects of Element P/D on Turbine Inlet Temperature.

As seen in Figure 28, the effect of varying the receiver length to diameter ratio is also small. Varying its value from 0.7 to 1.5 appears to decrease the turbine inlet temperature by about 15 degrees. This same variation occurs at both the peak and the minimum temperatures.

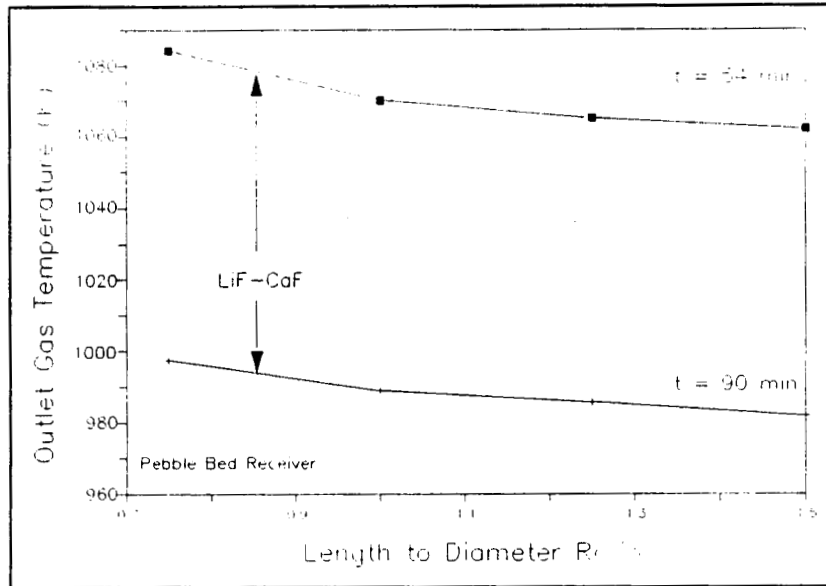


Figure 28. Effects of Receiver L/D on Turbine Inlet Temperature.

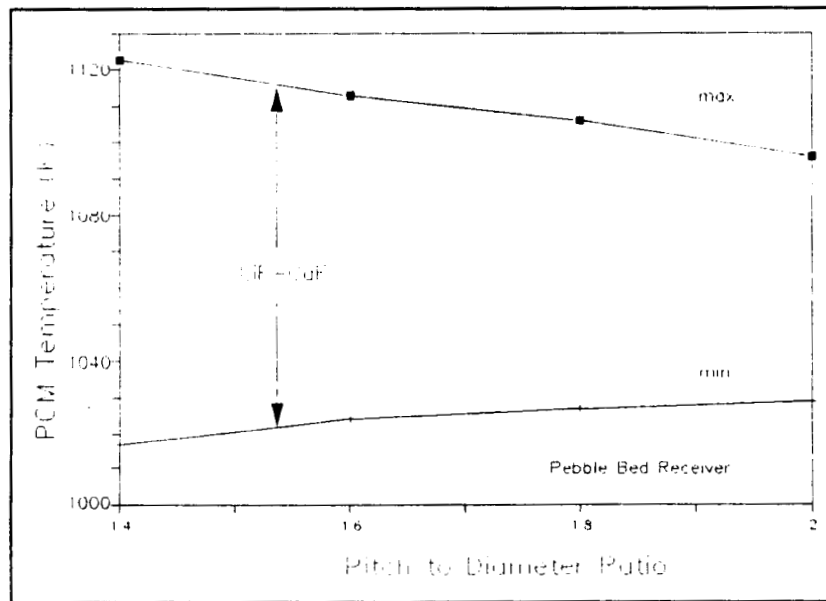


Figure 29. Effects of Element P/D on Canister Temperature Difference.

The effect of element pitch to diameter ratio on the PCM temperature is shown in Figure 29. The effect is somewhat greater than that seen on the turbine inlet temperature. Here the P/D is varied from 1.4 to 2 the maximum PCM temperature at 54 minutes is seen to decrease from about 1122 to 1095 K. At the same time the minimum PCM temperature increases from about 1017 to 1028 K. The overall variation across the element is then seen to decrease

by about 25%. Both effects would be thought to be beneficial toward reducing high temperature, stress related structural problems.

The PCM maximum temperature and temperature difference at 54 minutes is also seen to be a weak function of the receiver length to diameter ratio as seen in Figure 30. As L/D varies from 0.75 to 1.6 the peak PCM temperature is decreased from 1110 to 1100 K. The temperature difference over this same range decreases from about 95 to 70 degrees.

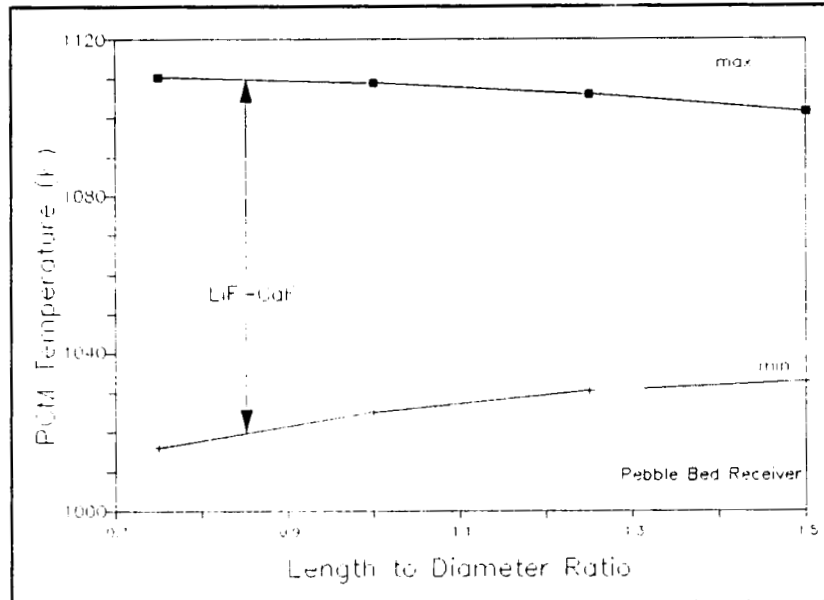


Figure 30. Effects of Receiver L/D on Canister Temperature Difference.

3.4 Cavity Heat Pipe Receiver.

As noted earlier each canister has associated with it a heat pipe wedge which serves effectively as a fin for thermal enhancement. Clearly the effect of additional fins will be to reduce temperature differentials within the element. Because the distances through which the energy is being driven is reduced with increased canisters, the temperature difference between the heat pipe fluid and the PCM melt temperature is reduced. The net effect is that cavity temperature variations between the end of the periods of solar incidence and solar eclipse are reduced. The requirement for small high temperature source variations is thought to be more severe for the Stirling engine than for the Brayton; it is noted that a Stirling receiver would therefore normally incorporate a higher number of elements than a corresponding Brayton receiver.

The results of the parametric study indicating the effect of number of canisters is shown in the Figure 31. Results indicate that temperature reductions average about 3.5 K per canister for the LiF 22 CaF₂ without enhancement and the BN enhanced PCM. The pyrolytic graphite demonstrates a somewhat reduced effect with only about a 2.5 K reduction per canister. For the 100% PCM case this would imply that doubling the number of canisters from 18 to 36 would decrease the cavity temperature variation from about 175 to about 115 K. While this trend is somewhat reduced with the enhanced materials, 18% pyrolytic graphite will still undergo an improvement of from about 125 to about 65 K. The Ge, having an extremely high thermal diffusivity, shows a quite low temperature variation. In spite of the low value overall trends appear the same as for the remaining materials. Clearly the number of canisters is seen to be a primary factor in determining the magnitude of cavity temperature variation.

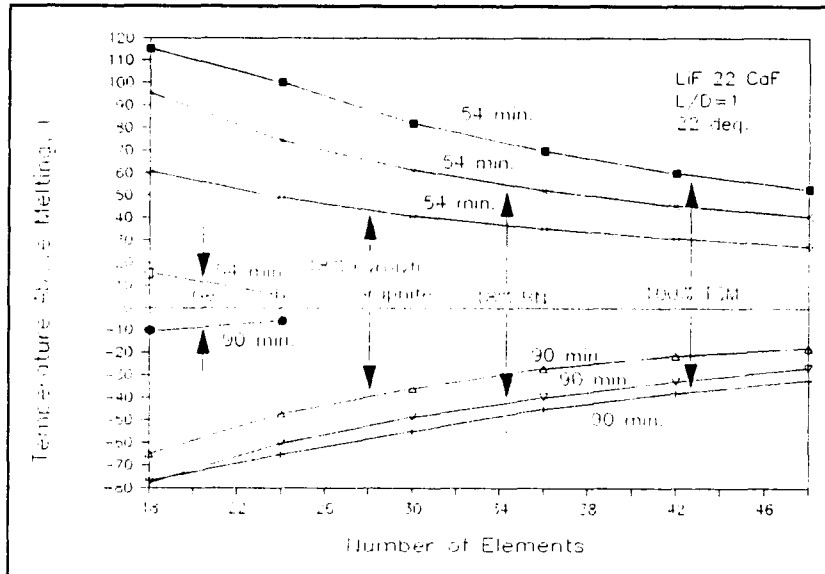


Figure 31. Effects of Element Number on Canister Temperature Difference.

A small apex angle will also tend to reduce temperature variations by reducing the maximum distance that heat must be transported into the solid. So long as a portion of the PCM remains partially melted the entire system is then coupled to the melting temperature. Short thermal distances are then seen to be close coupled whereas longer distances permit greater thermal swings. It is further noted that the small apex angles which tend to enhance heat transfer, involve configurations with large surface to volume ratios so that system weight will tend to suffer. Clearly additional trade-offs are required to optimize the system in this regard.

The effect of apex angle on cavity temperature oscillations is shown in the Figure 32. The relationship appears to be nearly linear over the range shown, about 3 K per degree. Earlier results, not shown here, indicate that the enhancement effects begin to decrease above angles of about 22 degrees so that cavity temperature swings approach an asymptotic value. In effect decreasing the apex angle from the asymptotic limit to about 15 degrees will only decrease temperature variations from about 125 to a little over 100 K. A further reduction to a very sharp angle of 10 degrees will only drop the variation to 90 K. It is concluded that apex angle provides only modest improvement in cavity temperature variation and generally will be of secondary importance.

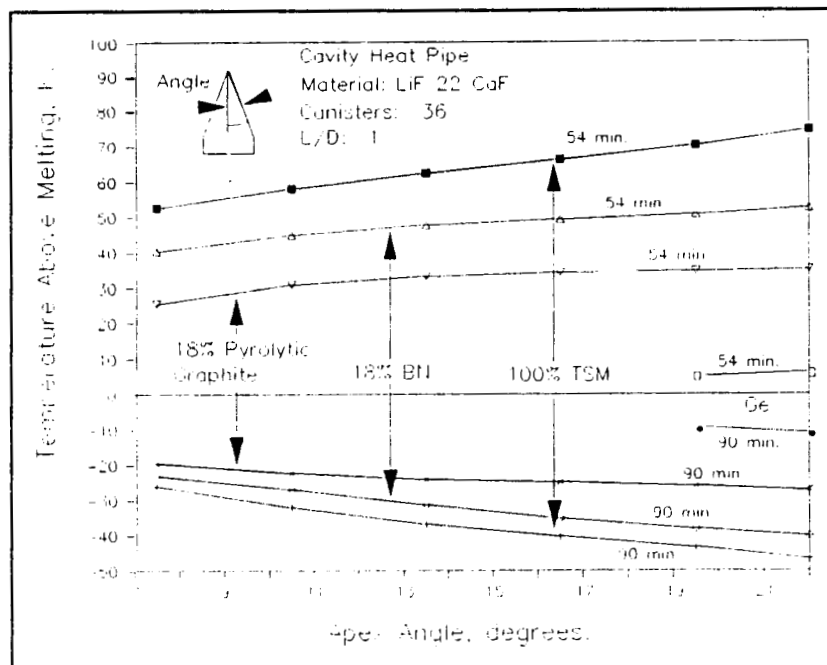


Figure 32. Effects of Element Apex Angle on Cavity Temperature Difference.

Increasing element length will have the effect of decreasing the other element dimensions, specifically the depth and width. Since the latter two dimensions are the most significant in terms of the heat transfer problem, the net effect will be to decrease cavity temperature variations.

As seen in Figure 33 for the unenhanced PCM, increasing the receiver length to diameter ratio from 0.5 to 2.0 produces a corresponding decrease in cavity temperature variations from about 160 to 80 K. For the two foam enhanced schemes the effect is similar; temperature variations are about halved. As would be expected the temperature variations for the metals, having very high thermal diffusivities, are quite small. As with the

salts, the overall trend is toward decreased variations with increased L/D. In all cases the cavity temperature variation is seen to be highly dependent on receiver L/D.

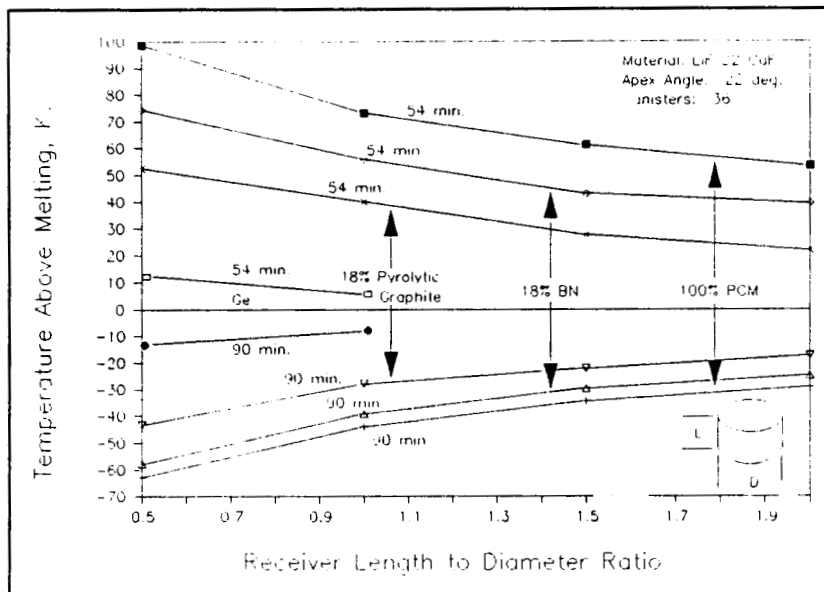


Figure 33. Effects of Receiver L/D on Cavity Temperature Difference.

The effects of thermal enhancement are shown in Figure 34. The effect of enhancement tends to be nonlinear and small additions tend to produce limited results. This tendency is particularly seen for the BN case where additions of less than 10% show no significant overall improvement in thermal performance. A 20% addition has the overall effect of reducing cavity temperature swings from about 115 to about 70 K. The pyrolytic graphite would appear to offer more substantial thermal improvement; cavity temperatures are reduced to 90 and 50 K for foam additions of 10 and 20%, respectively. Thermal enhancement is thereby seen to provide an effective means of further temperature control.

ORIGINAL PAGE IS
OF POOR QUALITY

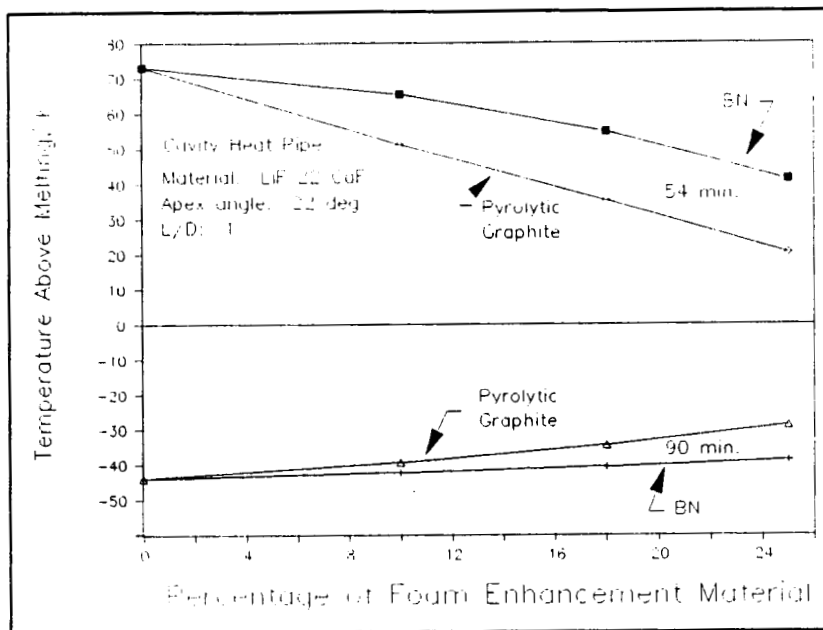


Figure 34. Effects of PCM Enhancement on Cavity Temperature Difference.

3.5 Cavity Receiver.

The variation in the turbine inlet temperature associated with the cavity receiver is shown in Figure 35. The range is seen to be relatively low with a minimum of 975 and a maximum of 1015. This is the least variability of any of the designs considered. The effect is thought to be closely related to the large number of corrugations considered. Each of the other designs showed a tendency toward decreasing variations with large number of elements. One advantage of this concept is that it seems to make the utilization of large numbers of PCM subdivisions without the weight and mechanical complexity of certain of the other designs.

The effect of the large number of corrugations is to overshadow the effects of other parameters on the turbine inlet temperature. Results showed little discernable variation in these temperatures with L/D, P/D enhancement, etc. Again, if the unit were designed with a number of corrugations more consistent with the number of elements in other receiver designs it is thought that this receiver would follow the established patterns. Because of the lack of variability in the parameters described the associated drawings have been omitted.

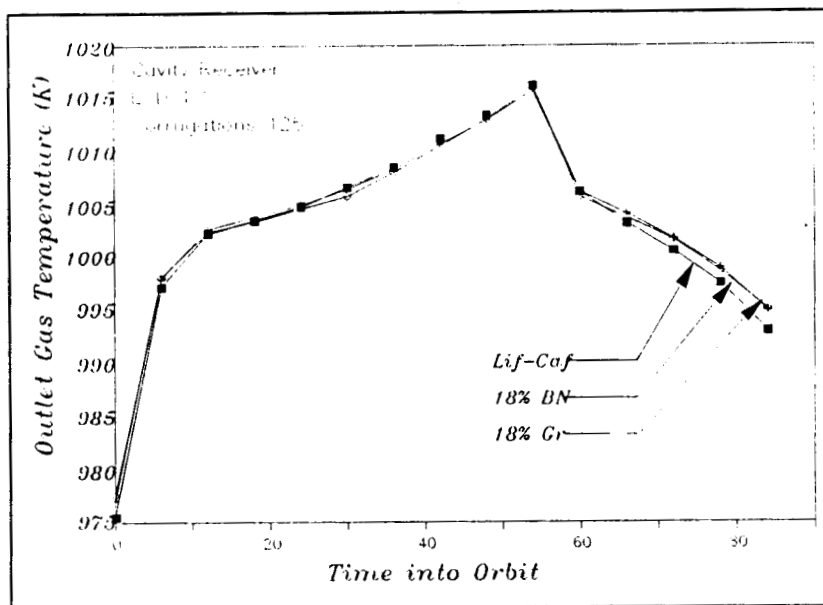


Figure 35. Turbine Inlet Temperatures Through Orbit.

The effects of PCM enhancement on the PCM maximum and minimum temperatures are seen in Figure 36. Effects are seen to follow a pattern similar to that of other receivers. Clearly there is a tendency to reduce peak temperatures as enhancement is added; minimum temperatures appear to remain virtually unchanged. However the effect is seen to be relatively small. The receiver is thought to be designed with sufficient corrugations that the dimensions on individual PCM "elements" are small. The peak temperature is seen to decrease by about 20 degrees with 18% BN, about 35 degrees with a similar amount of graphite addition. Improvements in the temperature differentials are also relatively small, on the order of 20 to 30%. It should be recognized that with the transparency of the PCM much of the thermal energy bypasses the PCM reducing the required differential to produce melting in the PCM.

A unique feature of this design is the ability to vary the energy distribution in the PCM by varying the absorptivity. This is done by controlling the quantity of absorbing material added. It would be anticipated that an optimal value of absorptivity could be found. A large value would tend to cause excessive heating at the PCM surface and result in increased temperature differentials. A low value would produce excessive absorption at the metal corrugation-PCM interface. Under an extreme condition virtually all energy would be added to the gas during periods of solar incidence with little storage occurring. Under these conditions no temperature difference would occur across the PCM. While the results shown in Figure 37 suggest that in the range indicated, the lower the absorptivity the better, this result is

misleading. Preliminary results suggest that a value of between 0.8 and 0.95 would provide a suitable balance between these two considerations.

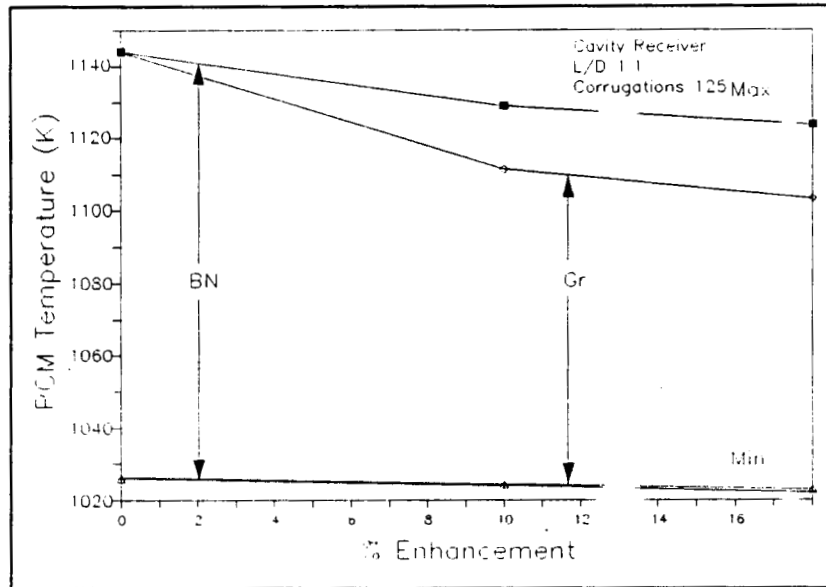


Figure 36. Effects of Element P/D on Canister Temperature Difference.

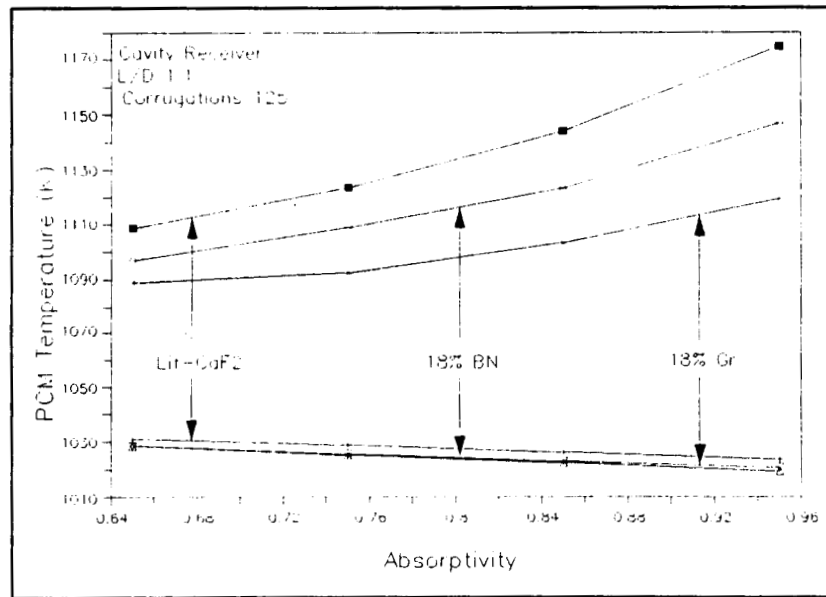


Figure 37. Effects of PCM Absorptivity on Canister Temperature Difference.

The effect of increasing the element length to diameter ratio on the PCM temperature and temperature difference are shown in Figure 38. The result may initially appear counter to those developed for other concepts in that temperatures and temperature

differences increase with increasing L/D. This is an artifact of the method used in varying the L/D in the parameter study. The decision was made to hold the minimum receiver diameter constant while allowing the larger diameter to vary with length (The corrugation angles were held fixed). The net result was to increase the PCM radial dimensions as length was added.

It may be observed that the minimum PCM temperature is held slightly below the melting point at all times so that this parameter shows little variability. The maximum temperature increases relatively rapidly as the radial PCM dimension increases. (Note that the added fraction of absorbing material must be continually adjusted to maintain a constant absorptivity.) Under these conditions the temperature differential is seen to nearly double, from 80 to 145 degrees as the L/D is increased from 0.66 to 1.33.

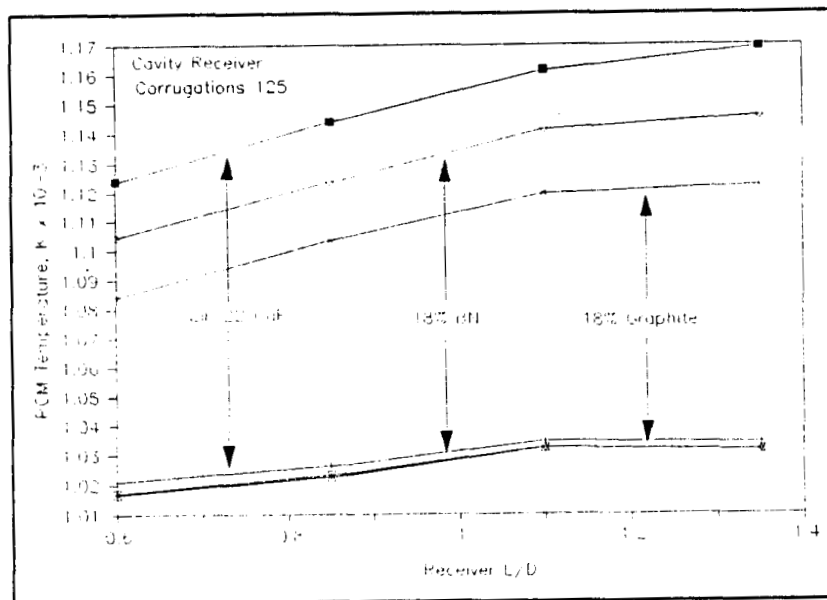


Figure 38. Effects of Receiver L/D on Canister Temperature Difference.

As seen in Figure 39 the effect of increasing the number of corrugations is similar to that of increasing the number of elements for other concepts. Here the range extends from 75 to 150. Under these conditions the minimum temperature shows little variation, remaining slightly below the melting point. The maximum temperature decreases from about 1165 to about 1130 for the unenhanced PCM. Additions of 18% BN decreased this peak temperature from 1135 to 1110 over this same range. Graphite provides for a further reduction ranging from 1110 to 1090 K. From the increasing slope of the curve it would appear that

ORIGINAL PAGE IS
OF POOR QUALITY

significant reductions in the number of corrugations below the indicated range would lead to rather large increases in these values.

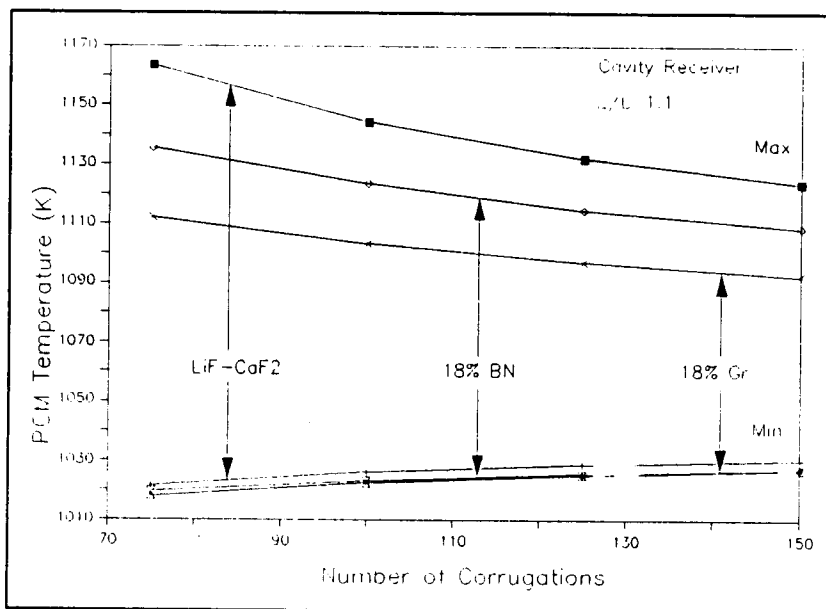


Figure 39. Effects of Element P/D on Canister Temperature Difference.

4 Discussion

It should be emphasized that in a evaluation of this type, including only thermal performance of the relative concepts, relative comparisons are somewhat limited and should not be used as a sole basis for receiver selection. Moreover there remain a certain arbitrariness in establishing certain of the configurations. Specifically those designs including canisters were not credited with the thermal enhancement properly attributed to that design. This was done in order to illustrate a continuity in the effects of thermal enhancement where it was assumed that PCM distribution would be accommodated by the foam filler itself. Further it is not clear to the authors that the effects of potential liquid PCM circulation and thermal insulation due to possible void coalescence and migration have been equitably evaluated between competing concepts. Finally the use of the CAV2 generated incident heat fluxes may unfairly penalize the non heat pipe concepts by failing to account for radiant redistribution of the incident heat flux within the receiver. Nevertheless it is believed that the results presented are useful in a number of ways. In a general sense they may serve to provide reasonable estimates of the performance achievable. They also provide an indication of the benefits attributable to various enhancement alternatives. Finally they serve to indicate that range of individual parameters which tend to optimize thermal performance within each of the respective designs.

4.1 Attainable Performance

Attainable thermal performance is evaluated here in two distinct ways. The first involves the variation in receiver outlet temperature, generally termed either turbine inlet temperature, heat pipe temperature, or engine head temperature. The second involves PCM peak temperatures or PCM thermal differences. These parameters relate to the thermal stress and thermal cycling within the PCM containment and have a direct bearing on the ultimate reliability of the receiver.

The cyclic thermal variation for the base line receiver is shown in Figure 12 where the overall variation is seen to be of the order of 60 K. The basic problem of optimizing performance with this design is the maldistribution of incident energy in the axial direction. Excess incident energy is provided at the aperture end of the receiver tending to provide excessive sensible heating of the PCM during the latter stages of the heating cycle. Insufficient heating occurs at the opposite end of the receiver so that complete solidification and sensible heat removal during the eclipse phase remains a problem. The design problem then becomes one of making a trade off between excess temperature near

the receiver inlet versus increased engine hot side temperature variations. The most direct solution of the problem is to increase the amount of PCM in the receiver.

The corresponding plot for the heat pipe receiver is shown in Figure 20. It is important to note here that the number of elements in the heat pipe system is reduced to 20 from the original 75 used in the base line receiver. It is also important to note that the calculated results for the heat pipe system do not include any enhancement effects from the canister side walls. As a consequence the LiF 22 CaF₂ results indicate somewhat larger temperature swings than would be observed in such a system. Based on prior runs a reasonable approximation for such a system would be to assume that the effects of adding 12% metal fins would be to produce about 2/3 of the improvement of adding 18% BN. Thus the anticipated temperature variation for the system is thought to be about 94 K. Increasing the number of elements from 20 to 30 with the heat pipe system, as seen in Figure 22, would serve to decrease the temperature difference to about 50 K. The two systems are strikingly similar in terms of individual components and would seem to offer the most viable direct comparison of any two receivers under consideration. The improvements associated with the heat pipe configuration may be attributed to a combination of factors. First the heat pipe serves to smooth the incident heat flux. Second, energy utilized by the engine during the period of solar incidence is not forced through the PCM, but rather is transported directly from the aperture section of the heat pipe directly to the engine. The resultant reduction in heat flux through the PCM can only serve to reduce the required temperature differential.

The engine hot side temperature variation for the cavity receiver is shown in Figure 35. This design also utilized a direct solar incidence on the PCM with the working fluid flowing past the PCM. As with the base case this design has the problem of excessive heat addition near the aperture and insufficient heat flux at the outlet end. It does benefit from a somewhat higher number of canisters than the base line receiver and from a truncated cone shape which redistributes the incident heat flux to an extent. The result of these two improvements is seen in reducing the working fluid temperature variation to about 47 K.

It is concluded that an overall temperature variation of between 50 and 100 K is reasonably achievable with an unenhanced LiF 22 CaF₂ PCM receiver. As will be noted in the following sections, the lower range of values will typically be associated with arrangements optimized for thermal performance rather than weight.

The range of radial temperature variation across the individual elements is also of importance, not to engine performance, but rather as an indication of the thermal stresses established within the PCM containment. This variation is normally a maximum at the end of solar incidence and is therefore evaluated at that time. Shown in Figure 19 is the maximum and minimum temperatures within that range of canisters nearest the aperture of the base line case. Since the reference condition is at a P/D of about 1.66 it can be seen that the maximum and minimum temperatures correspond to about 172 and 148 degrees above melting or 1211 and 1187 respectively. Note that the variation across the element is only 24 degrees but the absolute values are relatively large. This is due to the high axial incident flux near the aperture.

The cavity receiver, as shown in Figure 39, tends to have slightly improved PCM temperature differentials over the base line case. With 125 corrugations the PCM maximum is 1132 and minimum is 1022 K. The reduction in the maximum temperature can be attributed partially to the improved incident flux distribution associated with the truncated cone configuration. It is also important to note that the coolant passages in this design are suitable for conforming to axial needs. In this analysis it has been assumed that the convection coefficient is axially adjusted to provide an axial NTU distribution which matches the fraction of heat removal to the fraction of incident energy. Upon reviewing the final results it was realized that this effect could be carried to a greater extent. That is the matching of the rate of heat removal to the incident heat flux leads to a situation in which the orbital temperature variation tends to produce axial PCM temperature patterns in which the minimum temperature appears as something of a mirror image of the maximum temperature with an axis about the melting point. A further refinement of the method would increase the rate of heat removal at axial locations corresponding to the highest PCM temperatures. This would distort the mirror image decreasing the peak temperatures and producing significant sensible heat removal during the heat removal phase at these same locations.

In comparison both the heat pipe and the cavity heat pipe receivers operate at maximum and minimum PCM temperatures of about 60 and 0 degrees above melting or 1099 and 1039 K, respectively. The magnitude of the temperatures is significantly reduced due to smoothing of the axial flux in the heat pipe. The temperature differential is, however, considerably larger. This may be attributed to the reduced number of elements and the subsequent increase in individual canister radius.

The pebble bed arrangement is by its nature somewhat different in terms of element temperature variations. The values shown in Figure 30 indicate that the temperature difference across the PCM mass ranges from 1025 to 1110 K. Note that this difference is not across a single sphere but represents the temperature difference between spheres at the center and edge of the bed. For this reason comparisons of metal stress between these elements and the alternative designs are difficult. In this design the PCM sphere size is essentially 1/3 of the element containment ID. A simple analysis would then suggest a temperature difference across each sphere of about 30 to 35 degrees.

4.2 PCM Thermal Enhancement

The effects of thermal enhancement on the cycle hot side temperature are shown for the base line receiver in Figure 13. For the heat pipe receiver these same results are shown in Figure 20. Neither case provides a clear comparison of the various enhancement schemes. As noted earlier, the set of conditions chosen for the base line receiver do not lend themselves to the use of Ge or 18% additions of BN or pyrolytic graphite. As a consequence consideration has been limited to 10% additions of the latter two enhancement materials. Moreover both cases are somewhat complicated by the question of whether and how side wall should be considered. The approach proposed here is simply to compare the results neglecting the side walls but to weight certain of the other cases more heavily in making the final comparison.

In the base line case the cyclic variations are reduced from about 77 K to 43 and 37 K for a 10 % addition of BN and graphite, respectively. This corresponds to a 44% and a 52% reduction in variation from the base line. The enhancement of the heat pipe receiver is seen to reduce the variation from about 110 K to about 75, 60 and 5 K for the 18% BN 18% graphite and the Ge, respectively. This results in a 32% improvement for the BN, and a 45% improvement for the graphite. Note that while the while the enhancement fraction is much lower for the base line case the improvement achieved is greater. The introduction of Ge as a phase change material reduces the overall temperature variation to near zero and would clearly be the most advantageous choice from thermal considerations.

A somewhat simpler comparison is made in the various enhancement schemes in the cavity heat pipe receiver. Referring to Figure 31, it is seen that using the reference 36 elements the introduction of thermal enhancement reduces the variation from 115 to 90 and 62 K, respectively. The improvement is seen to be a reduction of 22% and 45% respectively. While the Ge PCM

has not been evaluated for this same number of elements, certainly the variation will be less than for the 24 element case or less than 15 K. The corresponding reduction is then greater than 87%.

The cavity receiver provides a second relatively direct comparison. As seen in Figure 34, the BN serves to reduce the variation from about 117 to 95 K, or about 19%. Similarly the graphite reduces the variation to about 70 K or about 40%.

Summarizing the cases above it is concluded that thermal enhancement with BN would normally be expected to decrease engine hot side temperature variations to between 20 and 25%, graphite to between 40 and 45% and Ge to between 85 and 95%.

Canister temperature differences are shown for the cavity heat pipe receiver can be taken from Figure 32 recognizing that at 54 minutes the minimum temperature will be at the back wall of the element where only a residual solid mass of PCM remains. As a consequence the element temperature difference will be between the melting temperature and the peak temperature. It would appear then that the addition of 18% BN would serve to reduce temperature variation across the element from 65 to 48 K or by 26%. Graphite enhancement reduces the differential to 32 K or by 51%. Germanium PCM would encounter only about a 5 K difference at this same time representing a reduction of 92%.

The cavity receiver indicates a much larger temperature difference across the elements as indicated in Figure 36. Here the unenhanced material operates with a peak temperature difference of about 120 K. Eighteen percent additions of BN reduce this to about 100 K or about 17% and similar additions of graphite to about 79 K or by 34%.

Summarizing these conclusions it appears that BN enhancement would potentially reduce peak PCM temperature differences by between 15 and 30%. Similar additions of graphite would reduce these same differences by between 35 and 50%. Germanium PCM would virtually eliminate such differences, reducing them by about 90% as compared to the unenhanced salt.

4.3 Parametric Studies

In reviewing the thermal performance of each of the design concepts, it becomes clear that most of the corresponding performance curves appear similar in general form. That is the cycle hot side temperature, whether it be termed the turbine inlet temperature or heat pipe temperature, tends to become more uniform as the effective thickness of the PCM is decreased. Several methods remain for controlling the effective thickness in each of these designs.

Generally, increasing the receiver length will tend to redistribute PCM so as to provide a smaller radial path for energy storage. In the study shown here this effect is shown as the receiver length to diameter (L/D) ratio. An apparent exception to decreased temperature variations with increased L/D is the case of the cavity receiver. This case involves the use of an absorbing phase in the PCM. It is thought that the higher temperatures are associated with the steeper energy gradient associated with the increased concentration of absorbing material utilized to maintain a constant average absorptivity.

In each of the designs it was found that increasing the number of elements, or corrugations in the case of the cavity receiver, tended to reduce variations in the cycle hot side temperature. This again is attributable to the reduction in the effective thickness of PCM through which the heat flux must travel. In those cases which did not utilize the heat pipe concept to redistribute the incident heat flux, it was found that increasing the element pitch to diameter ratio would tend to redistribute incident heat flux in a more uniform method also reducing temperature differences.

5 Conclusions.

While the base line concept represents a relatively high degree of development in thermal receiver design, substantial improvements in thermal performance may still be achieved. Generally these are accomplished through one of several methods including (1) the use of heat pipes to redistribute incident heat flux in a uniform manner, (2) better utilization of the PCM material with less sensible heating and cooling, (3) introduction of concepts which completely or partially bypass energy flow around the PCM and directly to the engine, (4) introduction of concepts which can practically accommodate larger number of elements or introduce other effective methods of reducing the thickness of PCM through which heat transport occurs or (5) introduction of enhanced thermal conductivity materials.

Within this range of design features it is possible to reduce peak PCM temperature from about 1210 to around 1090 K without the benefit of thermal enhancement. The base line receiver is found to provide relatively uniform engine hot side temperatures with variations of about 60 K. While certain of the concepts may in fact increase this value, reductions to about 45 K are possible while retaining the $\text{LiF } 22 \text{ CaF}_2$ PCM.

The introduction of BN enhancement is found to marginally beneficial in terms of improved thermal performance. The development of a graphite enhancement material would provide somewhat higher levels of performance and would receive a much higher priority. The development of Germanium or other metallic PCM offers a quite high level of thermal performance is, if containment or other potential development problems can be overcome, offer substantial improvements over all other enhancement schemes.

6 References

1. Wallin, W. E. & Dustin, M. O., "Advanced Space Solar Dynamic Power Systems Beyond IOC", 22nd IECEC, Philadelphia, Penn, Aug. 1987.
2. Vanco, M. R., "Analytical Comparison of Relative Heat Transfer Coefficients and Pressure Drops of Inert Gases and Their Binary Mixtures", Internal Report, NASA Lewis Research Center.
3. Strumpf, H.J. & Coombs, M.G., "Advanced Heat Receiver Conceptual Design Study", NASA CR-180901, December 1987.
4. Juhasz, J. J., Coles-Hamilton, C. E. and Lacy, D. E., "Impact of Thermal Energy Storage Properties on Solar Dynamic Space Power Conversion System Mass", 22nd IECEC, Philadelphia, August 10-14, 1987.
5. Kesseli, J. & Saunders, R., "Advanced Heat Receiver Conceptual Design Study", Presented at NASA Lewis Research Center, Oct. 1986.
6. Lacy, D. E. & Coles-Hamilton, C., "Selection of High Temperature Thermal Energy Storage Materials for Advanced Solar Dynamic Space Power Systems", 22nd IECEC, Philadelphia, Penn, Aug. 1987.
7. Diver, R. B. & Andraka, C. E., "CAV2-A PC Based Computer Program for Predicting Incident Solar Flux Distributions Inside Dish Cavity Receivers" Sandia Report SAND86-0927, Feb. 1987.
8. Patankar, S. V., Numerical Heat Transfer and Fluid Flow, Hemisphere Publishing Corp., New York, 1980.
9. Meredith, R. E. & Tobias, C. W., "Conductivities in Emulsions, Electrochemical Society Journal, Vol. 108, 286, 1961.

APPENDIX A

PROGRAM FOR THE THERMAL ANALYSIS
OF THE
BASE LINE RECEIVER
AND THE
HEAT PIPE RECEIVER

C TIME = Time into orbit run, min
 C TIMER = Time of orbit, min
 C TO = Previous relative temperature of node (I,J)
 C TP = Projected relative temperature of node (I,J)
 C WALLS = Ratio of wall conduction area to storage area
 C
 C Material properties
 C
 C CPGAS = Coolant specific heat, kJ/kg K
 C CVLIQ = Liquid specific heat, kJ/kg K
 C CVMET = Ring specific heat, kJ/kg K
 C CVPURE = Specific heat of PCM (solid & liquid) kJ/kg K
 C CVSOL = Solid specific heat, kJ/kg K
 C DENLIQ = Liquid density, kg/m**3
 C DENMET = Ring density, kg/m**3
 C DENPURE = Density of PCM (solid & liquid) kg/m**3
 C DENSOL = Solid density, kg/m**3
 C F = Smooth tube adiabatic friction factor
 C GASMIX = Fraction of gas 1 in coolant mix
 C H = Convection coefficient of gas W/m**2 K
 C HFL = Heat of fusion, kJ/kg
 C K = Eff. thermal conductivity of node (I,J), W/m K
 C KE = Thermal conductivity of node (I,J+1), W/m K
 C KN = Thermal conductivity of node (I+1,J), W/m K
 C KP = Thermal conductivity solid with void, W/m K
 C KS = Thermal conductivity of node (I-1,J), W/m K
 C KW = Thermal conductivity of node (I,J-1), W/m K
 C K_1 = Thermal conductivity constant (See GASPROP)
 C K_2 = Thermal conductivity constant (See GASPROP)
 C K_3 = Thermal conductivity constant (See GASPROP)
 C K_4 = Thermal conductivity constant (See GASPROP)
 C KLIQ = Liquid thermal conductivity, W/m K
 C KMET = Ring thermal conductivity, W/m K
 C KPURE = Eff. thermal cond. of PCM (solid & liq.) W/m K
 C KSOL = Solid thermal conductivity, W/m K
 C MW = Molecular weight of gas component
 C VISC_1 = Viscosity constant (see GASPROP)
 C VISC_2 = Viscosity constant (see GASPROP)
 C VISC_3 = Viscosity constant (see GASPROP)
 C VISC_4 = Viscosity constant (see GASPROP)
 C VOID = Void fraction in element
 C
 C Indices
 C
 C I = Counter in radial direction
 C ICOUNT = Loop counter
 C IFLAG = Flag to indicate insufficient convergence
 C IMAX = Maximum number of loops
 C J = Counter in azimuthal direction
 C L = Counter in axial direction

```

C      LIO      = Counter on output file
C      NORBIT   = Number of orbit cycles
C      NI      = Number of radial nodes
C      NJ      = Number of azimuthal nodes
C      NL      = Number of axial nodes
C      NTIME   = Number of time increments per orbit
C
C      Matrix coefficients
C
C      A      = Conduction matrix coefficient on I-1 node
C      B      = Conduction matrix coefficient on I node
C      C      = Conduction matrix coefficient on I+1 node
C      D      = Conduction matrix coefficient on constant vector
C
C      Thermal resistances & capacitances
C
C      AE     = Thermal conductance of J-1 node, W/K
C      AN     = Thermal conductance of I+1 node, W/K
C      AS     = Thermal conductance of I-1 node, W/K
C      AW     = Thermal conductance of J+1 node, W/K
C      AP0    = Thermal capacitance of node (I,J), kJ/m K
C
C      Heat fluxes
C
C      QAZ    = Outside surface heat flux, W/m**2
C      QDIR   = Direct solar heat flux, W/m**2
C      QGASP  = Total heat added to gas at position DZ/2, kJ
C      QGASDZ = Total heat added to gas at position DZ, kJ
C      QIJ    = Radiation to element (I,J), W/m**2
C      QIDIR  = Indirect solar heat flux, W/m**2
C      QINTR  = Heat input on internal surface, W/m**2
C      QZ     = Integrated avg. axial multiplier on heat flux
C      QZZ    = Local axial multiplier on heat flux
C      QZ_    = Constant on fit of QZ
C
C*****
C
C      PROGRAM SOLDTSS
C
C      REAL KLIQ, KMET, KSOL, LENGTH, MIN(11), NTU
C      DIMENSION FLOGAS(10), QDIR(10), QINDIR(10), QINT(10)
C      DIMENSION TGAS(10), THETA(10), THGAS(10,10,10), TP(15,10,10)
C
C      COMMON/BLOKA/CVLIQ, CVMET, CVSOL, DENLIQ, DENMET, DENSOL, HFL,
C      , KLIQ, KMET, KSOL, LENGTH, PI, RI, RICAN, RO, ROCAN,
C      , RMELT(15,10,10), ROMELT(15,10,10), VOID, WALLS
C      COMMON/BLOKB/F, GASMIX
C      COMMON/BLOKC/DR, DTIME, DPHI, DZ, HEAT, QAZ, QZ, T0(15,10,10)
C      COMMON/BLOKD/CPGAS, DELTDZ, DELTP, GASMAS, H, NTU, TGASIN, TGASP,
C      , THMELT

```

```

COMMON/BLOKE/A(15),B(15),C(15),D(15),T(15,10,10)
COMMON/BLOKF/I,J,L,NI,NJ,NL
COMMON/BLOKG/POS,QZ1,QZ2,QZ3,QZ4

```

```

C
C*****
C
C          OPEN INPUT AND OUTPUT FILES
C
C*****
C

```

```

OPEN(8,FILE='INPUT.TXT')
OPEN(7,FILE='OUTPUT.TXT')
II=1
PI=3.14159
READ(8,2100,ERR=93)IMAX,NORBIT,NI,NJ,NL,NTIME
READ(8,2200,ERR=94)RICAN,RI,RO,ROCAN,LENGTH,DUM1
READ(8,2200,ERR=95)CVLIQ,DENLIQ,KLIQ,WALLS,THMELT,DUM2
READ(8,2200,ERR=96)CVSOL,DENSOL,KSOL,ERRMAX,HFL,DUM3
READ(8,2200,ERR=97)CVMET,DENMET,KMET,GASMIX,TIMER,BORL
READ(8,2200,ERR=98)QZ1,QZ2,QZ3,QZ4,SORL
1 READ(8,2200,ERR=99,END=5)MIN(II),TGAS(II),FLOGAS(II),
,QDIR(II),QINDIR(II),QINT(II)
II=II+1
MIN(II)=1.E9
GO TO 1

```

```

C
C*****
C
C          INITIALIZE LOOP COUNTERS AND ERROR FLAGS
C
C*****
C

```

```

5 DELTP=0.0
ITEMP=0
DR=(RO-RI)/FLOAT(NI-2)
DPHI=PI/FLOAT(NJ)
DZ=LENGTH/FLOAT(NL)
DTIME=60.0*TIMER/FLOAT(NTIME)

```

```

C
DO 10 II=1,NI
DO 10 JJ=1,NJ
DO 10 LL=1,NL
T(II,JJ,LL)=-50.0
TP(II,JJ,LL)=T(II,JJ,LL)
C
IF(II.LT.NI)THEN
RMELT(II,JJ,LL)=0.0
ELSE
RMELT(II,JJ,LL)=1.0
ENDIF

```

```

C
  10 CONTINUE
C*****
C
C   BEGIN CALCULATIONAL LOOPS ON LENGTH, TIME, ANGLE
C
C*****
C
  DO 100 NO=1,NORBIT
    NPUT=0
    TIME=0.0
C
  DO 100 N=1,NTIME
    IF(MIN(NPUT+1) .LE. TIME+0.1E-6)NPUT=NPUT+1
    GASMAS=FLOGAS(NPUT)
    THGAS(N,NO,1)=TGAS(NPUT)
    TIME=FLOAT(N)*DTIME/60.0
C
  DO 100 L=1,NL
    POS=DZ*FLOAT(L)
    TGASIN=THGAS(N,NO,L)
C
    DO 20 II=1,NI
      DO 20 JJ=1,NJ
        ROMELT(II,JJ,L)=RMELT(II,JJ,L)
        TO(II,JJ,L)=T(II,JJ,L)
20    CONTINUE
C
    ICOUNT=0
30    IFLAG=0
    ICOUNT=ICOUNT+1
    TGASP=THGAS(N,NO,L)+DELTP
C
    DO 40 J=1,NJ
      CALL GASPROP(RICAN,T(1,J,L),DZ)
      CALL SOLAR(LENGTH,QDIR(NPUT),QINDIR(NPUT),ROCAN)
      CALL CONDUCT(BORL,SORL,QINT(NPUT))
      CALL SOLVER
      CALL HEATGAS(T(1,J,L))
40    CONTINUE
C
    DO 50 II=1,NI
      DO 50 JJ=1,NJ
        ERROR=ABS(T(II,JJ,L)-TP(II,JJ,L))/THMELT
        IF(ERROR .GT. ERRMAX)IFLAG=2
        IF(ERROR .GT. ERRMAX)ITEMP=ITEMP+1
        TP(II,JJ,L)=T(II,JJ,L)
50    CONTINUE
C
    IF(ICOUNT .GT. IMAX)THEN

```

```

        WRITE(7,1000) ITEMP
        IFLAG=0
    ENDIF
C
    IF(IFLAG .GE. 1)GO TO 30
    THGAS(N,NO,L+1)=THGAS(N,NO,L)+DELTDZ
    IF(NO .LT. NORBIT)GO TO 100
C
    WRITE(7,1050)
    WRITE(7,1250)
    WRITE(7,1100) POS, TIME, NO
    WRITE(7,1150) QZ, HEAT
    DO 70 I=1,NI
        DO 60 J=1,NJ
            THETA(J)=T(I,J,L)+THMELT
60        CONTINUE
            WRITE(7,1200) (THETA(J),J=1,NJ)
70        CONTINUE
C
    WRITE(7,1300) TGASP, THGAS(N,NO,L+1),H
C
    WRITE(7,1050)
    WRITE(7,1250)
    DO 80 I=1,NI-1
        WRITE(7,1350) (RMELT(I,J,L),J=1,NJ)
80        CONTINUE
        WRITE(7,1350) (RMELT(1,J,L),J=1,NJ)
C
100 CONTINUE
C
C*****
C
C          INPUT AND OUTPUT FORMAT STATEMENTS
C
C*****
C
1000 FORMAT(1X,'FAILED TO CONVERGE AFTER ',I6,' ITERATIONS.')
1050 FORMAT(1X,' ')
1100 FORMAT(1X,'Axial Position = ',1F5.3,' m. Time = ',
& 1F6.1,' min. Cycle = ',I1,'.')
1150 FORMAT(1X,'Heat Input Frac. = ',1F6.4,' Heat = ',1F9.4)
1200 FORMAT(10F7.1)
1250 FORMAT(1X,'=====
&==','=====')
1300 FORMAT(1X,'Avg. Gas Temp. = ',F6.1,'K Out. Gas temp.',
& F6.1,'K H = ',F7.4,'KW/m2-K')
1350 FORMAT(10F7.4)
1400 FORMAT(1X,'INPUT FORMAT ERROR IN 1ST LINE')
1401 FORMAT(1X,'INPUT FORMAT ERROR IN 2ND LINE')
1402 FORMAT(1X,'INPUT FORMAT ERROR IN 3RD LINE')

```

```
1403 FORMAT(1X,'INPUT FORMAT ERROR IN 4TH LINE')
1404 FORMAT(1X,'INPUT FORMAT ERROR IN 5TH LINE')
1405 FORMAT(1X,'INPUT FORMAT ERROR IN 6TH LINE')
1406 FORMAT(1X,'INPUT FORMAT ERROR IN TRANSIENT SECTION')
2100 FORMAT(I6,5I10,2F10.0)
2200 FORMAT(2F10.4,4E10.4)
  STOP
  93 WRITE(*,1400)
  STOP
  94 WRITE(*,1401)
  STOP
  95 WRITE(*,1402)
  STOP
  96 WRITE(*,1403)
  STOP
  97 WRITE(*,1404)
  STOP
  98 WRITE(*,1405)
  STOP
  99 WRITE(*,1406)
  STOP
  END
```

```

C*****
C*****
C
C          SUBROUTINE SOLAR
C
C      This program calculates the solar incidence on
C      the outside perimeter of the containment ring
C
C          q" = q"(direct)*cos(angle) + q"(indirect)
C
C*****
C*****
C
C      SUBROUTINE SOLAR(LENGTH,QDIR,QINDIR,ROCAN)
C
C      DIMENSION CS(21)
C      REAL LENGTH
C      COMMON/BLOK/DR,DTIME,DPHI,DZ,HEAT,QAZ,QZ,T0(15,10,10)
C      COMMON/BLOK/I,J,L,NI,NJ,NL
C      COMMON/BLOK/POS,QZ1,QZ2,QZ3,QZ4
C      DATA CS(1),CS(3),CS(5),CS(7),CS(9),CS(11),CS(13)/
C      /1.0,6*2.0/
C      DATA CS(15),CS(17),CS(19),CS(2),CS(4),CS(6),CS(8)/
C      /3*2.0,4*4.0/
C      DATA CS(10),CS(12),CS(14),CS(16),CS(18),CS(20),CS(21)/
C      /6*4.,1./
C      DATA PI/3.14159/
C
C*****
C
C      QZ USES SIMPSON'S 1/3 INTEGRATION TO FIND THE
C      INTTEGRATED AVERAGE VALUE OF THE AXIAL POWER CURVE
C      OVER THE INTERVAL DZ
C
C*****
C
C      XL=(POS-DZ)/LENGTH
C      QZ=0.0
C
C      DO 15 II=1,21
C          IF(II .GT. 1)XL=XL+0.05*DZ/LENGTH
C          QZZ=QZ1*XL*EXP(1.0-(XL/QZ2)**QZ3)+QZ4*(XL)**0.5
C          QZ=QZ+CS(II)*(QZZ)/60.0
C      15 CONTINUE
C
C*****
C
C      FIND THE PROJECTION OF THE DIRECT SOLAR INCIDENCE
C
C*****

```

```
C
  ANGLE1=PI*FLOAT(J)/FLOAT(NJ)
  ANGLE2=PI*FLOAT(J-1)/FLOAT(NJ)
C
  IF (J+J-2 .GT. NJ) THEN
    SINANGLE=0.0
  ELSEIF (J+J .GT. NJ) THEN
    SINANGLE=1.0-SIN(ANGLE2)
  ELSE
    SINANGLE=SIN(ANGLE1)-SIN(ANGLE2)
  ENDIF
C
C*****
C
C  ADD DIRECT AND INDIRECT INCIDENT SOLAR RADIATION
C
C*****
C
  QAZ=(QDIR*SINANGLE + QINDIR*DPHI)*ROCAN*DZ*QZ
  IF(J .EQ. 1) HEAT=0.0
  HEAT=HEAT+2.0*QAZ
C
  RETURN
  END
```

```

C*****
C*****
C
C          SUBROUTINE GASPROP
C
C      This program calculates the effective thermal
C      properties and convective coefficients for the gas coolant
C      The gas coolant is assumed to be a mixture of He and Xe.
C      Properties for these two constituents are included as
C      curve fits with the corresponding coefficients included
C      as data within the subroutine.
C
C*****
C*****
C
C      REFERENCES
C      M. R. Vanco, "Analytical Comparison of Relative Heat
C      Transfer Coefficients and Pressure Drops of Inert
C      Gases and Their Binary Mixtures", Lewis Research Center
C
C      A. J. Chapman "Fundamentals of Heat Transfer"
C      Macmillan, 1987, p 329.
C
C*****
C*****
C
C      EQUATIONS
C
C      K1 = K11 + K12*(TGASP - K13)**K14
C      K2 = K21 + K22*(TGASP - K23)**K24
C
C      VISC1 = VISC11 + VISC12*(TGASP - VISC13)**VISC14
C      VISC2 = VISC21 + VISC22*(TGASP - VISC23)**VISC24
C
C*****
C
C      SUBROUTINE GASPROP(RICAN,T1J,DZ)
C
C      REAL K,K1,K2,K11,K12,K13,K14,K21,K22,K23,K24,KGAS,
C      +MW,MW1,MW2,NTU,NU
C
C      COMMON/BLOKB/F,GASMIX
C      COMMON/BLOKD/CPGAS,DELTDZ,DELTP,GASMAS,H,NTU,TGASIN,TGASP,
C      ,THMELT
C
C      DATA GAMMA,PI,RUNIV,MW1,MW2/1.66,3.14159,8.31434,4.,131./
C      DATA K11,K12,K13,K14/0.1580E-3,0.9086E-6,333.333,0.794/

```

```

DATA K21,K22,K23,K24/0.6404E-5,0.0454E-6,333.333,0.800/
DATA VISC11,VISC12,VISC13,VISC14/
/.2158E-4,.1022E-6,333.3,.825/
DATA VISC21,VISC22,VISC23,VISC24/
/.253E-4,.2452E-6,333.333,.77/

```

```

C
F1(X,Y) = (1.0+2.41*(X-Y)*(X-0.142*Y)/(X+Y)**2)
F2(X1,X2,X3,X4,X5,X6)=
=((1.0+(X1/X2)**0.5*(X3/X4)**0.25)**2)/
/(2.0*2.0**0.5*(1.0+X5/X6)**0.5)

```

```

C
C*****
C
C FIND THE THERMAL CONDUCTIVITY & VISCOSITY OF PURE GASES *
C
C*****
C

```

```

K1=K11+K12*(TGASP-K13)**K14
K2=K21+K22*(TGASP-K23)**K24
VISC1=VISC11+VISC12*(TGASP-VISC13)**VISC14
VISC2=VISC21+VISC22*(TGASP-VISC23)**VISC24
VISCW1=VISC11+VISC12*(T1J+THMELT-VISC13)**VISC14
VISCW2=VISC21+VISC22*(T1J+THMELT-VISC23)**VISC24

```

```

C
C*****
C
C FIND THE WEIGHTING PARAMETERS FROM REFERENCE *
C
C*****
C

```

```

PHI12=F2(VISC1,VISC2,MW2,MW1,MW1,MW2)
PHI21=PHI12*(VISC2*MW1)/(VISC1*MW2)
PSI12=F2(K1,K2,MW1,MW2,MW1,MW2)*F1(MW1,MW2)
PSI21=F2(K2,K1,MW2,MW1,MW2,MW1)*F1(MW2,MW1)

```

```

C
C*****
C
C SOLVE FOR THERMAL CONDUCTIVITY AND VISCOSITY OF GAS MIX *
C
C*****
C

```

```

VISC=VISC1/(1.0+PHI12*(1.0-GASMIX)/GASMIX)+
+ VISC2/(1.0+PHI21*(GASMIX/(1.0-GASMIX)))
VISCW=VISCW1/(1.0+PHI12*(1.0-GASMIX)/GASMIX)+
+ VISCW2/(1.0+PHI21*(GASMIX/(1.0-GASMIX)))
KGAS=K1/(1.0+PSI12*(1.0-GASMIX)/GASMIX)+
+ K2/(1.0+PSI21*(GASMIX/(1.0-GASMIX)))

```

```

C
C*****
C

```

```

C      SOLVE FOR SPECIFIC HEAT OF GAS MIX      *
C      *
C*****
C
      MW=GASMIX*MW1+(1.0-GASMIX)*MW2
      CPGAS=GAMMA*RUNIV/((GAMMA-1.0)*MW)
C
C
C*****
C      .SOLVE FOR CONVECTION COEFFICIENT      *
C      USING THE SIEDER-TATE CORRELATION FOR TURBULENT FLOW *
C      AND THE NUSSELT CORRELATION FOR LAMINAR FLOW      *
C      FIND THE NUMBER OF TRANSFER UNITS      *
C      *
C*****
C
      PR=CPGAS*VISC/(KGAS)
      RE=2.0*GASMAS/(PI*RICAN*VISC)
C
      IF(RE .LT. 10000.0) THEN
          F=64.0/RE
          NU=3.66
      ELSE
          F=(1.82*ALOG10(RE)-1.64)**(-2)
          NU=0.027*RE**0.8*PR**0.333333*(VISC/VISCW)**0.14
      ENDIF
C
      H=KGAS*NU/(2.0*RICAN)
      NTU=H*2.0*PI*RICAN*DZ/(GASMAS*CPGAS)
C
      RETURN
      END

```

```

C*****
*
C*****
C
C          SUBROUTINE CONDUCT
C
C          PROGRAM DEVELOPS FINITE DIFFERENCE MATRIX
C          FOR CONDUCTION ANALYSIS IN CYLINDRICAL COORDINATES
C
C*****
C*****
C          REFERENCE:  Pantankar, S. V., "Numerical Heat Transfer and
C          Fluid Flow", McGraw Hill, 1980, pp. 64-74.
C
C*****
C
C          SUBROUTINE CONDUCT(BORL,SORL,QINT)
C
C          REAL K,KE,KLIQ,KMET,KN,KP,KS,KSOL,KW,LENGTH,NTU
C
C          COMMON/BLOKA/CVLIQ,CVMET,CVSOL,DENLIQ,DENMET,DENSOL,HFL,
+KLIQ,KMET,KSOL,LENGTH,PI,RI,RICAN,RO,ROCAN,
+RMELT(15,10,10),ROMELT(15,10,10),VOID,WALLS
COMMON/BLOKCDR,DTIME,DPHI,DZ,HEAT,QAZ,QZ,T0(15,10,10)
COMMON/BLOKD/CPGAS,DELTDZ,DELTP,GASMAS,H,NTU,TGASIN,TGASP,
,THMELT
COMMON/BLOKE/A(15),B(15),C(15),D(15),T(15,10,10)
COMMON/BLOKF/I,J,L,NI,NJ,NL
C
C          DO 50 I=1,NI
C
C          IF (J .EQ. 1) THEN
C              AE=0.0
C              TE=0.0
C          ELSE
C              TE=T(I,J-1,L)
C          ENDIF
C
C          IF (J .EQ. NJ) THEN
C              AW=0.0
C              TW=0.0
C          ELSE
C              TW=T(I,J+1,L)
C          ENDIF
C
C
C*****
C
C          SET NODAL CONSTANTS FOR INSIDE RING
C

```

```

C
C*****
C
IF (I .EQ. 1) THEN
  R=RICAN
  RN=RI
  VOID=(1.0-DENLIQ/DENSOL)*(1.0-RMELT(2,J,L))
  CALL PROPERTY (CV,DEN,2,J,KN,L)
  AA=0.5*(RN*RN-R*R)*DPHI*KMET/DZ
  AB=0.5*(RN*RN-R*R)*DPHI*KMET/DZ
  AN=KMET*KN*RN*DPHI*DZ/(0.5*KMET*DR+KN*(RI-RICAN))
  AS=0.0
  IF(J .GT. 1)
&   AE=KMET*(RI-RICAN)*DZ/(0.5*(RI+RICAN)*DPHI)
  IF(J .LT. NJ)
&   AW=KMET*(RI-RICAN)*DZ/(0.5*(RI+RICAN)*DPHI)
  APO=DENMET*CVMET*0.5*(RI*RI-RICAN*RICAN)*DPHI*DZ/DTIME
  TCIJ=TGASIN-THMELT
  HIJ=GASMAS*CPGAS*(1.0-EXP(-NTU))/FLOAT(2*NJ)
  QIJ=QINT/(2.0*PI*R*LENGTH)
C
C*****
C
C           SET NODAL CONSTANTS FOR OUTSIDE RING
C
C*****
C
ELSEIF (I .EQ. NI) THEN
  R=ROCAN
  RS=RO
  VOID=(1.0-DENLIQ/DENSOL)*(1.0-RMELT(NI-1,J,L))
  CALL PROPERTY (CV,DEN,I-1,J,KS,L)
  AA=0.5*(R*R-RS*RS)*DPHI*KMET/DZ
  AB=0.5*(R*R-RS*RS)*DPHI*KMET/DZ
  AS=KMET*KS*RS*DPHI*DZ/(0.5*KMET*DR+KS*(ROCAN-RO))
  AN=0.0
  IF(J .GT. 1)
&   AE=KMET*(ROCAN-RO)*DZ/((.5*(ROCAN-RO)+RO)*DPHI)
  IF(J .LT. NJ)
&   AW=KMET*(ROCAN-RO)*DZ/((.5*(ROCAN-RO)+RO)*DPHI)
  APO=DENMET*CVMET*0.5*(ROCAN*ROCAN-RO*RO)*DPHI*DZ/DTIME
  TCIJ=0.0
  HIJ=0.0
  QIJ=QAZ
C
C*****
C
C           SET NODAL CONSTANTS FOR PHASE CHANGE MATERIAL
C
C*****

```

```

C
ELSE
  R=RI+(FLOAT(I)-1.5)*DR
  RN=R+0.5*DR
  RS=R-0.5*DR
  VOID=(1.0-DENLIQ/DENSOL)*(1.0-RMELT(I,J,L))
  CALL PROPERTY (CV,DEN,I,J,K,L)
  AA=0.5*(RN*RN-RS*RS)*DPHI*K/DZ
  AB=0.5*(RN*RN-RS*RS)*DPHI*K/DZ
C
  IF (I .EQ. 2) THEN
    AS=KMET*K*RI*DPHI*DZ/(0.5*KMET*DR+K*(RI-RICAN))
    TS=T(2,J,L)+DR*AS*(T(1,J,L)-T(2,J,L))/
      / (2.0*K*RI*DPHI)+
+    0.125*(T(2,J,L)-2.0*T(3,J,L)+T(4,J,L))
  ELSE
    CALL PROPERTY (CV,DEN,I-1,J,KS,L)
    KP=2.0*K*KS/(K+KS)
    AS=KP*RS*DPHI*DZ/DR
    TS=0.5*(T(I,J,L)+T(I-1,J,L))+
+    0.125*(T(I+1,J,L)-2.0*T(I,J,L)+T(I-1,J,L))
  ENDIF
C
  IF (I .EQ. NI-1) THEN
    AN=KMET*K*RO*DPHI*DZ/(0.5*KMET*DR+K*(ROCAN-RO))
    TN=T(NI-1,J,L)+DR*AN*(T(NI,J,L)-T(NI-1,J,L))/
/    (2.*K*RO*DPHI)+0.125*(T(NI-1,J,L)-
-    2.0*T(NI-2,J,L)+T(NI-3,J,L))
  ELSE
    CALL PROPERTY (CV,DEN,I+1,J,KN,L)
    KP=2.0*K*KN/(K+KN)
    AN=KP*RN*DPHI*DZ/DR
    TN=0.5*(T(I,J,L)+T(I+1,J,L))+
+    0.125*(T(I+1,J,L)-2.0*T(I,J,L)+T(I-1,J,L))
  ENDIF
C
C*****
C
C      Calculate the melt front movement
C
C*****
C
  IF (TS*TN .GE. 0.0) THEN
    OVRRLX = BORL*ABS(T(I,J,L))
    DMELT = OVRRLX*0.5*(TN+TS)*CV/HFL
    IF (TS .GE. 0.0) THEN
      DMELT=AMIN1(DMELT,1.0-RMELT(I,J,L))
    ELSE
      DMELT=AMAX1(DMELT,0.0-RMELT(I,J,L))
    ENDIF
  
```

```

ELSE
  IF(T(I,J,L)*TN .GE. 0.0) THEN
    IF(TN .GE. 0.0) THEN
      DMELT=(0.5*TN/(TN-T(I,J,L))-RMELT(I,J,L))*SORL
    ELSE
      DMELT=((0.5*TN-T(I,J,L))/
/          (TN-T(I,J,L))-RMELT(I,J,L))*SORL
    ENDIF
  ELSE
    IF(TN .LE. 0.0) THEN
      DMELT=(.5*TS/(TS-T(I,J,L))-RMELT(I,J,L))*SORL
    ELSE
      DMELT=((0.5*TS-T(I,J,L))/
/          (TS-T(I,J,L))-RMELT(I,J,L))*SORL
    ENDIF
  ENDIF
ENDIF
ENDIF

C
C*****
C
C Check melt front movement to ensure that it meets
C thermodynamic limitations.
C
C*****
C
  IF(DMELT .GE. 0.0) THEN
    DO 40 II=I+1,NI-1
      IF(RMELT(II,J,L) .LT. 0.99) DMELT=0.0
40    CONTINUE
  ENDIF

C
  IF(I .EQ. 2) THEN
    IF(DMELT .LT. 0.0) THEN
      IF((RMELT(I+1,J,L) .LE. .01) .OR.
&      (T(I-1,J,L) .LE. 0.0))
&      RMELT(I,J,L)=RMELT(I,J,L)+DMELT
    ELSE
      IF((RMELT(I+1,J,L) .GE. 0.99) .OR.
&      (T(I-1,J,L) .GE. 0.0))
&      RMELT(I,J,L)=RMELT(I,J,L)+DMELT
    ENDIF
  ELSEIF(I .EQ. NI-1) THEN
    IF(DMELT .GE. 0.0) THEN
      IF((T(NI,J,L) .GE. 0.0) .OR.
&      (QAZ .GE. 0.0))
&      RMELT(I,J,L)=RMELT(I,J,L)+DMELT
    ELSE
      IF((T(NI,J,L) .LE. 0.0) .OR.
&      (RMELT(NI-2,J,L) .LE. .01))
&      RMELT(I,J,L)=RMELT(I,J,L)+DMELT

```

```

      ENDIF
    ELSE
      IF(DMELT .LT. 0.0) THEN
        IF((RMELT(I-1,J,L) .LE. .01) .OR.
          & (RMELT(I+1,J,L) .LE. .01))
          & RMELT(I,J,L)=RMELT(I,J,L)+DMELT
        ELSE
          IF((RMELT(I-1,J,L) .GE. .99) .OR.
            & (RMELT(I+1,J,L) .GE. .99))
            & RMELT(I,J,L)=RMELT(I,J,L)+DMELT
          ENDIF
        ENDIF
      ENDIF

      RMELT(I,J,L)=AMAX1(0.0,RMELT(I,J,L))
      RMELT(I,J,L)=AMIN1(1.0,RMELT(I,J,L))

      IF (J .GT. 1) THEN
        CALL PROPERTY (CV,DEN,I,J-1,KE,L)
        KP=2.0*K*KE/(K+KE)
        AE=KP*DR*DZ/(R*DPHI)
      ENDIF

      IF(J .LT. NJ) THEN
        CALL PROPERTY (CV,DEN,I,J+1,KW,L)
        KP=2.0*K*KW/(K+KW)
        AW=KP*DR*DZ/(R*DPHI)
      ENDIF

      APO=DEN*CV*R*DPHI*DR*DZ/DTIME
      TCIJ=0.0
      HIJ=0.0
      PCMMASS=R*DPHI*DR*DENLIQ*(1.0-WALLS)*DZ
      QIJ=(ROMELT(I,J,L)-RMELT(I,J,L))*PCMMASS*HFL/DTIME
    ENDIF

    IF (L .EQ. 1) THEN
      AA=0.0
      TA=0.0
    ELSE
      TA=T(I,J,L-1)
    ENDIF

    IF (L .EQ. NL) THEN
      AB=0.0
      TB=0.0
    ELSE
      TB=T(I,J,L+1)
    ENDIF

    A(I)=-AS

```

$$B(I) = AA + AB + AN + AS + AE + AW + APO + HIJ$$
$$C(I) = -AN$$
$$D(I) = APO * T0(I, J, L) + HIJ * TCIJ + QIJ + AE * TE + AW * TW + AA * TA + AB * TB$$

C

50 CONTINUE

C

RETURN

END

```

C*****
C*****
C
C          SUBROUTINE PROPERTY
C
C          This program calculated the effective thermal
C properties of the solid & liquid phases of the storage media*
C
C*****
C*****
C*****
C
C REFERENCES  Y. S. Touloukian et.al. "Thermophysical
C Properties of Matter", Vol. 2, 1970.
C
C R. P. Wichner, ORNL "Boundary Conditions and Thermophysical
C Properties of LiF-CaF2", Presented to NASA Lewis Research
C Center, June 10, 1987.
C
C R. I. Vachon, et.al, "Thermal Conductivity of Heterogeneous
C Mixtures & Lunar Soils", NAS8-26579, October 1973.
C
C*****
C
C          SUBROUTINE PROPERTY (CV,DEN,I,J,K,L)
C
C          COMMON/BLOKA/CVLIQ,CVMET,CVSOL,DENLIQ,DENMET,DENSOL,HFL,
C          +KLIQ,KMET,KSOL,LENGTH,PI,RI,RICAN,RO,ROCAN,
C          ,RMELT(15,10,10),ROMELT(15,10,10),VOID,WALLS
C
C          REAL K,KLIQ,KMET,KP,KPSOL,KPURE,KSOL,LENGTH
C
C
C*****
C
C          FIND THE THERMAL PROPERTIES OF THE PURE MATERIALS
C
C          CALCULATE EFFECT OF VOID ON PROPERTIES OF SOLID
C USE CORRELATION BY MEREDITH & TOBIAS TO CORRECT CONDUCTIVITY*
C
C*****
C
C          KPSOL=KSOL*(2.0*(1.0-VOID)+0.6135*VOID**2.333-1.6*VOID**
C          & 3.333)/(2.0+VOID+0.6135*VOID**2.333-0.6975*VOID**3.333)
C          DENPSOL= DENLIQ
C
C          KPURE=1.0/(RMELT(I,J,L)/KLIQ+(1.0-RMELT(I,J,L))/KPSOL)
C          CVPURE=RMELT(I,J,L)*CVLIQ+(1.0-RMELT(I,J,L))*CVSOL
C          DENPURE=RMELT(I,J,L)*DENLIQ+(1.0-RMELT(I,J,L))*DENPSOL

```

```
C
C*****
C
C   PUT PURE STORAGE MATERIAL IN PARALLEL WITH CAN MATERIAL
C
C*****
C
C   K=KPURE*(1.0-WALLS)+KMET*WALLS
C   DEN=DENPURE*(1.0-WALLS)+WALLS*DENMET
C   CV=(CVPURE*DENPURE*(1.0-WALLS)+WALLS*CVMET*DENMET)/DEN
C
C   RETURN
C   END
```

```

C*****
C*****
C
C          SUBROUTINE SOLVER
C
C          This program solves a tridiagonal matrix using
C          an elimination method
C
C          [A]T(I-1) + [B]T(I) + [C]T(I+1) = [D]
C
C*****
C*****
C
C          SUBROUTINE SOLVER
C          COMMON/BLOKE/A(15),B(15),C(15),D(15),T(15,10,10)
C          COMMON/BLOKF/I,J,L,NI,NJ,NL
C
C*****
C          PROCEED WITH GAUSSIAN ELIMINATION TO DEVELOP A
C          UPPER DIAGONAL MATRIX
C*****
C
C          DO 1, I=1,NI-1
C              R=A(I+1)/B(I)
C              B(I+1)=B(I+1)-R*C(I)
C              D(I+1)=D(I+1)-R*D(I)
C          1 CONTINUE
C
C*****
C          BEGIN BACK SUBSTITUTION
C*****
C
C          T(NI,J,L)=D(NI)/B(NI)
C
C          DO 2, I=NI-1,1,-1
C              T(I,J,L)=(D(I)-C(I)*T(I+1,J,L))/B(I)
C          2 CONTINUE
C          RETURN
C          END

```

APPENDIX B
PROGRAM FOR THE THERMAL ANALYSIS
OF THE
CAVITY RECEIVER

```

C*****
C*****
C*****
C
C
C          PROGRAM SOLDTESS
C
C          SOLAR DYNAMIC TRANSIENT ENERGY STORAGE SIMULATION
C
C          This program is the main routine for the TESS code.
C          Its purpose is to read & print data and to call
C          calculational subroutines so as to complete the thermal
C          analysis. Checks for convergence are made here.
C*****

```

NOMENCLATURE

System dimensions

```

C  CS = Coefficient for Simpson 1/3 Integration
C  DR = Diff. element dimension in radial direction, m
C  DPHI = Diff. element dim. in azimuthal direction, rad
C  DMAX = Maximum move in melt position in one iteration
C  DMELT = Fractional movement of melt position in element
C  DTIME = Time increment, sec
C  DZ = Diff. element dimension in axial direction, m
C  GASMAS = Coolant flow rate, kg/sec
C  LENGTH = Axial length of stack, m
C  OVRRLX = Over relaxation factor on melt movement
C  POS = Axial position of current node, m
C  R = Radius of element (I,J), m
C  RI = Outside radius of inner can ring, m
C  RICAN = Inside radius of inner can ring, m
C  RMELT = Fraction of PCM in element melted
C  RN = Radius at outside edge of element (I,J), m
C  RO = Inside radius of outer can ring, m
C  ROCAN = Outside radius of outer can ring, m
C  RS = Radius at inside edge of node (I,J), m
C  ROMELT = Previous fraction of PCM melted
C  T = Projected relative temperature of node
C  TCIJ = Absolute coolant temperature of gas at pos., K
C  TGAS = Relative coolant temperature at axial position
C  TGASIN = Absolute coolant temp. entering axial position, K
C  TGASP = Absolute coolant temperature at mid DZ, K
C  THGAS = Absolute coolant temperature at inlet, K
C  THETA = Absolute temperature of node (I,J), K
C  THETAG = Absolute temperature of gas, K
C  THMELT = Absolute melting temperature of storage media, K
C  TIME = Time into orbit run, min
C  TIMER = Time of orbit, min

```

C TO = Previous relative temperature of node (I,J)
 C TP = Projected relative temperature of node (I,J)
 C WALLS = Ratio of wall conduction area to storage area
 C

Material properties

C CPGAS = Coolant specific heat, kJ/kg K
 C CVLIQ = Liquid specific heat, kJ/kg K
 C CVMET = Ring specific heat, kJ/kg K
 C CVPURE = Specific heat of PCM (solid & liquid) kJ/kg K
 C CVSOL = Solid specific heat, kJ/kg K
 C DENLIQ = Liquid density, kg/m**3
 C DENMET = Ring density, kg/m**3
 C DENPURE = Density of PCM (solid & liquid) kg/m**3
 C DENSOL = Solid density, kg/m**3
 C F = Smooth tube adiabatic friction factor
 C GASMIX = Fraction of gas 1 in coolant mix
 C H = Convection coefficient of gas W/m**2 K
 C HFL = Heat of fusion, kJ/kg
 C K = Eff. thermal conductivity of node (I,J), W/m K
 C KE = Thermal conductivity of node (I,J+1), W/m K
 C KN = Thermal conductivity of node (I+1,J), W/m K
 C KP = Thermal conductivity solid with void, W/m K
 C KS = Thermal conductivity of node (I-1,J), W/m K
 C KW = Thermal conductivity of node (I,J-1), W/m K
 C K_1 = Thermal conductivity constant (See GASPROP)
 C K_2 = Thermal conductivity constant (See GASPROP)
 C K_3 = Thermal conductivity constant (See GASPROP)
 C K_4 = Thermal conductivity constant (See GASPROP)
 C KLIQ = Liquid thermal conductivity, W/m K
 C KMET = Ring thermal conductivity, W/m K
 C KPURE = Eff. thermal cond. of PCM (solid & liq.) W/m K
 C KSOL = Solid thermal conductivity, W/m K
 C MW_ = Molecular weight of gas component _
 C VISC_1 = Viscosity constant (see GASPROP)
 C VISC_2 = Viscosity constant (see GASPROP)
 C VISC_3 = Viscosity constant (see GASPROP)
 C VISC_4 = Viscosity constant (see GASPROP)
 C VOID = Void fraction in element
 C

Indicies

C I = Counter in radial direction
 C ICOUNT = Loop counter
 C IFLAG = Flag to indicate insufficient convergence
 C IMAX = Maximum number of loops
 C J = Counter in azimuthal direction
 C L = Counter in axial direction
 C LIO = Counter on output file
 C NORBIT = Number of orbit cycles
 C NI = Number of radial nodes
 C NJ = Number of azimuthal nodes

```

C      NL = Number of axial nodes
C      NTIME = Number of time increments per orbit
C
C      Matrix coefficients
C      A = Conduction matrix coefficient on I-1 node
C      B = Conduction matrix coefficient on I node
C      C = Conduction matrix coefficient on I+1 node
C      D = Conduction matrix coefficient on constant vector
C
C      Thermal resistances & capacitances
C      AE = Thermal conductance of J-1 node, W/K
C      AN = Thermal conductance of I+1 node, W/K
C      AS = Thermal conductance of I-1 node, W/K
C      AW = Thermal conductance of J+1 node, W/K
C      APO = Thermal capacitance of node (I,J), kJ/m K
C
C      Heat fluxes
C      QAZ = Outside surface heat flux, W/m**2
C      QDIR = Direct solar heat flux, W/m**2
C      QGASP = Total heat added to gas at position DZ/2, kJ
C      QGASDZ = Total heat added to gas at postion DZ, kJ
C      QIJ = Radiation to element (I,J), W/m**2
C      QIDIR = Indirect solar heat flux, W/m**2
C      QINTR = Heat input on internal surface, W/m**2
C      QZ = Integrated avg. axial multiplier on heat flux
C      QZZ = Local axial multiplier on heat flux
C      QZ_ = Constant on fit of QZ
C
C*****
C
C      PROGRAM SOLDTESS
C
C      REAL KLIQ, KMET, KSOL, LENGTH, MIN(11), NTU
C      DIMENSION THETA(10), TP(15,10)
C
C      COMMON/BLOKA/CVLIQ, CVMET, CVSOL, DENLIQ, DENMET, DENSOL, HFL,
C      , KLIQ, KMET, KSOL, LENGTH, RMELT(25,20), ROMELT(25,20), VOID
C      COMMON/BLOKC/DTIME, DX, DY, TO(25,20)
C      COMMON/BLOKE/A(25), B(25), C(25), D(25), Q(10), QNA(20), T(25,20)
C      COMMON/BLOKF/I, J, NI, NJ
C      DATA U/400.0/
C
C*****
C
C      OPEN INPUT AND OUTPUT FILES
C*****
C
C      OPEN(8, FILE='INPUT.TXT')
C      OPEN(7, FILE='OUTPUT.TXT')

```

```

II=1
READ(8,2100,ERR=93) IMAX,NORBIT,NI,NJ,NTIME
READ(8,2200,ERR=94) H,H1,W,BORL,SORL
READ(8,2200,ERR=95) CVLIQ,DENLIQ,KLIQ,LENGTH,THMELT
READ(8,2200,ERR=96) CVSOL,DENSOL,KSOL,ERRMAX,HFL
READ(8,2200,ERR=97) CVMET,DENMET,KMET,GASMIX,TIMER
1 READ(8,2200,ERR=99,END=5) MIN(II),Q(II),DUM2,DUM3,DUM4
II=II+1
MIN(II)=1.E9
GO TO 1

```

```

C
C*****
C
C          INITIALIZE LOOP COUNTERS AND ERROR FLAGS          *
C
C*****
C

```

```

5 ITEMP=0
DX=H1/FLOAT(NJ)
NI=INT(H/DX+0.5)
DXX=H-DX*FLOAT(NI-1)
DY=W/FLOAT(2*NJ)
DTIME=60.0*TIMER/FLOAT(NTIME)

```

```

C
DO 10 II=1,NI
DO 10 JJ=1,NJ
    T(II,JJ)=-1.0
    TP(II,JJ)=T(II,JJ)
    RMELT(II,JJ)=0.0
10 CONTINUE
T1AVG=T(1,1)

```

```

C
C*****
C
C          BEGIN CALCULATIONAL LOOPS ON LENGTH, TIME, ANGLE          *
C
C*****
C

```

```

DO 100 NO=1,NORBIT
NPUT=0
TIME=0.0
DO 100 N=1,NTIME

```

```

IF(MIN(NPUT+1) .LE. TIME+0.1E-6)NPUT=NPUT+1

```

```

DO 20 JJ=1,NJ
    QNA(JJ)=Q(NPUT)/FLOAT(NJ)
DO 20 II=1,NI
    ROMELT(II,JJ)=RMELT(II,JJ)
    TO(II,JJ)=T(II,JJ)

```

```
20      CONTINUE
C
      ICOUNT=0
30      IFLAG=0
      ICOUNT=ICOUNT+1
C
      CALL SODIUM(NPUT, THMELT, TKNA, TNA, U)
C
      DO 40 J=1, NJ
          CALL CONDUCT(BORL, DXX, SORL, TNA, U)
          CALL SOLVER
40      CONTINUE
C
      DO 50 II=1, NI
      DO 50 JJ=1, NJ
          ERROR=ABS(T(II, JJ) - TP(II, JJ)) / THMELT
          IF(ERROR .GT. ERRMAX) IFLAG=2
          IF(ERROR .GT. ERRMAX) ITEMP=ITEMP+1
          TP(II, JJ)=T(II, JJ)
50      CONTINUE
C
      IF(ICOUNT .GT. IMAX) THEN
          WRITE(7, 1000) ITEMP
          IFLAG=0
      ENDIF
C
      IF(IFLAG .GE. 1) GO TO 30
      TIME=TIME+DIME/60.0
      IF(NO .LT. NORBIT) GO TO 100
C
      WRITE(7, 1050)
      WRITE(7, 1250)
      WRITE(7, 1100) TIME, TKNA
      DO 70 II=1, NI
          DO 60 JJ=1, NJ
              THETA(JJ)=T(II-(JJ-1), JJ)+THMELT
60          CONTINUE
          JJJ=AMINO(II, NJ)
          WRITE(7, 1200) (THETA(JJ), JJ=1, JJJ)
70          CONTINUE
C
          WRITE(7, 1050)
          WRITE(7, 1250)
          DO 80 I=1, NI
              JJJ=AMINO(NJ, I)
              WRITE(7, 1350) (RMELT(I-(JJ-1), JJ), JJ=1, JJJ)
80          CONTINUE
C
100 CONTINUE
C
```

```

C*****
C
C          INPUT AND OUTPUT FORMAT STATEMENTS
C
C*****
C
1000 FORMAT(1X,'FAILED TO CONVERGE AFTER ',I6,' ITERATIONS.')
1050 FORMAT(1X,' ')
1100 FORMAT(1X,' Time = ', 1F6.1,' min.      Sodium Temp. = ',
, 1F6.1,' K.')
1200 FORMAT(10F7.1)
1250 FORMAT(1X,'=====',
+ '=====')
1300 FORMAT(1X,'Avg. Gas Temp. = ',F6.1,'K  Out. Gas temp.',F6.1,'K H =
+ ',F7.4,'KW/m2-K')
1350 FORMAT(10F7.4)
1400 FORMAT(1X,'INPUT FORMAT ERROR IN 1ST LINE')
1401 FORMAT(1X,'INPUT FORMAT ERROR IN 2ND LINE')
1402 FORMAT(1X,'INPUT FORMAT ERROR IN 3RD LINE')
1403 FORMAT(1X,'INPUT FORMAT ERROR IN 4TH LINE')
1404 FORMAT(1X,'INPUT FORMAT ERROR IN 5TH LINE')
1405 FORMAT(1X,'INPUT FORMAT ERROR IN 6TH LINE')
1406 FORMAT(1X,'INPUT FORMAT ERROR IN TRANSIENT SECTION')
2100 FORMAT(I6,4I10)
2200 FORMAT(5F10.4)
STOP
93 WRITE(*,1400)
STOP
94 WRITE(*,1401)
STOP
95 WRITE(*,1402)
STOP
96 WRITE(*,1403)
STOP
97 WRITE(*,1404)
STOP
98 WRITE(*,1405)
STOP
99 WRITE(*,1406)
STOP
END

```

APPENDIX C

PROGRAM FOR THE THERMAL ANALYSIS
OF THE
PEBBLE BED RECEIVER

```

PROGRAM MAIN
C*****
C*****
C
C
C          TEST COEFF
C
C*****
C*****
C
DIMENSION TL(15,10,20),RL(15,10,20)
COMMON/BLOKF/I,J,L,NI,NJ,NL,ITIME,MODE
COMMON/BLOKA/RMELT(15,10),KLIQ,KSOL,KGAS,KMET,VOID,EPS,
,          DRM,RO,DENLIQ,CVLIQ,CVSOL,DENMET,CVMET,HFL,
,          SAPUV,PI,PR,REP,H,CVPURE,DENPURE,DENSOL,
,          ROMELT(15,10),RPMELT(15,10)
COMMON/BLOKB/DZ,DTIME,DR,QAQ,QZ,HEAT
COMMON/BLOKD/TGAS(50),TO(15,10),T(15,10),AREA,GASMAS,
,          TGASO(50),GASMIX,TGASIN,DP,VF,DPHI,CPGAS,
,          DENGAS,TP(15,10),TGASP(50),TGAST(50,100)
COMMON/BLOKG/KE(15,10),KW(15,10),KN,KS,HWGAS(10),HWSOL
COMMON/BLOKJ/A(15),B(15),C(15),D(15)
COMMON/BLOKO/KPSOL,KPURE,K(3,3)
COMMON/BLOKX/FCTR
COMMON/BLOKS/Q1DIR,Q1IN,Q2DIR,Q2IN

REAL KPSOL,KSOL,KPURE,DFT,DF,KSTAG,KCOND,KRAD,KRO,FS,KWKF
REAL KFSTAG,KFF,KWALL,KWRAD,K,KLIQ,KGAS,KMET,LENGTH
REAL KN,KS,KE,KW
INTEGER DTIME
OPEN(8,FILE='INPDATA.TXT')

READ(8,*)NI,NJ,NL,NTIME,DTIME,NORBIT
READ(8,*)DP,DRM,RO,LENGTH,VF,SAPUV,SAPUVW
READ(8,*)KLIQ,CVLIQ,DENLIQ,THMELT
READ(8,*)KSOL,CVSOL,DENSOL,HFL
READ(8,*)KMET,CVMET,DENMET,EPS
READ(8,*)TGASIN,GASMAS,GASMIX
READ(8,*)FCTR,ERRMAX,Q1DIR,Q1IN,Q2DIR,Q2IN,IMAX

PI=3.14159
DPHI=3.14159/NJ
AREA=PI*RO**2
DR=RO/(NI-1)
DZ=LENGTH/NL
OPEN(5,FILE='TEMP.TXT')
DO 12 IORBIT=1,NORBIT
DO 12 MODE=1,2
  IF (MODE .EQ. 2) NTIME=2160
  IF (MODE .EQ. 1) NTIME=3240

```

```

DO 12 L=1,NL
DO 12 ITIME=1,NTIME/DTIME
IF ((ITIME .EQ. 1).AND.(MODE .EQ. 1)
& .AND.(IORBIT .EQ. 1)) THEN
    TGAS(L)=TGASIN
    TGASO(L)=TGASIN
    DO 6 II=1,NI
    DO 6 JJ=1,NJ
        T(II,JJ)=1218.0
        TO(II,JJ)=1218.0
        TP(II,JJ)=1218.0
        ROMELT(II,JJ)=0.0
        RMELT(II,JJ)=0.0
6    CONTINUE
    ELSEIF (ITIME .EQ. 1) THEN
        TGASO(L)=TGAST(L,NTIME/DTIME)
        TGAS(L)=TGASO(L)
        TGASP(L)=TGASO(L)
        DO 7 II=1,NI
        DO 7 JJ=1,NJ
            TO(II,JJ)=TL(II,JJ,L)
            T(II,JJ)=TO(II,JJ)
            TP(II,JJ)=TO(II,JJ)
            ROMELT(II,JJ)=RL(II,JJ,L)
            RMELT(II,JJ)=ROMELT(II,JJ)
7    CONTINUE
    ENDIF
    JKJ=0
400    HEAT=0.0
    DO 11 J=1,NJ
        CALL TGAS2(KGAS,H,PR,REP)
500        DO 10 I=1,NI
            CALL TCON
            CALL TCOEFF
10        CONTINUE
            CALL TSOLVER
            CALL TMELT(THMELT)
11    CONTINUE
    CALL TGASTEMP
2200    FORMAT(1X,'TGAS(',I1,')=' ,F7.2)
    DO 30 J=1,NJ
    DO 30 I=1,NI
        IF (ABS(T(I,J)-TP(I,J)) .GE. ERRMAX) THEN
            DO 40 JJ=1,NJ
            DO 40 II=1,NI
                TP(II,JJ)=T(II,JJ)
40        CONTINUE
            JKJ=JKJ+1
            WRITE(*,2216) IORBIT,MODE,L,ITIME,JKJ
2216    FORMAT('+',4I3,5X,I4)

```

```

                IF (JKJ .GT. IMAX) THEN
                WRITE(5,7000)JKJ
7000          FORMAT(1X,'FAILED TO CONVERGE AFTER',I4,'
& ITERATIONS')
                GO TO 700
                ENDIF
                GO TO 400
                ENDIF
30          CONTINUE
          SUMT2=0.0
          SUMR2=0.0
          DO 28 I=1,NI
            SUMT1=0.0
            SUMR1=0.0
            DO 29 J=1,NJ
              CVPURE=RMELT(I,J)*CVLIQ+
+              (1.0-RMELT(I,J))*CVSOL
              SUMT1=SUMT1+(T(I,J)-TO(I,J))*CVPURE
              IF (I .EQ. 1) GO TO 29
              SUMR1=SUMR1+(RMELT(I,J)-ROMELT(I,J))
29          CONTINUE
            RS=(NI-I)*RO/(NI-1)
            RN=RS+RO/(NI-1)
            VOLUME=(DPHI/2)*(RN-RS)*(RN+RS)*DZ
            PRODT=VOLUME*SUMT1
            PRODR=VOLUME*SUMR1
            SUMT2=SUMT2+PRODT
            SUMR2=SUMR2+PRODR
28          CONTINUE
          QLAT=2*(1-VF)*DENPURE*SUMR2*HFL/DTIME
          QSENS=2*(1-VF)*DENPURE*SUMT2/DTIME
          IF (L .EQ. 1) THEN
            TGASB=TGASIN
          ELSE
            TGASB=TGAST(L-1,ITIME)
          ENDIF
          QGAS=GASMAS*CPGAS*(TGAS(L)-TGASB)
700          TGASO(L)=TGAS(L)
          TGAST(L,ITIME)=TGAS(L)
          WRITE(5,*)
          WRITE(5,*)
          WRITE(5,*)
          WRITE(5,3500)IORBIT,MODE,ITIME,L
3500          FORMAT(1X,'IIIIII ORBIT # ',I1,' IIIIII MODE ',I1,'
&          IIIIII TIME=',I1,' IIIIII L=',I1,' IIIIII')
          WRITE(5,*)
          DO 15 I=1,NI
            WRITE(5,2000)(T(I,J),J=NJ,1,-1)
2000          FORMAT(1X,10(F6.1,1X))

```

```
15      CONTINUE
        WRITE(5,*)
        DO 18 I=1,NI
          WRITE(5,2100) (RMELT(I,J),J=NJ,1,-1)
2100      FORMAT(1X,10(F6.3,1X))
        18      CONTINUE
        WRITE(5,*)
        WRITE(5,8000) KGAS,H,PR,REP
8000      FORMAT(1X,'KGAS=',F9.7,3X,'H=',F6.4,3X,'PR=',F6.4,
&          3X,'REP=',F8.3)
        WRITE(5,2200) L,TGAS(L)
        HEAT=HEAT*DZ
        WRITE(5,8001) QZ,HEAT
8001      FORMAT(1X,'HEAT INPUT FRAC. =',F8.5,3X,'HEAT=',F8.5)
        WRITE(5,*)
        WRITE(5,8002) QGAS,QLAT,QSENS
8002      FORMAT(1X,'QGAS=',F7.5,5X,'QLAT=',F7.5,5X,
&          'QSENS=',F7.5)
        DO 16 I=1,NI
        DO 16 J=1,NJ
          TO(I,J)=T(I,J)
          TP(I,J)=T(I,J)
          TL(I,J,L)=T(I,J)
          ROMELT(I,J)=RMELT(I,J)
          RL(I,J,L)=RMELT(I,J)
        16      CONTINUE
        12      CONTINUE
5000  END
```

```

C
C
C *****
C *****
C
C
C          SUBROUTINE GASPROP
C
C This program calculates the effective thermal properties*
C and convective coefficients for the gas coolant.
C The gas coolant is assumed to be a mixture of He and Xe.*
C Properties of these two constituents are included as
C curve fits with the corresponding coefficients included *
C as data in the subroutine.
C
C *****
C *****
C
C *****
C
C REFERENCES
C M. R. Vanco, "Analytical Comparison of Relative Heat
C Transfer Coefficients & Pressure Drops of Inert Gases
C and Their Binary Mixtures", Lewis Research Center
C
C A. J. Chapman "Fundamentals of Heat Transfer"
C Macmillan, 1978, p 329.
C
C *****
C
C *****
C
C EQUATIONS
C      K1 = K11 + K12*(TGAS - K13)**K14
C      K2 = K21 + K22*(TGAS - K23)**K24
C
C      VISC1 = VISC11 + VISC12*(TGAS - VISC13)**VISC14
C      VISC2 = VISC21 + VISC22*(TGAS - VISC23)**VISC24
C
C *****
C
C SUBROUTINE TGAS2(KGAS,H,PR,REP)
C REAL K,K1,K2,K11,K12,K13,K14,K21,K22,K23,K24,MW,MW1,MW2,
C ,KGAS
C COMMON/BLOKD/TGAS(50),TO(15,10),T(15,10),AREA,GASMAS,
C ,TGASO(50),GASMIX,TGASIN,DP,VF,DPHI,CPGAS,
C ,DENGAS,TP(15,10),TGASP(50),TGAST(50,100)
C COMMON/BLOKF/I,J,L,NI,NJ,NL,ITIME,MODE
C COMMON/BLOKG/KE(15,10),KW(15,10),KN,KS,HWGAS(10),HWSOL
C DATA GAMMA,PI,RUNIV,MW1,MW2/
C /1.66,3.14159,8.31434,4.0,131.0/
C DATA K11,K12,K13,K14/0.1580E-3,0.9086E-6,333.333,0.794/

```

```

DATA K21,K22,K23,K24/0.640E-5,0.0454E-6,333.333,0.800/
DATA VISC11,VISC12,VISC13,VISC14/
/.2158E-4,.1022E-6,333.333,.825/
DATA VISC21,VISC22,VISC23,VISC24/
/0.253E-4,0.2452E-6,333.333,0.77/
F1(X,Y)=(1.0+2.41*(X-Y)*(X-0.142*Y)/(X+Y)**2)
F2(X1,X2,X3,X4,X5,X6)=
=((1.0+(X1/X2)**0.5*(X3/X4)**0.25)**2)/
/(2.0*2.0**0.5*(1.0+X5/X6)**0.5)
C
C *****
C
C FIND THE THERMAL CONDUCTIVITY & VISCOSITY OF PURE GASES *
C
C *****
C
K1=K11+K12*(TGAS(L)-K13)**K14
K2=K21+K22*(TGAS(L)-K23)**K24
VISC1=VISC11+VISC12*(TGAS(L)-VISC13)**VISC14
VISC2=VISC21+VISC22*(TGAS(L)-VISC23)**VISC24
C
C *****
C
C FIND THE WEIGHTING PARAMETERS FROM REFERENCE *
C
C *****
C
PHI12=F2(VISC1,VISC2,MW2,MW1,MW1,MW2)
PHI21=PHI12*(VISC2*MW1)/(VISC1*MW2)
PSI12=F2(K1,K2,MW1,MW2,MW1,MW2)*F1(MW1,MW2)
PSI21=F2(K2,K1,MW2,MW1,MW2,MW1)*F1(MW2,MW1)
C
C *****
C
C SOLVE FOR THE THERMAL CONDUCTIVITY *
C AND VISCOSITY OF GAS MIX *
C
C *****
C
VISC=VISC1/(1.0+PHI12*(1.0-GASMIX)/GASMIX)+
/ VISC2/(1.0+PHI21*(GASMIX/(1.0-GASMIX)))
KGAS=K1/(1.0+PSI12*(1.0-GASMIX)/GASMIX)+
/ K2/(1.0+PSI21*(GASMIX/(1.0-GASMIX)))
C *****
C
C SOLVE FOR SPECIFIC HEAT OF GASMIX *
C
C *****
C
MW=GASMIX*MW1+(1.0-GASMIX)*MW2

```

```

      CPGAS=GAMMA*RUNIV/((GAMMA-1.0)*MW)
C
C
C*****
C
C CORRELATION RECOMMENDED FOR GAS FLOW IN A BED OF SPHERES*
C
C           $(\bar{e}_j)_h = (\bar{e}_j)_m = 2.06 (Re)^{-0.575}$ 
C
C j are the Colburn j factors, and e is the void fraction *
C
C REFERENCE
C Incropera, Frank P. , "Fundamentals of Heat and Mass
C Transfer", 2nd Edition, John Wiley & Sons Inc., 1981.
C p 292,352.
C
C*****
C
C PR=CPGAS*VISC/(KGAS)
C REP=GASMAS*DP/(VISC*AREA)
C H=(2.06/VF)*(KGAS/DP)*PR**(1.0/3)*REP**0.425
C DENGAS=11.22
C
C RETURN
C END

```

```

C
C *****
C *****
C
C
C          SUBROUTINE COEFF
C
C      This program develops finite difference matrix for
C      conduction analysis in cylindrical coordinates.
C
C *****
C *****
C
C      SUBROUTINE TCOEFF
C      COMMON/BLOKA/RMELT(15,10),KLIQ,KSOL,KGAS,KMET,VOID,EPS,
C      ,          DRM,RO,DENLIQ,CVLIQ,CVSOL,DENMET,CVMET,HFL,
C      ,          SAPUV,PI,PR,REP,H,CVPURE,DENPURE,DENSOL,
C      ,          ROMELT(15,10),RPMELT(15,10)
C      COMMON/BLOKB/DZ,DTIME,DR,QAZ,QZ,HEAT
C      COMMON/BLOKD/TGAS(50),TO(15,10),T(15,10),AREA,GASMAS,
C      ,          TGASO(50),GASMIX,TGASIN,DP,VF,DPHI,CPGAS,
C      ,          DENGAS,TP(15,10),TGASP(50),TGAST(50,100)
C      COMMON/BLOKF/I,J,L,NI,NJ,NL,ITIME,MODE
C      COMMON/BLOKG/KE(15,10),KW(15,10),KN,KS,HWGAS(10),HWSOL
C      COMMON/BLOKJ/A(15),B(15),C(15),D(15)
C
C      INTEGER DTIME
C      REAL KN,KS,KE,KW
C
C      CVPURE=RMELT(I,J)*CVLIQ+(1.0-RMELT(I,J))*CVSOL
C      DENPURE=DENLIQ
C      DR=RO/(NI-1)
C      RS=(NI-I)*DR
C
C      IF(I.EQ.1) THEN
C          DR=DRM
C          DRS=((RO/(NI-1))+DR)/2
C          GO TO 100
C      ELSEIF (I.EQ.2) THEN
C          DRN=(DR+DRM)/2
C          DRS=DR
C          GO TO 100
C      ELSEIF (I.EQ.NI) THEN
C          RS=0.0
C          DRN=DR
C          GO TO 100
C      ELSE
C          GO TO 90
C      ENDIF
C
C 90 DRN=DR

```

C-2

```
DRS=DR
100 RN=RS+DR
RE=RS+DR/2
RW=RE
DV=(DPHI/2)*(RN-RS)*(RN+RS)
PF=1-VF
AE=KE(I,J)*DR/(RE*DPHI)
AW=KW(I,J)*DR/(RW*DPHI)
C
IF (I.EQ.NI) THEN
  C(I)=0.0
  GO TO 250
ENDIF
C
AWALL=PI*RO/NJ
C(I)=- (KS*RS*DPHI/DRS)
C
IF (I.EQ.1) GO TO 290
C
250 A(I)=- (KN*RN*DPHI/DRN)
BC=H*SAPUV*DV*TGAS(L)+PF*DENPURE*CVPURE*DV*TO(I,J)/DTIME
/+PF*DENPURE*HFL*DV*(ROMELT(I,J)-RMELT(I,J))/DTIME
B(I)=AE+AW-C(I)-A(I)+H*SAPUV*DV+PF*DENPURE*CVPURE*DV/DTIME
D(I)=AE*T(I,J-1)+AW*T(I,J+1)+BC
GO TO 300
C
290 C(I)=C(I)
B(I)=AE+AW-C(I)+DENMET*CVMET*DV/DTIME+HWGAS(J)*AWALL
CALL TSOLAR
BC=(DENMET*CVMET*DV*TO(I,J)/DTIME)+QAZ+HWGAS(J)*AWALL*
*TGAS(L)
D(I)=AE*T(I,J-1)+AW*T(I,J+1)+BC
A(I)=0.0
C
300 RETURN
END
```

```

C          *****
C          *****
C          C
C          C          SUBROUTINE CONDUCT          *
C          C          *
C          C          *
C          C This program calculates the interface conductivities to*
C          C the north, south, east, and west of the element (I,J). *
C          C          *
C          C*****
C          C*****
C          C
C          SUBROUTINE TCON
C
C          COMMON/BLOKF/I,J,L,NI,NJ,NL,ITIME,MODE
C          COMMON/BLOKA/RMELT(15,10),KLIQ,KSOL,KGAS,KMET,VOID,EPS,
C          ,
C          ,          DRM,RO,DENLIQ,CVLIQ,CVSOL,DENMET,CVMET,HFL,
C          ,          SAPUV,PI,PR,REP,H,CVPURE,DENPURE,DENSOL,
C          ,          ROMELT(15,10),RPMELT(15,10)
C          COMMON/BLOKD/TGAS(50),TO(15,10),T(15,10),AREA,GASMAS,
C          ,          TGASO(50),GASMIX,TGASIN,DP,VF,DPHI,CPGAS,
C          ,          DENGAS,TP(15,10),TGASP(50),TGAST(50,100)
C          COMMON/BLOKG/KE(15,10),KW(15,10),KN,KS,HWGAS(10),HWSOL
C          COMMON/BLOKO/KPSOL,KPURE,K(3,3)
C
C          REAL KPSOL,KPURE,DFT,DF,KSTAG,KCOND,KRAD,KRO,FS,KWKF
C          REAL KFSTAG,KFF,KWALL,KWRAD,K,KLIQ,KSOL,KGAS,KMET,KWGRAD
C          REAL KN,KS,KE,KW,NUM
C
C          DO 110 II=2,3
C          IF ((I.EQ.1).AND.(II.NE.3)) GO TO 110
C
C          IF ((I.EQ.NI).AND.(II.EQ.3)) THEN
C             KN=KS
C             KS=0.0
C             GO TO 155
C          ENDIF
C
C          DO 120 JJ=2,3
C
C          IF (II.EQ.2) THEN
C             IF (JJ.EQ.2) THEN
C                VOID=(1.0-DENLIQ/DENSOL)*(1.0-RMELT(I,J))
C             ELSE
C                VOID=(1.0-DENLIQ/DENSOL)*(1.0-RMELT(I,J+1))
C             ENDIF
C          ELSE
C             VOID=(1.0-DENLIQ/DENSOL)*(1.0-RMELT(I+1,J))
C          ENDIF
C
C          IJ=J

```

```

IF (II.EQ.2) IJ=J-2+JJ
IF ((J.EQ.NJ).AND.(JJ.EQ.3)) THEN
  KW(I,J)=0.0
  GO TO 105
ENDIF
C
C *****
C
C CALCULATE THE EFFECT OF VOID ON CONDUCTIVITY OF SOLID *
C USE CORRELATION BY MEREDITH & TOBIAS TO CORRECT *
C CONDUCTIVITY *
C *****
C
KPSOL=KSOL*(2.0*(1.0-VOID)+0.6135*VOID**2.333-1.6*
*VOID**3.333)/
/(2.0+VOID+0.6135*VOID**2.333-0.6975*VOID**3.333)
C
C *****
C FIND CONDUCTIVITY OF PURE MATERIAL *
C *****
C
JI=I
IF (II .EQ. 3) JI=I+1
KPURE=1.0/((RMELT(JI,IJ)/KLIQ)+((1.0-RMELT(JI,IJ))/KPSOL))
HRS=0.227*(EPS/(2.0-EPS))*(T(I,J)**3)*10E-9
HRV=.227*T(I,J)**3*10E-9/(1+VF*(1.0-EPS)/(2*(1-VF)*EPS))
C
C *****
C FIND THE EFFECTIVE CONDUCTIVITY OF THE BED USING METHOD*
C OF SUMMED RESISTANCE OVER VARIOUS HEAT TRANSFER PATHS *
C " HANDBOOK OF HEAT TRANSFER APPLICATIONS, *
C 2nd EDITION, 1985, pp. 6-10,6-18. *
C *****
C
DFT=((KPURE-KGAS)/KPURE)**2
DF=((0.25*DFT)/(ALOG(KPURE/KGAS)-DFT))-KGAS/(3*KPURE)
NUM=((KPURE-KGAS)/KPURE)**2
D1=ALOG((KPURE/KGAS)-.9128*((KPURE/KGAS)-1.0))
D2=((KPURE-KGAS)/KPURE)*.0872
PHI=((1.0/12)*NUM/(D1-D2))-(2.0/3)*(KGAS/KPURE)
D=(1/PHI)+(DP*HRS/KGAS)
KSTAG=VF*(1+HRV*DP/KGAS)+(1-VF)/
/(1.0/D)+(2.0/3)*KGAS/KPURE)
KCOND=(KSTAG+0.11*PR*REP)*KGAS
K(II,JJ)=KCOND

```

```

105 IF (II.EQ.3) GO TO 110
120 CONTINUE
110 CONTINUE
C      C
C      C*****
C      C  FIND WALL-TO-BED CONDUCTIVITY USING THE METHOD OF
C      C
C      C          "EFFECTIVE PATH LENGTH"
C      C
C      C "HANDBOOK OF HEAT TRANSFER APPLICATIONS 2nd EDITION,
C      C 1985, pp. 6-10,6-18.
C      C*****
C      C
C      C IF (I.EQ.1) THEN
190    KWKF=2.0*0.7+(1.0-0.7)/(DF+(KGAS/(3.0*KPURE)))
        KFSTAG=1.0/KWKF-(0.5*KGAS/KSTAG)
        KFF=1.0/KFSTAG+0.054*PR*REP
        KWALL=KFF*KGAS/DP
        DEN=(VF*(1.0-EPS)*10E+6)/(2.0*(1-VF)*EPS)
        KWGRAD=(0.227*T(I,J)**3/(DEN+1.0))/1000
        HWGAS(J)=KWALL
        HWSOL=((0.227*(EPS/(2.0-EPS))*(T(I,J)**3*10E-6))/1000)+
+      KWRAD
        KE(I,J)=KMET
        IF (J .EQ. 1) KE(I,J)=0.0
        KW(I,J)=KMET
        IF (J .EQ. NJ) KW(I,J)=0.0
        FS=DRM/(DRM+RO/(NI-1.0))
        K(3,2)=KWKF*KGAS+0.11*PR*REP*KGAS+HWSOL*
*      (RO/(NI-1.0)+DRM)/2.0
        KS=1.0/(FS/KMET+(1.0-FS)/K(3,2))
        KN=0.0
        GO TO 200
    ENDIF
C
    KN=KS
    KS=1.0/(0.5/K(2,2)+0.5/K(3,2))
C
155 IF (J.EQ.1) THEN
        KE(I,J)=0.0
        GO TO 195
    ELSE
        KE(I,J)=KW(I,J-1)
    ENDIF
C
    IF ((KW(I,J).EQ.0) .AND. (J .EQ. NJ)) GO TO 200
195 KW(I,J)=1.0/(0.5/K(2,2)+0.5/K(2,3))
200 RETURN
    END

```

```

C
C *****
C *****
C
C
C          SUBROUTINE GASPROP
C
C
C This program calculates the effective thermal properties*
C and convective coefficients for the gas coolant.
C The gas coolant is assumed to be a mixture of He and Xe.*
C Properties of the two constituents are included as curve*
C fits with the corresponding coefficients included as
C data in the routine.
C
C *****
C *****
C
C *****
C
C REFERENCES
C M. R. Vanco, "Analytical Comparison of Relative Heat
C Transfer Coefficients and Pressure Drops of Inert
C Gases and Their Binary Mixtures", Lewis Research Center*
C
C A. J. Chapman "Fundamentals of Heat Transfer"
C Macmillan, 1978, p 329.
C
C *****
C *****
C
C EQUATIONS
C
C      K1 = K11 + K12*(TGAS - K13)**K14
C      K2 = K21 + K22*(TGAS - K23)**K24
C
C      VISC1 = VISC11 + VISC12*(TGAS - VISC13)**VISC14
C      VISC2 = VISC21 + VISC22*(TGAS - VISC23)**VISC24
C
C *****
C
C SUBROUTINE TGAS2(KGAS,H,PR,REP)
C REAL K,K1,K2,K11,K12,K13,K14,K21,K22,K23,K24,MW,MW1,MW2,
C ,KGAS
C COMMON/BLOKD/TGAS(50),TO(15,10),T(15,10),AREA,GASMAS,
C ,
C , TGASO(50),GASMIX,TGASIN,DP,VF,DPHI,CPGAS,
C , DENGAS,TP(15,10),TGASP(50),TGAST(50,100)
C COMMON/BLOKF/I,J,L,NI,NJ,NL,ITIME,MODE
C COMMON/BLOKG/KE(15,10),KW(15,10),KN,KS,HWGAS(10),HWSOL
C DATA GAMMA,PI,RUNIV,MW1,MW2/
C /1.66,3.14159,8.31434,4.0,131.0/
C DATA K11,K12,K13,K14/0.1580E-3,0.9086E-6,333.333,0.794/

```

```

DATA K21,K22,K23,K24/0.640E-5,0.0454E-6,333.333,0.800/
DATA VISC11,VISC12,VISC13,VISC14/
/.2158E-4,.1022E-6,333.333,.825/
DATA VISC21,VISC22,VISC23,VISC24/
/0.253E-4,0.2452E-6,333.333,0.77/
F1(X,Y)=(1.0+2.41*(X-Y)*(X-0.142*Y)/(X+Y)**2)
F2(X1,X2,X3,X4,X5,X6)=
=((1.0+(X1/X2)**0.5*(X3/X4)**0.25)**2)/
/(2.0*2.0**0.5*(1.0+X5/X6)**0.5)
C
C
C*****
C
C FIND THE THERMAL CONDUCTIVITY & VISCOSITY OF PURE GASES *
C
C*****
C
K1=K11+K12*(TGAS(L)-K13)**K14
K2=K21+K22*(TGAS(L)-K23)**K24
VISC1=VISC11+VISC12*(TGAS(L)-VISC13)**VISC14
VISC2=VISC21+VISC22*(TGAS(L)-VISC23)**VISC24
C
C
C*****
C
C FIND THE WEIGHTING PARAMETERS FROM REFERENCE *
C
C*****
C
PHI12=F2(VISC1,VISC2,MW2,MW1,MW1,MW2)
PHI21=PHI12*(VISC2*MW1)/(VISC1*MW2)
PSI12=F2(K1,K2,MW1,MW2,MW1,MW2)*F1(MW1,MW2)
PSI21=F2(K2,K1,MW2,MW1,MW2,MW1)*F1(MW2,MW1)
C
C
C*****
C
C SOLVE FOR THE THERMAL CONDUCTIVITY & VISCOSITY OF MIX *
C
C*****
C
VISC=VISC1/(1.0+PHI12*(1.0-GASMIX)/GASMIX)+
/
VISC2/(1.0+PHI21*(GASMIX/(1.0-GASMIX)))
KGAS=K1/(1.0+PSI12*(1.0-GASMIX)/GASMIX)+
/
K2/(1.0+PSI21*(GASMIX/(1.0-GASMIX)))
C
C
C*****
C
C SOLVE FOR SPECIFIC HEAT OF GASMIX *
C
C*****
C
MW=GASMIX*MW1+(1.0-GASMIX)*MW2
CPGAS=GAMMA*RUNIV/((GAMMA-1.0)*MW)

```

```

C
C
C *****
C
C CORRELATION RECOMMENDED FOR GAS FLOW IN A BED OF SPHERES*
C
C          (eh) = (em) = 2.06 (Re)-0.575
C
C j are the Colburn j factors, and e is the void fraction *
C
C REFERENCE
C Incropera, Frank P. , "Fundamentals of Heat and Mass
C Transfer", 2nd Edition, John Wiley & Sons Inc., 1981,
C p 292,352.
C *****
C
C PR=CPGAS*VISC/(KGAS)
C REP=GASMAS*DP/(VISC*AREA)
C H=(2.06/VF)*(KGAS/DP)*PR**(1.0/3.0)*REP**0.425
C DENGAS=11.22
C
C RETURN
C END
C

```

```

C *****
C *****
C
C          SUBROUTINE GASTEMP
C
C This program solves for the temperature of the working
C fluid. The energy equation has been discretized using
C the upwind scheme to calculate the convection term.
C   Ref: " Numerical Heat Transfer And Fluid Flow ",
C   Suhas V. Patankar.
C *****
C *****
C
C          SUBROUTINE TGASTEMP
C
C          COMMON/BLOKA/RMELT (15,10) , KLIQ, KSOL, KGAS, KMET, VOID, EPS,
C          , DRM, RO, DENLIQ, CVLIQ, CVSOL, DENMET, CVMET, HFL,
C          , SAPUV, PI, PR, REP, H, CVPURE, DENPURE, DENSOL,
C          , ROMELT (15,10) , RPMELT (15,10)
C          COMMON/BLOKD/TGAS (50) , TO (15,10) , T (15,10) , AREA, GASMAS,
C          , TGASO (50) , GASMIX, TGASIN, DP, VF, DPFI, CPGAS,
C          , DENGAS, TP (15,10) , TGASP (50) , TGAST (50,100)
C          COMMON/BLOKB/DZ, DTIME, DR, QAZ, QZ, HEAT
C          COMMON/BLOKF/I, J, L, NI, NJ, NL, ITIME, MODE
C          COMMON/BLOKG/KE (15,10) , KW (15,10) , KN, KS, HWGAS (10) , HWSOL
C
C          REAL KGAS
C          INTEGER DTIME
C
C          DR=RO/(NI-1)
C          QWALL1=0.0
C          QWALL2=0.0
C          QBED1=0.0
C          QBED2=0.0
C          AWALL=(PI*RO/NJ)*DZ
C          DO 11 JQ=1,NJ
C          DO 11 IQ=2,NI
C             RS=(NI-IQ)*DR
C             RN=RS+DR
C             DV=(DPFI/2)*(RN-RS)*(RN+RS)*DZ
C
C          IF (IQ .EQ. 2) THEN
C             QWALL1=QWALL1+2*HWGAS (JQ) *AWALL*T (1, JQ)
C             QWALL2=QWALL2+2*HWGAS (JQ) *AWALL
C          ENDIF
C
C          QBED1=QBED1+2*H*SAPUV*DV*T (IQ, JQ)
C          QBED2=QBED2+2*H*SAPUV*DV
11 CONTINUE

```

```
C
VOLUME=(PI*RO**2)*DZ
AB=GASMAS*CPGAS
B=(QWALL1+QBED1)+DENGAS*VF*CPGAS*TGASO(L)*VOLUME/DTIME
A=AB +(DENGAS*VF*CPGAS*VOLUME/DTIME)+QWALL2+QBED2
C
IF (L.EQ.1) THEN
    TB=TGASIN
ELSE
    TB=TGAST(L-1,ITIME)
ENDIF
C
TGAS(L)=(AB*TB+B)/A
RETURN
END
```



```
        RMELT(I,J)=RMELT(I,J)+DMELT
    ELSE
        RMELT(I,J)=0.0
    ENDIF
C
    RMELT(I,J)=AMAX1(0.0,RMELT(I,J))
    RMELT(I,J)=AMIN1(1.0,RMELT(I,J))
11  CONTINUE
C
    DO 13 I=1,NI
        T(I,J)=T(I,J)+THMELT
13  CONTINUE
C
    RETURN
    END
```

```

C*****
C*****
C
C
C          SUBROUTINE SOLAR
C
C          This program calculates the solar incidence on
C          the outside perimeter of the containment ring
C
C           $q'' = q''(\text{direct}) \cdot \cos(\text{angle}) + q''(\text{indirect})$ 
C
C*****
C*****
C
C          SUBROUTINE TSOLAR
C
C          DIMENSION CS(21)
C          REAL LENGTH
C          COMMON/BLOKF/I,J,L,NI,NJ,NL,ITIME,MODE
C          COMMON/BLOKB/DZ,DTIME,DR,QAZ,QZ,HEAT
C          COMMON/BLOKS/Q1DIR,Q1IN,Q2DIR,Q2IN
C          DATA CS(1),CS(3),CS(5),CS(7),CS(9),CS(11),CS(13)/
C          /1.0,6*2.0/
C          DATA CS(15),CS(17),CS(19),CS(2),CS(4),CS(6),CS(8)/
C          /3*2.0,4*4.0/
C          DATA CS(10),CS(12),CS(14),CS(16),CS(18),CS(20),CS(21)/
C          /6*4.,1./
C          DATA PI/3.14159/
C          DATA QZ1,QZ2,QZ3,QZ4/24.28,0.08,0.75,0.26244/
C
C*****
C
C          QZ USES SIMPSON'S 1/3 INTEGRATION TO FIND THE
C          INTTEGRATED AVERAGE VALUE OF THE AXIAL POWER CURVE
C          OVER THE INTERVAL DZ
C
C*****
C
C          LENGTH=0.9144
C          POS=DZ*L
C          XL=(POS-DZ)/LENGTH
C          QZ=0.0
C
C          DO 15 II=1,21
C             IF(II .GT. 1) XL=XL+0.05*DZ/LENGTH
C             QZZ=QZ1*XL*EXP(1.0-(XL/QZ2)**QZ3)+QZ4*(XL)**0.5
C             QZ=QZ+CS(II)*(QZZ)/60.0
C 15 CONTINUE
C
C*****
C

```

```

C      FIND THE PROJECTION OF THE DIRECT SOLAR INCIDENCE      *
C                                                                *
C*****
C
C      ANGLE1=PI*FLOAT(J)/FLOAT(NJ)
C      ANGLE2=PI*FLOAT(J-1)/FLOAT(NJ)
C
C      IF (J+J-2 .GT. NJ) THEN
C          SINANGLE=0.0
C      ELSEIF (J+J .GT. NJ) THEN
C          SINANGLE=1.0-SIN(ANGLE2)
C      ELSE
C          SINANGLE=SIN(ANGLE1)-SIN(ANGLE2)
C      ENDIF
C
C*****
C      ADD DIRECT AND INDIRECT INCIDENT SOLAR RADIATION      *
C                                                                *
C*****
C
C      IF (MODE .EQ. 1) THEN
C          QDIR=Q1DIR
C          QINDIR=Q1IN
C      ELSE
C          QDIR=Q2DIR
C          QINDIR=Q2IN
C      ENDIF
C      DPHI=PI/NJ
C      ROCAN=0.04191+0.00127
C      QAZ=(QDIR*SINANGLE + QINDIR*DPHI)*ROCAN*QZ
C      IF(J .EQ. 1) HEAT=0.0
C      HEAT=HEAT+2.0*QAZ
C
C      RETURN
C      END

```


APPENDIX D

PROGRAM FOR THE THERMAL ANALYSIS
OF THE
CAVITY RECEIVER

```

program main
C
common/bloka/a(15),b(15),c(15);d(15)
common/blokb/ni,ne(10),j,t(15,10)
common/blokc/thmelt,tgasin,gasmas,cpgas,ntu,deltp,
+      deltdz
common/blokd/tgasp,gasmix,ro(15),ht,w,dxx,p
common/bloke/rmelt(15,10),denliq,densol,walls,cvmet,
+      denmet,kmet,kliq,ksol,cvliq,cvsol
common/blokf/dz,dtime,rpo(10),gaz,hfl,romelt(15,10),c1,wf,
+      to(15,10),rpmelt(15,10),dx,dy,th,qt,le(15),
+      apoo(15,10),apon(15,10)
common/blokg/k,kn,ks,ke,kw,den,cv
dimension cs(21),q(20),tp(15,10),thgas(20,20),
+      theta(20,10),thn(15,10),rmel(15,10),nn(10)
real ntu,length,kliq,ksol,kmet,k,kn,ks,ke,kw,den,cv,le
C
data cs(1),cs(3),cs(5),cs(7),cs(9),cs(11),cs(13)/
/1.0,6*2.0/
data cs(15),cs(17),cs(19),cs(2),cs(4),cs(6),cs(8)/
/3*2.0,4*4.0/
data cs(10),cs(12),cs(14),cs(16),cs(18),cs(20),cs(21)/
/6*4.,1./
open (8,file='ginput.txt')
open (7,file='goutput.txt')
C
read(8,*)imax,norbit,nj,nl,ntime
read(8,*)length,ht,w,th,sl
read(8,*)gasmas,borl,c1,wf,tr
read(8,*)cvliq,denliq,kliq,walls,thmelt
read(8,*)cvsol,densol,ksol,errmax,hfl
read(8,*)cvmet,denmet,kmet,gasmix,timer
read(8,*)qz1,qz2,qz3,qz4,qz5,qz6
read(8,*)qd,qn,tgas,cor,ft
C*****
p = 3.14
ni = nj
tgasp = tgas
dy = ht/nj
dz = length/float(nl)
dtime = 60.0*timer/float(ntime)
qtime = 54.0*60.0/dtime
C
do 2 j = 1,nj
ro(j) = ni*dy
ne(j) = ni-j+2
2 continue
C
do 100 l = 1,nl
w = p*((nl-l+.5)*dz/sl+tr)/cor

```

```

dx = w/nj
dxx = (dx*dx+dy*dy)**0.5
c
do 10 jj = 1,nj
do 10 ii = 1,15
c
if (ii .gt. ne(jj)) then
  t(ii,jj) = 0.0
else
  t(ii,jj) = -0.00001
endif
c
tp(ii,jj) = t(ii,jj)
rmelt(ii,jj) = 0.0
apon(ii,jj) = 0.0
10 continue
pos = l*dz
xl = pos/length
qzz = qz1+qz2*xl+qz3*xl*xl+qz4*(xl)**3.0+qz5*(xl)**4.0
+      +qz6*(xl)**5.0
qz = qzz-qzzp
qzzp = qzz
c
do 100 no = 1,norbit
do 100 n = 1,ntime
c
if (l .eq. 1) thgas(n,no) = tgas
c
do 30 jj = 1,nj
do 30 ii = 1,15
c
if (ii.gt.ne(jj)) then
  t(ii,jj) = 0.0
  apon(ii,jj) = 0.0
endif
c
to(ii,jj) = t(ii,jj)
romelt(ii,jj) = rmelt(ii,jj)
apoo(ii,jj) = apon(ii,jj)
30 continue
c
if (n.gt.qtime) then
  q(n) = qn
else
  q(n) = qd
endif
c
qaz = q(n)*qz/nj
icount = 0
35 iflag = 0

```

```

        icount = icount+1
        tgasin = thgas(n,no)
        ta=0.0
        tt=0.0
c
        do 24 j = 1,nj
            tt = tt + ne(j)-1
            le(j) = ro(j)-(j-1)*dy
            f = (1-exp(-c1*le(j)))
            ta = ta+f
24 continue
c
        qt = qaz*(nj-ta)*(1-wf)
        qt = qt/tt
        qlat = 0.0
        qsens = 0.0
        grad = 0.0
        tac = 0
        heat = 0.0
        hd = 0.0
c
        do 80 j = 1,nj
            rpo(j) = ro(j)
80 continue
c
        do 40 j = 1,nj
            call gasprop(dz,nj,h,1)
            heat = heat + qaz*dz
            hd = hd+h
            call conduct(borl,i,nj,icount,ft,qlat,qsens,grad,tac)
            call heatgas(nj)
            call solver(i)
40 continue
c
        hd = hd/nj
c
        do 50 jj = 1,nj
            do 50 ii = 1,ne(jj)
                error = abs(t(ii,jj)-tp(ii,jj))
                if (error .gt. errmax) iflag = 2
                tp(ii,jj) = t(ii,jj)
                rpmelt(ii,jj) = rmelt(ii,jj)
50 continue
c
        qgas = gasmas*cpgas*delt dz
        qtotal = qlat+qsens+qgas
        qerror = abs(1.0-qtotal/heat)
c
        if (n .gt. qtime) then
            if (qerror .gt. 0.01) iflag = 2

```

```
    else
      if (qerror .gt. 0.001) iflag = 2
    endif
c
  tgasp = thgas(n,no)+deltp
c
  if (iflag .gt. 1) then
    if (icount .ge. imax) then
      write (7,1000) icount
    else
      goto 35
    endif
  endif
c
  thgas(n,no) = thgas(n,no)+deltdz
c
  do 47 j =1,nj
47 continue
c
  if (no .lt. norbit) goto 100
  write(7,1050)
  write(7,1250)
  write(7,1100)1,no,n
  write(7,1150)heat,qz
  write(7,1151)qtotal
1151 format(1x,'qtotal = ',f10.8)
  nr = 0.0
c
  do 83 j = 1,nj
    nn(j)=ne(j)+j-1
83 continue
c
  do 34 j = 1,nj
    nr = amax1(nr,nn(j))
34 continue
c
  do 36 j = 1,nj
  do 37 i = 1,nr
c
    if (i.gt.ne(j)) then
      rmelt(i,j) = 0.0
      theta(i,j) = 0.0
    else
      theta(i,j) = t(i,j)+thmelt
    endif
c
  37 continue
  36 continue
c
  do 85 j = 1,nj
```

```

do 85 i = 1,nr
c
  if (j.ne.1) then
    thn((i+j-1),j) = theta(i,j)
    rmel((i+j-1),j) = rmelt(i,j)
  else
    thn(i,j) = theta(i,j)
    rmel(i,j) = rmelt(i,j)
  endif
c
85 continue
c
do 70 i = nr,1,-1
write(7,1200)i,(thn(i,j),j=1,nj)
70 continue
c
write(7,1300)tgasp,thgas(n,no),hd
write(7,1050)
write(7,1250)
c
do 82 i = nr,1,-1
write(7,1350)i,(rmel(i,j),j=1,nj)
82 continue
c
100 continue

c*****
c
c          input and output format statements
c
c*****
1000 format(1x,'failed to converge after',i6,'iterations')
1050 format(1x,'          ')
1250 format(1x,'=====')
    ==', '=====')
1100 format(1x,'axial position = ',i1,' orbit = ',i1,' orbit
    & position = ',i2)
1150 format(1x,'net solar heat input = ',1f10.8,'qz = ',1f9.4)
1200 format(1x,'i = ',i2,20f7.1)
1300 format(1x,'avg gas temp = ',f6.1,'k out gas temp ',
    ,f6.1,'kh = ',f7.4,'kw/m2-k')
1350 format(1x,'i = ',i2,20f7.4)
close(8)
close(7)
stop
end

```

```

subroutine gasprop(dz,nj,h,l)
c
real k,k1,k2,k11,k12,k13,k14,k21,k22,k23,k24,kgas,
+   mw,mw1,mw2,ntu,nu
common/blokb/ni,ne(10),j,t(15,10)
common/blokc/thmelt,tgasin,gasmas,cpgas,ntu,delp,
+   deltdz
common/blokd/tgasp,gasmix,ro(15),ht,w,dxx,p
c
data gamma,pi,runiv,mw1,mw2/1.66,3.14159,8.31434,4,131/
data k11,k12,k13,k14/0.1580e-3,0.9086e-6,333.333,0.794/
data k21,k22,k23,k24/0.6404e-5,0.0454e-6,333.333,0.800/
data viscl1,viscl2,viscl3,viscl4/
/.2158e-4,.1022e-6,333.3,.825/
data visc21,visc22,visc23,visc24/
/.253e-4,.2452e-6,333.333,.77/
f1(x,y) = (1+2.41*(x-y)*(x-0.142*y))/(x+y)**2.0)
f2(x1,x2,x3,x4,x5,x6) =
= ((1+(x1/x2)**.5*(x3/x4)**.25)**2.0)/
+   (2.0*2.0**.5*(1+x5/x6)**0.5)
c
k1 = k11+k12*(tgasp-k13)**k14
k2 = k21+k22*(tgasp-k23)**k24
viscl = viscl1+viscl2*(tgasp-viscl3)**viscl4
visc2 = visc21+visc22*(tgasp-visc23)**visc24
viscw1 = viscl1+viscl2*(t(1,j)+thmelt-viscl3)**viscl4
viscw2 = visc21+visc22*(t(1,j)+thmelt-visc23)**visc24
c
phi12 = f2(viscl,visc2,mw2,mw1,mw1,mw2)
phi21 = phi12*(visc2*mw1)/(viscl*mw2)
psi12 = f2(k1,k2,mw1,mw2,mw1,mw2)*f1(mw1,mw2)
psi21 = f2(k2,k1,mw2,mw1,mw2,mw1)*f1(mw2,mw1)
c
visc = viscl/(1+phi12*(1 - gasmix)/gasmix)+
+   visc2/(1+phi21*(gasmix/(1 - gasmix)))
viscw = viscw1/(1+phi12*(1 - gasmix)/gasmix)+
+   viscw2/(1+phi21*(gasmix/(1 - gasmix)))
kgas = k1/(1+psi12*(1 - gasmix)/gasmix)+
+   k2/(1 +psi21*(gasmix/(1 - gasmix)))
c
mw = gasmix*mw1+(1-gasmix)*mw2
cpgas = gamma*runiv/((gamma-1)*mw)
c
pr = cpgas*visc/(kgas)
dt = 2.0*ht*w/(dxx*nj)
re = 2.0*gasmas/((p*.5*dt)*visc)
nut = .027*re**.8*pr**.333333*(visc/viscw)**.14
c
if ((1.eq.1).and.(re.lt.2100.0))then
nu = .44*(dz/(re*pr*dt))**(-.66)

```

```
elseif (re .lt. 2100.0) then
  nu = 2.35
elseif ((re.gt.2100.0).and.(re.lt.10000.0)) then
  nu = amax1(2.35,nut)
else
  nu = nut
endif
```

c

```
h = kgas*nu/dt
ntu = h*dxx*dz*nj/(gasmass*cpgas)
if (l.eq.1) ntu = .2337841
if (l.eq.2) ntu = .5330746
if (l.eq.3) ntu = .4739715
if (l.eq.4) ntu = .4153427
if (l.eq.5) ntu = .41995574
```

c

```
return
end
```

```

subroutine conduct
+(borl,i,nj,icount,ft,qlat,qsens,grad,tac)
c
common/bloka/a(15),b(15),c(15),d(15)
common/blokb/ni,ne(10),j,t(15,10)
common/blokc/thmelt,tgasin,gasmas,cpgas,ntu,deltp,
+      deltdz
common/blokd/tgasp,gasmix,ro(15),ht,w,dxx,p
common/bloke/rmelt(15,10),denliq,densol,walls,cvmet,
+      denmet,kmet,kliq,ksol,cvliq,cvsol
common/blokf/dz,dtime,rpo(10),qaz,hfl,romelt(15,10),c1,wf,
+      to(15,10),rpmelt(15,10),dx,dy,th,qt,le(15),
+      apoo(15,10),apon(15,10)
common/blokg/k,kn,ks,ke,kw,den,cv
real k,kn,ks,ke,kw,kmet,ntu,ksol,kliq,le
c
ne(j) = 200
i = 1
as = 0
c
1 if (j .eq. 1) then
    aw = 0
    tw = 0
elseif (i.eq.1) then
    tw = t(i,j-1)
else
    tw = t(i+1,j-1)
endif
c
if (j .eq. nj) then
    ae = 0.0
    te = 0.0
elseif (i.eq.1) then
    te = t(i,j+1)
else
    te = t(i-1,j+1)
endif
c
if (i .ge. 2) then
    r = (float(i)+j-2.5)*dy
    rn = r + .5*dy
    rs = r - .5*dy
endif
c
c*****
c      set nodal constants for the wall      *
c*****
c
if (i .eq. 1) then
    an = kmet*dxx/th

```

```

    if (j .ne. 1) aw = kmet*th/dxx
    if (j .ne. nj) ae = kmet*th/dxx
    apon(i,j) = denmet*cvmet*th*dxx/dtime
    apo = apon(i,j)
    dapo = 0.0
    dtapo = 0.0
    tcij = tgasin-thmelt
    hij = gasmas*cpgas*(1-exp(-ntu))/(dz*nj)
    abw = wf*(exp(-c1*le(j)))
    qr = qaz*abw
    qij = qr
    goto 40
endif
c
c*****
c      set nodal constants for outermost elements      *
c*****
c
    if (rpo(j) .gt. rn) then
        if (rpo(j) .le. (rn+dy)) ne(j) = i+1
    endif
c
    if ((j .eq. nj).and.(i .eq. 2)) then
        if (rpo(j).le.rn) ne(j) = i
    endif
c
    if (i .gt. (ni-j+2)) then
        rmelt(i,j) = 1.0
c
        if (i .eq. ne(j)) then
            an = 0.0
        elseif (i .eq. (ne(j)-1)) then
            an = kliq*dx/(.5*(rpo(j)-rn)+.5*dy)
        else
            an = kliq*dx/dy
        endif
c
        if (i .eq. (ni-j+3)) then
            call property (cv,den,i-1,j,ks)
            if (i.eq.ne(j)) then
                as = kliq*ks*dx/(kliq*.5*dy+ks*(rpo(j)-rs)*.5)
            else
                as = kliq*ks*dx/((kliq+ks)*.5*dy)
            endif
        elseif (i .eq. ne(j)) then
            as = kliq*dx/(.5*(rpo(j)-rs+dy))
        else
            as = kliq*dx/dy
        endif
c

```

```

if (j .ne. nj) then
  if (rpo(j+1).ge.rn) then
    if (i.eq. ne(j)) then
      ae = kliq*((rpo(j)+rn)*.5-rs)/dx
    else
      ae = (kliq*dy)/dx
    endif
  elseif(rpo(j+1).le.rs) then
    ae = 0.0
  elseif (i.eq.ne(j)) then
    ae = (kliq*((rpo(j)+rpo(j+1))* .5-rs))/dx
  else
    ae = kliq*((rn+rpo(j+1))* .5-rs)/dx
  endif
endif

```

c

```

if (j .ne.1) then
  if (rpo(j-1).ge.rn) then
    if (i.eq. ne(j)) then
      aw = kliq*((rpo(j)+rn)*.5-rs)/dx
    else
      aw = (kliq*dy)/dx
    endif
  elseif(rpo(j-1).le.rs) then
    aw = 0.0
  elseif (i.eq.ne(j)) then
    aw = (kliq*((rpo(j)+rpo(j-1))* .5-rs))/dx
  else
    aw = kliq*((rn+rpo(j-1))* .5-rs)/dx
  endif
endif

```

c

```

if (i .eq. ne(j)) then
  apon(i,j) = denliq*cvliq*(1.0 - walls)*(rpo(j)-rs)*
* dx/dtime
else
  apon(i,j) = denliq*cvliq*(1.0 - walls)*dy*dx/dtime
endif

```

c

```

if (apoo(i,j).eq.0.0) apoo(i,j) = apon(i,j)
if (qaz .gt. 0.0) then
  apo = apoo(i,j)
  dapo = apon(i,j) - apo
  dtapo = 0.0
else
  apo = apon(i,j)
  dapo = 0.0
  dtapo = apoo(i,j) - apon(i,j)
endif
tcij = 0.0

```

```

      hij = 0.0
      if (i .eq. ne(j)) then
        abm = 1 - exp(-c1*(rpo(j)-rs))
      else
        abm = (-exp(-c1*(rpo(j)-rs))+exp(-c1*(rpo(j)-rn)))
      endif
      qr = qaz*abm + qt
      qij = qr
      goto 40
    endif
  c
  c*****
  c          set nodal constants for the inner pcm          *
  c*****
  23      call property (cv,den,i,j,k)
  c
      if (i .eq. 2) then
        apon(i,j) = den*cv*.5*dx*dy/dtime
        pcmmass = .5*dx*dy*densol*(1-walls)
      else
        apon(i,j) = den*cv*dx*dy/dtime
        pcmmass = dx*dy*densol*(1-walls)
      endif
  c
      if (apoo(i,j) .eq. 0.0) apoo(i,j) = apon(i,j)
      if (qaz.gt.0.0) then
        apo = apon(i,j)
        dapo = 0.0
        dtapo = apoo(i,j) - apon(i,j)
      else
        apo = apoo(i,j)
        dapo = apon(i,j) - apoo(i,j)
        dtapo = 0.0
      endif
  c
      tcij = 0.0
      hij = 0.0
      dmelt = t(i,j)*cv*borl/hfl
  c
      if (i.eq. ne(j)) then
        an = 0.0
      elseif (i.eq.(ni-j+2)) then
        if ((i+1).eq.ne(j)) then
          an = k*kliq*dx/(k*(rpo(j)-rn)*.5+kliq*.5*dy)
        else
          an = k*kliq*dx/((k+kliq)*.5*dy)
        endif
      else
        call property(cv,den,i+1,j,kn)
        an = k*kn*dx/((k+kn)*.5*dy)
      endif

```



```

else
  if (dmelt.gt.0.0) then
    if (rmelt(i+1,j) .ge. 1.0)
      &      rmelt(i,j) = rmelt(i,j)+dmelt
    else
      if ((rmelt(i-1,j) .le. 0.0) .or. (qaz .lt. 0.0))
        &      rmelt(i,j) = rmelt(i,j)+dmelt
      endif
    endif
  endif

c
  if (rmelt(i,j).gt.1.0) rmelt(i,j) = 1.0
  if (rmelt(i,j) .lt. 0.0) rmelt(i,j) = 0.0
  qij = (romelt(i,j)-rmelt(i,j))*pcmmass*hfl/dtime
  qlat = qlat-qij*dz
  abm = (-exp(-c1*(rpo(j)-rs))+exp(-c1*(rpo(j)-rn)))
  qr = qaz*abm + qt
  qij = qij + qr

c
  if (i .le. (ni-j+2)) then
    if (i.eq.2) then
      odmelt = (rmelt(i,j)-rpmelt(i,j))*0.5*dy*
      *      (densol/denliq-1)
    else
      *      odmelt = (rmelt(i,j)-rpmelt(i,j))*dy*
      *      (densol/denliq-1)
    endif
    ro(j) = ro(j) + odmelt
  endif

c
  if (rmelt((ni-j+2),j)-0.0.le.0.000001) then
    ro(j) = ni*dy
    ne(j) = ni-j+2
  endif

c
  odmelt = 0.0
40 a(i) = -as
  b(i) = an+as+ae+aw+apo+dapo+hij
  c(i) = -an
  d(i) = (apo+dtapo)*to(i,j)+qij+ae*te+aw*tw+hij*tcij
c  delapo = apoo(i,j) - apon(i,j)
c  if (delapo.ge.0.0) then
c    qmove = delapo*(0.0-to(i,j))*dz
c  else
c    qmove = delapo*(0.0-t(i,j))*dz
c  endif
  qsens = qsens+(apo+dapo)*dz*t(i,j)-(apo+dtapo)*dz*to(i,j)
  qgrad = qgrad + qr*dz
  if (i.ne.1) tac = tac+abm
  if (i .eq. ne(j)) goto 60
50 i = i+1

```

```
goto 1  
60 return  
end
```

```
subroutine property(cv,den,i,j,k)
C
common/bloke/rmelt(15,10),denliq,densol,walls,cvmet,denmet,
+      kmet,kliq,ksol,cvliq,cvsol
real kliq,ksol,kmet,k,kpure
C
kpure = 1.0 / (rmelt(i,j)/kliq + (1-rmelt(i,j))/ksol)
cvpure = rmelt(i,j)*cvliq + (1-rmelt(i,j))*cvsol
denpur = rmelt(i,j)*denliq + (1-rmelt(i,j))*densol
C*****
C      put storage material in parallel with can material      *
C*****
k = kpure*(1-walls)+kmet*walls
den = denpur*(1-walls)+denmet*walls
cv = (cvpure*denpur*(1-walls)+walls*cvmet*denmet)/den
return
end
```

```
subroutine solver(i)
common/bloka/a(15),b(15),c(15),d(15)
common/blokb/ni,ne(10),j,t(15,10)
m = ne(j)
c
do 1 i = 1,m-1
    r = a(i+1)/b(i)
    b(i+1) = b(i+1)-r*c(i)
    d(i+1) = d(i+1)-r*d(i)
1 continue
c
t(m,j) = d(m)/b(m)
c
do 2 i = m-1,1,-1
    t(i,j) = (d(i)-c(i)*t(i+1,j))/b(i)
2 continue
c
return
end
```

```
subroutine heatgas(nj)
real ntu
common/blokb/ni,ne(10),j,t(15,10)
common/blokc/thmelt,tgasin,gasmas,cpgas,ntu,deltp,
+      deltdz
c
  if (j .eq. 1) then
    qgasp = 0.0
    qgasdz = 0.0
  endif
c
  temp=(t(1,j)+thmelt)-tgasin
  qgasp=qgasp+gasmas*cpgas*temp*(1-exp(-0.5*ntu))/(nj)
  qgasdz=qgasdz+gasmas*cpgas*temp*(1-exp(-ntu))/(nj)
c
  if (j .eq. nj) then
    deltp=qgasp/(gasmas*cpgas)
    deltdz=qgasdz/(gasmas*cpgas)
  endif
c
10 continue
return
end
```

1. Report No. NASA CR-185117		2. Government Accession No.		3. Recipient's Catalog No.	
4. Title and Subtitle Thermal Evaluation of Advanced Solar Dynamic Heat Receiver Performance				5. Report Date March 1989	
				6. Performing Organization Code	
7. Author(s) Roger A. Crane				8. Performing Organization Report No. None	
				10. Work Unit No. 506-41-31	
9. Performing Organization Name and Address University of South Florida Tampa, Florida 33620				11. Contract or Grant No. NAG3-851	
				13. Type of Report and Period Covered Contractor Report Final	
12. Sponsoring Agency Name and Address National Aeronautics and Space Administration Lewis Research Center Cleveland, Ohio 44135-3191				14. Sponsoring Agency Code	
15. Supplementary Notes Project Manager, Miles O. Dustin, Power Technology Division, NASA Lewis Research Center.					
16. Abstract <p>The work described herein addresses the thermal performance of a variety of concepts for thermal energy storage as applied to solar dynamic applications. It is recognized that designs providing large thermal gradients or large temperature swings during orbit are susceptible to early mechanical failure. Concepts incorporating heat pipe technology may encounter operational limitations over sufficiently large ranges. By reviewing the thermal performance of basic designs the relative merits of the basic concepts are to be compared. In addition the effect of thermal enhancement and metal utilization as applied to each design provides a partial characterization of the performance improvements to be achieved by developing these technologies.</p>					
17. Key Words (Suggested by Author(s)) Solar Dynamic Heat Receiver Thermal Energy Storage			18. Distribution Statement Unclassified-Unlimited		
19. Security Classif. (of this report) Unclassified		20. Security Classif. (of this page) Unclassified		21. No of pages 140	22. Price* A07